UNIVERSITY OF LIVERPOOL

Interference effects in molecular nanojunctions

Thesis submitted in accordance with the requirements of the University of Liverpool
for the degree of Doctor of Philosophy by

Nicolò Ferri

October 2018

Abstract

Nicolò Ferri: Interference effects in molecular nanojunctions

From the earliest theoretical investigation of the possibility of single molecule conductance, to today where single molecule conductance techniques are becoming routine operations, the field of molecular electronics has grown exponentially, becoming an important research topic with possible future applications.

Understanding electron transport in nanojunctions has lately been a hot topic and represents a fundamental step for the advancement of molecular electronics. This thesis aims at unravelling some of the mysteries and mechanisms that revolve around the behaviour of some molecular wires.

This thesis focusses its attention towards interference effects in organic molecular wires: in this thesis two main types of interferences are studied: one located on the contacts of a series of molecular wires and one regarding the structure-property relationships within molecular wires. The novelty of this work lies in the synthesis of new molecular wires and their conductance studies with STM-based techniques.

The first project demonstrated the existence of strong interactions between thiol contacts and gold electrodes (so-called 'gateway states') that were interfering with the conductance decay of a series of double barrier tunnelling molecular wires of increasing length by suppressing the attenuation of their conductance over their length. A simple experiment supported by theoretical calculations featuring the synthesis of molecular wires with thiols replaced by thioether contacts demonstrated the existence of these interactions by cancelling their effects.

The second project was focussed on the study of interference effects in thiophene-based molecular wires. Several series of molecular wires were synthesized in multiple subprojects to gain a better understanding of these effects by finely tuning the molecular wires structures such as the introduction of heteroatom bridges and the insertion of carbonyl moieties as cross conjugation points within the backbone of a molecular wire. On this project some unusual switching properties of some of the wires were discovered and investigated.

Finally, this study managed to shed some light on the behaviour of all the bithiophene-based molecular wires analysed and the information discovered will be useful in the tool-box for finely tuning properties of molecular wires.

Table of Contents

List of Abbreviations

Ac	Acetyl
ADT	Alkanedithiols
AFM	Atomic Force Microscope
CI	Chemical Ionisation
DCM	Dichloromethane
DFT	Density Functional Theory
DHP	Dihydropyran
DIPA	Di*iso*propylamine
DMF	*N,N*-Dimethylformamide
DPPE	1,2-Bis(diphenylphosphino)ethane
DTB	Double Tunnelling Barrier
EI	Electron Ionisation
HOMO	Highest Occupied Molecular Orbital
HRMS	High Resolution Mass Spectrometry
IR	Infrared
ITO	Indium-Tin Oxide
IUPAC	International Union of Pure and Applied Chemistry
LUMO	Lowest Unoccupied Molecular Orbital
MCBJ	Mechanically Controlled Break Junction
MI	Matrix Isolation
MS	Mass Spectrometry
NBS	*N*-Bromosuccinimide
n-BuLi	n-Butyllithium
NDR	Negative Differential Resistance
NEGF	Non-Equilibrium Green's Function
NMR	Nuclear Magnetic Resonance
OPE	Oligophenyleneethynylene

[Ph]	Phenyl
RT	Room Temperature
SAM	Self Assembled Monolayer
SPM	Scanning Probe Microscope
STM	Scanning Tunnelling Microscope
STM-BJ	Scanning Tunnelling Microscope – Break Junction
STS	Scanning Tunnelling Spectroscopy
[T3]	α-Terthiophene (2,2’:5’,2”-terthiophene)
TBPT	4,4'-bis(5-(methylthio)thiophen-2-yl)-1,1'-biphenyl
TFT	2,7-bis(5-(methylthio)thiophen-2-yl)-9*H*-fluorene
TPDT	2,7-bis(5-(methylthio)thiophen-2-yl)phenanthrene-9,10-dione
TFOT	2,7-bis(5-(methylthio)thiophen-2-yl)-9*H*-fluoren-9-one
$TCMe_2T$	4,4-dimethyl-2,6-bis(methylthio)-4H-cyclopenta[2,1-b:3,4-b']dithiophene
TDKT	2,7-bis(methylthio)benzo[2,1-b:3,4-b']dithiophene-4,5-dione
TKT	2,6-bis(methylthio)-4*H*-cyclopenta[2,1-*b*:3,4-*b’*]dithiophen-4-one
$TCPh_2T$	2,6-bis(methylthio)-4,4-diphenyl-4H-cyclopenta[2,1-b:3,4-b']dithiophene
$TGePh_2T$	2,6-bis(methylthio)-4,4-diphenyl-4H-germolo[3,2-b:4,5-b']dithiophene
$TSiPh_2T$	2,6-bis(methylthio)-4,4-diphenyl-4H-silolo[3,2-b:4,5-b']dithiophene
TCNQ	Tetracyanoquinodimethane
TEA	Triethylamine
THF	Tetrahydrofuran
THP	Tetrahydropyran
TMS	Trimethylsilyl
TTF	Tetrathiafulvalene
UV-Vis	Ultraviolet – Visible
[V]	Viologen (4,4’-bipyridinium)

During this PhD the following papers were produced:

A. Vezzoli, R. J. Brooke, N. Ferri, S. J. Higgins, W. Schwarzacher and R. J. Nichols, Single-Molecule Transport at a Rectifying GaAs Contact, *Nano Lett.*, 2017, **17**, 1109–1115.

A. Vezzoli, R. Brooke, N. Ferri, C. Brooke, S. Higgins, W. Schwarzacher and R. J. Nichols, Charge Transport at a Molecular GaAs Nanoscale Junction, *Faraday Discuss.*, 2018, **210**, 397-408.

S. Sangtarash, A. Vezzoli, H. Sadeghi, N. Ferri, H. M. O 'brien, I. Grace, L. Bouffier, S. J. Higgins, R. J. Nichols and C. J. Lambert, Gateway state-mediated, long-range tunnelling in molecular wires, *Nanoscale*, 2018, **10**, 3060-3067.

The following manuscript is currently available online as a preprint on the *ChemRxiv* repository, item #7275005 but has not been published yet.

N. Ferri, N. Algethami, A. Vezzoli, S. Sangtarash, M. McLaughlin, H. Sadeghi, C. J. Lambert, R. J. Nichols, S. J. Higgins, Large-Amplitude, High-Frequency Single-Molecule Switch.

Chapter 1: Introduction

1.0 Background and context

In April 1965 the chemist and director of research and development at Fairchild Semiconductor Gordon Earle Moore predicted, on the basis of empirical observations of the evolution of semiconductor device processing technology since the invention of the integrated circuit in 1958, that computing processing power would likely double every 2 years for the foreseeable future[1]. This later became known as 'Moore's law' and in conjunction with Dennard's scaling rules[2] held its validity until approximately 2010. The advance in technology was mainly due to an efficient miniaturization of transistors; unfortunately this scaling is, at the moment, already slowing down[3]. Leakage of current and limitation of lithographic processes are challenging difficulties that arise from transistor scaling[4]. In order to produce devices with even more computing power several alternatives have been tried. A promising way could be the bottom up approach offered by molecular electronics that one day may revolutionize today's nanotechnologies.

1.1 Molecular electronics: the origin

The first reliable molecular conductance study was reported in 1971 by Hans Kuhn and Bernard Mann; they electrically characterized devices consisting of organic monolayers of long-chain fatty acid salts deposited by the Langmuir-Blodgett technique on aluminium electrodes, with a top contact of Hg, or a second evaporated metal.[5] That publication demonstrated empirically that the mechanism of conductance was tunnelling, and subsequently in 1974 Arieh Aviram and Mark Ratner discussed theoretically the electronic transport through a simple rectifier,[6] a single molecule containing a donor group (TTF) and an acceptor group (TCNQ) bridged by a short alkane chain. The main idea was to model a small device with one side of the molecule having the LUMO aligned with the Fermi level of the metal to favour the injection of electrons, a molecular bridge, and a second moiety having the HOMO aligned with the Fermi level of the second metal, allowing the electrons to flow with a small bias in one direction, but a significantly higher bias in the reverse direction because of the misalignments of the orbital energies and the electrodes.

Molecular electronics in the 70s was slowly attracting increasing interest and finally in the 1980s the most important discovery in this field occurred: the invention of the scanning tunnelling microscope (STM) and atomic force microscope (AFM) by the IBM labs in Zurich. With these tools the possibility to perform single molecule conductance studies became a reality. Unfortunately, due to technical difficulties the first studies on electron transfer in single molecular junctions were published more than ten years later starting with the introduction of another important technique: the mechanically controlled break junction. In 1997 Reed[7] developed a stable system that consisted of a gold wire glued to a flexible structure that was stretched in a solution of benzene-1,4- dithiol until breakage in order to form two atomically-sharp tips covered by a molecular monolayer. At this point the solvent was evaporated under argon and the two tips were brought close to each other and current-voltage measurements were recorded. The position of the gold tips was controlled using a piezoelectric tube connected to a piezo rod and from this information it was possible to recover the distance between the electrodes during the experiments. Conductance values, electrode separation and a good reproducibility gave a powerful push forward to the molecular electronics field giving the ultimate tool to understand charge transport at molecular level. In Figure 1.1**Error! Reference source not found.** is shown a schematic of the MCBJ described above.

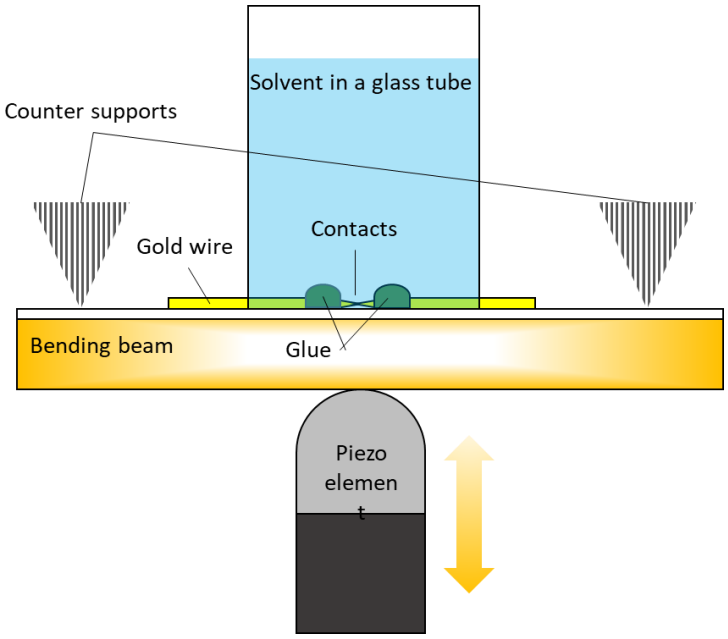

Figure 1.1 *Schematic of a Mechanically Controlled Break-Junction (MCBJ)*

Other methodologies were developed later, combining more advanced technologies to study molecular nanojunctions (such as the STM-based techniques), but this research field is still facing challenges and unexplained phenomena. Even after almost 50 years of molecular electronics on the nanoscale there are so many factors, effects and variables that are still a mystery. And this is only one of the fascinating aspects of molecular electronics.

1.2 Scanning Tunnelling Microscopy

The Scanning Tunnelling Microscope was invented in 1981 by Roher and Binning; how it works is shown in Figure 1.1 and is well explained by Julian Chen in 'Introduction to Scanning Tunnelling Microscopy'.[8] It is composed of a probe tip, generally made of tungsten or platinum-iridium, connected to a *piezodrive* (a set of three piezoelectric transducers mounted at 90° to each other in the three direction *x*, *y* and *z)*. The application of a sawtooth voltage to the *x* piezo while increasing voltage on the *y* piezo make possible the scan of the plane xy on the sample (generally made of Au (110) or GaAs (111) or Si (111)). The movement of the coarse positioner combined with the control over the z piezo gives the possibility to position the tip at just a few nanometres from the surface. To ensure the exact position of the tip the system must be isolated from external vibrations with springs or bungee cords. At this moment the tip is kept between 0.4 and 0.7 nm from the sample; in this point, if a bias voltage is applied between tip and substrate, tunnelling current is generated.[8]

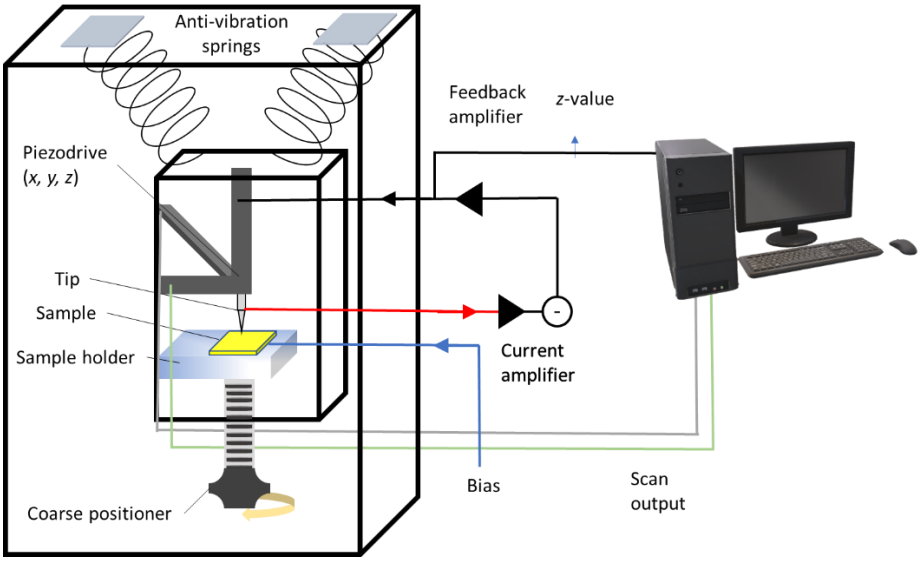

Figure 1.2 *Schematic of a STM*

Usually STM experiments are executed *via* two different methods: constant current mode and constant height mode. The former consists of maintaining the same current value while the height is adjusted by the piezo during the scan and the latter consists of maintaining the voltage and height while the resulting current is measured. The two methods are similar, but the latter is slightly quicker, because in the constant current mode the feedback electronics need to adjust the piezo every time while the constant-height mode the current is recorded directly. The output is an image in grayscale that may be enriched by addition of colours in post-production.

1.3 How does charge pass through molecules?

The charge transport through a nanojunction formed by a molecule bridging two electrodes depends on several factors including the type of backbone or molecule used, and the distance between the two electrodes, which is governed by the length of the molecule. The electronic transport studied in this thesis consists of coherent tunnelling and is typical for short molecules (< 3 nm).[9] Tunnelling is defined as coherent if the electron maintains phase information through the transport. This means that when an electron tunnels through a barrier it retains part of the wave

information and it that can be defined with a single wavefunction. This kind of transport is temperature-independent, in contrast to the hopping mechanism which is typical of longer molecules; in the latter case the electrons hop from one part of the molecule to another, losing all the phase information during the process. Hopping transport, an activated process, is temperature-dependent and is much slower than coherent tunnelling. Hopping typically consists of a transport of charge that progresses from site to site within a molecule.

In a metal/molecule/metal nanojunction, the Fermi energy of the electrodes changes when a bias is applied to promote electron transport. More specifically, when a bias is applied to a junction, the Fermi energy (E_F) of one electrode is increased, making the tunnelling of the electron to the other one possible through the HOMO or the LUMO orbitals of the molecular wires as shown in Figure 1.3.

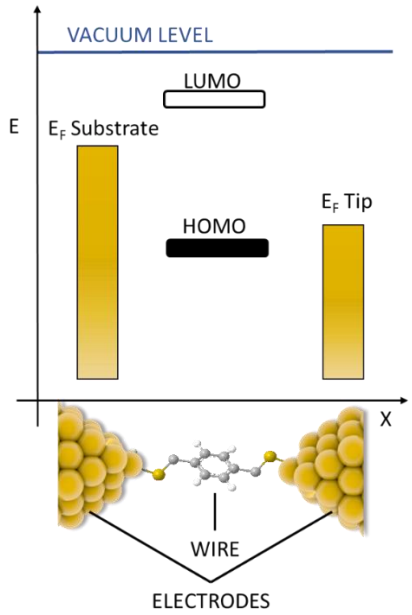

Figure 1.3 *Schematic diagram of a nanojunction showing the position of the orbitals of a molecular wire between the Fermi energy (E_F) of the two electrodes*

Figure 1.3 exemplifies coherent tunnelling found for short molecular wires in the case of small bias voltages. If the bias used is greater than the barrier height, a different type of transport takes place (Fowler-Nordheim tunnelling). Alternatively, for longer

molecules (> 3-4 nm), charge can be transported through a hopping mechanism. In the figure is also present the vacuum level which is located at higher energy, this because tunnelling through a molecular wire is more convenient than tunnelling through vacuum.

The tunnelling of electrons from one electrode (substrate) to the other (tip) happens through the wire's orbitals (in Figure 1.3 is shown a thiol-based molecular wire that uses his HOMO for the charge transport); this thesis will be focused in reporting interference effects in molecular wires and whenever there is an interference event, the position of the HOMO and LUMO will be slightly shifted resulting in a positive or a negative increase in the conductance value of a molecular wire.

In Chapter 2 will be presented two interferences effect called Gateway states and Coupling states while in Chapter 3 and 4 will be discussed the Fano resonance. The Gateway states are couplings between the orbitals of the contact of a series of molecular wires studied (alkane dithiols wires with a conjugated core in the middle) and the metal electrodes, while the Coupling states are the results of the influence of the Gateway states combined with the presence of a conjugated core in the middle of the molecular wires. These two interferences produced a significant shift of the position of the HOMO producing a boost in the conductance of the molecular wires and a decrease of the conductance decay over the length of the wires. The Fano resonance on the other hand is an interference effect that is predicted for molecular wires with cross conjugated moieties in the conductance pathway, that can lead to a significant boost or a significant decrease in conductance of the wire when compared with a similar wire without the cross conjugated part. Unfortunately, it is very difficult to predict the exact position of the Fano resonance; if the Fano resonance lies between the HOMO-LUMO gap it might change the position of the orbitals in the energy diagram and thus produce a decrease or an increase of the conductance; (a more detailed description of the transmission profile of the Fano resonance can be found in Figure 3.11).

In this thesis the molecular wires studied are very short and therefore their charge transport will be within the *coherent tunnelling* regime, nonetheless all the measurements have been executed at the same temperature and conditions.

1.4 Single Molecule Conductance Techniques

One of the first techniques used to conduct single molecule conductance experiments was the Matrix Isolation (MI) method reported in 2001 by Cui et al.[10] They fabricated a mixed SAM (Self-Assembled Monolayer) consisting of a small proportion of alkanedithiol diluted into alkanethiol on gold, then attached gold nanoparticles to the alkanedithiol molecules using the free thiol moieties not attached to the gold substrate. Then they used a conductive atomic force microscope (C-AFM) to locate and electrically contact the individual gold nanoparticles and were thus able to measure I/V traces. This demonstrated the feasibility of single molecule conductance measurements. Unfortunately, the experimental technique is both tedious to perform and technically challenging and the data analysis was also non-trivial, but later different techniques were developed in order better understand the behaviour of single molecule nanojunctions.

1.4.1 Scanning Tunnelling Microscope Break junction technique: STM-BJ

This technique is one of the most common ones used in molecular electronics along with the MCBJ described earlier. This technique uses a modified Scanning Tunnelling Microscope for performing single molecule conductance studies but is not limited to break junctions; it can be used also for monolayers and other devices. In a typical single molecule STM-BJ experiment, a gold (111) substrate is approached by a STM tip (usually gold as well) until it crashes, and a metallic contact is formed. At this point the tip is retracted while the current is measured. If a molecule, in our case, is trapped during the tip retraction, the current decay will show a small signal, usually a little step or plateau. When the molecule is fully stretched, the junction will break, resulting in an abrupt current decay. If no molecule bridges the gap, a simple exponential decay is observed instead throughout the retraction process (Figure 1.4). After this routine have been repeated around 5-10 thousand times, the data is processed, and the current decays are analysed to form a histogram with details over the conductance of the molecular wires studied. This technique possesses some

positive factors such as simpler substrate preparation as there is no need of a clean room for the device formation, it can be performed at room temperature and under ambient conditions. But at the same time during the measurements some drifting of the probe over the substrate can occur.

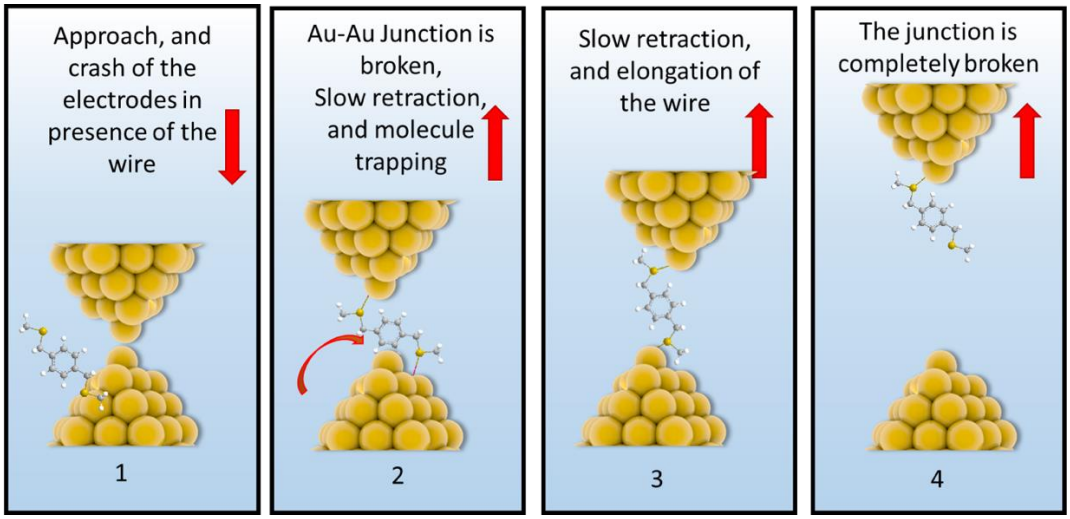

Figure 1.4 *Schematics of a STM-BJ measurement: the tip is approached and crashed on the gold electrode (1) in presence of a solution of the molecular wire and afterwards slowly retracted (2). A gold-gold junction is broken during the withdrawing of the tip and eventually a molecule bridges the gap and is fully elongated (3). Finally, the junction is fully broken and an abrupt decay in current is observed.*

In this thesis, the STM-BJ technique will be used for the majority of the molecules studied and it is nowadays considered one of the most reliable and widely-used methods for single molecule measurements. In addition, it usually does not require any data selection for the generation of the conductance histogram. Another technique used in this thesis was a similar STM-based technique: STM-I(s).

A more detailed description of the techniques used can be found in Chapter 6.

1.4.2 STM-I(s)

This technique is distinct from the STM-BJ method because it does not involve any contact between the tip and the gold substrate. Instead of relying on a physically-created junction between electrodes, this technique uses the charge of the tip to make a metal/molecule/metal nanojunction.

The set up and functioning is very similar to the previous technique (Figure 1.5): it starts with the approach of the tip to the gold surface where a sub-monolayer of molecular wires is present. The tip is then withdrawn before contacting the substrate, from a certain predefined height. At this point a molecule might fill the gap pushed by the electrostatic charge of the tip/substrate. As in the previous technique, the junction is then stretched until it breaks and the current decays. In this technique the data from the measurements is then analysed to form a histogram. Unfortunately, this technique has a much lower ''hit rate'' than the STM-BJ (usually *ca*. 10 times lower) and often, data selection by the user is needed in order to build a histogram, selecting only those traces where a molecular nanojunction is present. Even though this technique might require data selection and is a more time-consuming technique, it can be used for wires with a very low conductance and can resolve different geometries of contact.

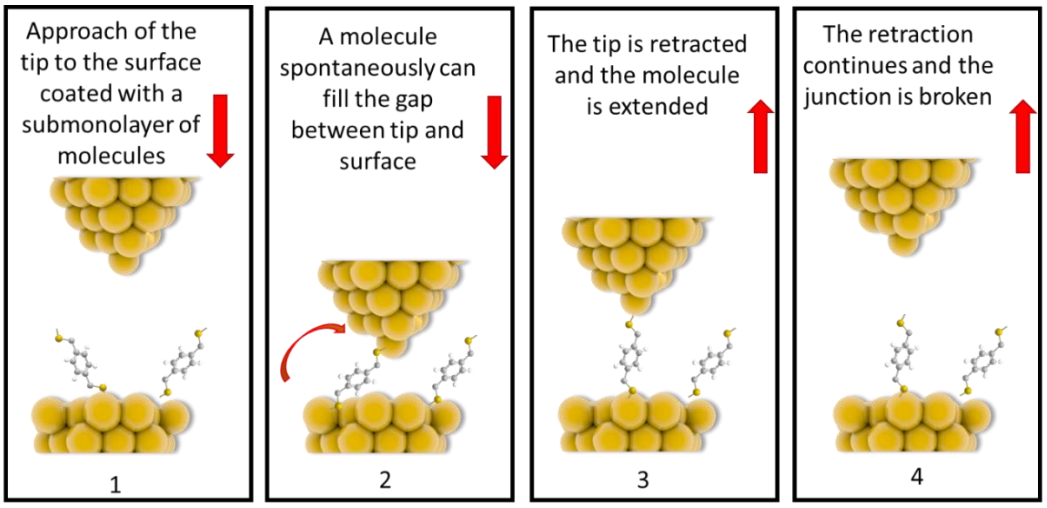

Figure 1.5 *Schematics of a STM-I(s) measurement: the tip is approached but not crashed on the gold electrode (1) in presence of a submonolayer of the molecular wires on air and eventually (2) a molecule might fill the gap between the electrodes. The tip is withdrawn and the molecule in the gap is fully elongated (3). Finally, the retraction brakes the junction and an abrupt decay in current is observed.*

1.4.3 Additional Techniques

The I(t) technique is similar to the I(s) technique in that it involves no contact between tip and substrate. This method is mainly used to analyse dithiol monolayers

but can be used for other purposes. It consists of holding the tip on the top of the surface of a monolayer while maintaining the same height; during this process current steps are recorded and later statistically analysed. This method has been used for studying the behaviour of dithiol SAMs on GaAs substrates.[11,12]

The I/V measurements are instead a modification of the STM-BJ technique; they have been used in this thesis to study the behaviour of different wires in a wider range of voltage. Usually STM-BJ measurements are recorded at a defined bias voltage (100-300 mV); once the nanojunction is formed, a rapid voltage ramp from -1V to +1V is performed and the current is measured as a function of bias voltage. Afterwards the traces are analysed to provide a picture of the conductance of the wire at different biases.

Another modification of the STM-BJ technique is the modulation experiment. It consists of the initial entrapment of the wire in a nanojunction as for a normal STM-BJ experiment, followed by pushing and pulling the tip by a few Ångstroms. This experiment provides useful information on the possibility of different types of possible contacts inside the molecule. If a molecule changes shape or possesses more than one contact group within the wire, the increase or decrease of distance between the electrodes decreases or increases the observed conductance. If a wire does not possess this capacity, its conductance will remain comparatively stable during the process.

All the techniques mentioned so far were used to test different properties of molecular wires in this thesis. A more technical description will be offered in Chapter 6 while the full list of all the measurements can be found in the Appendix.

1.5 Anchoring groups in a nanojunction

A nanojunction as described in this thesis is composed of a molecular wire and two electrodes and they are connected through molecular moieties called anchoring groups or contacts. The type of molecular moieties used as contacts is directly influenced by the electrode material. The most widely used type of metallic electrode is certainly gold, thanks to its resistance to oxidation and its low reactivity with other compounds. Alternative electrodes that have been investigated include GaAs, copper, and indium-doped tin oxide (ITO). Molecular moieties used as contacts, are generally, sulfur- and nitrogen-based contacts due to the lone pair that easily binds to gold and creates sigma bonds. Some examples are thiols, thioethers, thioesters, thiophenes, amines, nitriles and pyridines.[7,13–17] Also, carbon-based contacts have been reported: alkynes, carbenes, carboxylic acids, and fullerenes.[18] Some less used contacts include Trimethylsilyl-ethynyl, and phosphines[19,20].

Each contact influences the value of conductance of a molecular wire. In a study by Tao et al.[21], variations in conductance of a series of molecular wires with same backbone structure but different contacts have been reported, but the influence of the contact over the conductance of a molecular wire is not fully understood and multiple factors such as quantum interferences on the contacts or couplings with the metal electrodes might play a major role in the behaviour of a molecular wire.

One example that will be studied in this thesis (chapter 2) is the influence of thiol contacts on the conductance decay over increasing length of a series of double tunnelling barrier (DTB) molecular wires. A simple DTB wire consists in a conjugated molecular moiety in the centre of the wire connected to the electrodes by non-conjugated spacer (such as alkane chains). The conjugated centre should favour charge transport while the alkane chains should behave as tunnelling barriers. In this case, the interplay between sulfur and gold directly influences the conductance decay of a series of molecular wires by attenuating it under certain circumstances.

1.6 Quantum interference

For simple systems such as alkanedithiols or oligophenylene-based molecular wires it has been empirically demonstrated that conjugated molecules conduct significantly better than equivalent length molecules with only σ bonds, and that barriers such as alkane chains can decrease the conductance of a molecular wire. This is because in a molecular junction, the Fermi level must fall somewhere between the HOMO and LUMO of the molecule and the conductance and the rate of decay of conductance with length will both be related to the energy separation between the Fermi energy and the nearest frontier orbital[22–24]; this will clearly be smaller for π-conjugated systems. For more complicated systems there are many additional factors to consider. Interference effects in nanojunctions are becoming a hot topic in molecular electronics and they play a crucial role in defining the conductance behaviour of molecular wires with peculiar structures or having multiple conductance pathways. In fact, when more than one pathway is present, each of them must be considered when theoretical studies are performed. Several studies[25–27] predicted and demonstrated differences in conductance in some particular molecular wires. An example is the different effects observed in a benzene-based molecular wire when the contacts are connected in positions which are either mutually *meta* or *para*; changing the connection directly influences the behaviour of the wire; in this case the π-system is interfering directly on the charge transport and thus creating significant differences in the charge transport profile of the different molecular wires.[28]

Quantum interferences might increase (constructive interference) or decrease (destructive interference) the conductance of a molecular wire and theoretical calculations are useful tools to predict the behaviour of systems with multiple pathways but must be accompanied by strong experimental results. The understanding and the mastery of quantum interference effects can be very useful tools for the future development of molecular electronics and most importantly for the development of single molecule devices.[29]

Colin Lambert explained in a tutorial review in 2015[30] how to predict quantum interferences by tuning the structure of a molecular wire. Different types of interferences and examples are also discussed including the Fano resonances which are the responsible for the interference effects that will be discussed in the third and fourth chapter of this thesis.

1.7 Thesis outline

Fully understanding the charge transport in single molecule measurements has always been one of the most important desires in molecular electronics. The main aim of this thesis is to shed some light on some interesting interference effects predicted in single molecule conductance measurements.

The first work discussed in the second chapter will focus its attention towards the study of double tunnelling barrier-based molecular wires and especially on the influence of the nature of contacts over the length dependent conductance decay. In this case, the interplay between thiols, used as contacts, and the metal electrodes generated some resonances that influenced the behaviour of the wires analysed.

The third chapter is focused on the introduction of interference effects in bithiophene-based molecular wires by incorporating in the wires' molecular backbone different moieties such as heteroatom bridges or one or two carbonyl groups, to tune and influence the conductance behaviour of the molecules.

The fourth chapter will be split in two sub-projects; firstly the interference effect studies were extended by comparing molecular wires with a longer, but still conjugated backbone, based on an elongated version of the wires studied in the previous chapter and likewise focused on the introduction of Fano resonances in the conductance profile by the addition of ketones in the backbone of the wires as a cross-conjugated node. Secondly, interference effects in a set of molecules consisting of bipyridine-based ligands complexed with transition metal carbonyl centres to create multiple Fano resonances in the transmission profile of the junctions. The second sub-project is focused on an unusual and different type of molecule but still

helps giving a wider overview of interference effects that might tune or interfere with the conductance pathway of molecular wires.

The fifth chapter will be focused on the syntheses of the molecules used to form junctions in this thesis and will provide a general overview of the synthetic route followed and also on the procedures executed to create the wires for conductance studies.

The sixth chapter will provide some more information on the measurements executed with the Scanning Tunnelling Microscope and on the techniques used.

The thesis will then be concluded in Chapter 7 followed by the collection of all the measurements in the appendix.

Chapter 2: Gateway state-mediated tunnelling in molecular wires

2.0 Introduction

In a nanojunction, a fundamental goal in molecular electronics is the complete understanding of the electron transport. The conductance of a molecular wire in a MMM (metal-molecule-metal) junction depends on a series of factors, including the nature of the molecule, the contact group used, and its interaction with the metal (usually, gold).

According to tunnelling theory, the conductance across a nanojunction follow the general rule: $\mathbf{G = Ae^{-\beta L}}$, where **A** is the pre-exponential factor which derives from the junction contacts and from the nature of metallic leads, and **L** is simply the length of the junction. The exponential attenuation factor **β** is influenced strongly by the nature of the molecular wire itself.

The attenuation factor β is an important feature of nanoelectronic junctions and it has been determined for several systems: in a oligophenylene-based series of molecular wires the correlation between an increasing number of phenyl unit and the conductance value decay was previously measured[31] to have β value of 0.41 $Å^{-1}$. In other studies similar β values were measured for oligophenyleneimine[32] and oligonaphthalenefluoreneimine[33] molecular wires, while very low β values were observed in oligoporphyrins[31,34–36]and oligoynes[37]. Oligothiophenes were the subject of studies but their conductance decay was found to depend on others factors such as the conformational effects[38] or water-dependent switching.[39] The length dependent conductance of more simple molecules such as alkanedithiols was investigated thoroughly showing an exponential decrease of the conductance with the increase of the molecular length for short chains (up to 7-8 methylene units) and a much higher decay for longer molecules.[16,40,41]From the study of alkanedithiols a broad resonance in the transmission profile placed next to the Fermi level of the gold contact was noticed and described as a ''gateway state'' [42] (or contact level[16]). Previously Kim et al. noticed a similar phenomenon while studying a series of alkane-based molecular wires: a small peak close to the Fermi energy and a broad one about −1 eV from the Fermi energy. They showed that the resonances effect arising at these energies were due to molecular orbitals localized on sulfur contacts.[43] This peak was

also reported in the theoretical calculations of Hüser et al. for the case of thiol end-groups connected to a tip ending with one gold atom.[44]

It is often thought that in the relationship $\mathbf{G = Ae^{-\beta L}}$, the attenuation coefficient **β** is peculiar to the molecular backbone and the value of the electrode Fermi energy E_F with respect to the frontier orbital of the molecule measured, while at a given Fermi energy the prefactor **A** is only controlled by the coupling between contacts and electrodes. In fact, this is true only if the molecule considered has a large length **L** but it is not necessarily the case for some shorter molecules. As reported previously by Xie *et al*., studies on monolayers of series of oligophenyl dithiols and thiols (using a C-AFM) suggested that the coefficient **β** was a property not only of the backbone but also of the contacts, since different **β** values were obtained for monothiol and dithiol series.[45]

In this study a series of molecules containing a conjugate core and alkane chains of different length were studied in this work in order to observe the effects of the predicted resonances and to demonstrate that the contacts play a role not only for the prefactor **A** but also for the coefficient **β**.

2.1 Scope and previous work

The main aims of this work are to obtain a wider understanding of the conductance decay of series of molecular wires of increasing length and to investigate the factors contributing to the value of **β**. Specifically, we have studied both experimentally and theoretically the length-dependent conductance of a series of molecular wires based on a conjugated central unit connected on either side to alkane chains of varying length with thiol contacts.

The work described here is the culmination of a wider study that has been carried out over almost 6 years and It has involved the collaboration of people from different backgrounds: organic chemists, electrochemists and physicists. The present project has enabled the publication of the overall results in 2017. My contribution consisted in the synthesis of the molecular wires with thioethers contacts and the measurements of their conductance profile with the STM-I(s) and STM-BJ (described

in this chapter) in order to demonstrate the existence of the ''gateway states'' by suppressing their effects.

Our research group previously synthesised a series of molecular wires with various conjugated central units (viologen, phenyl or terthiophene) as shown in Figure 2.1 sandwiched between thiol-terminated alkane chains of increasing length and measured their conductance with STM-based techniques. Although in each series only the alkane chain length changes, it was found that the nature of the central unit had a strong effect on the conductance decay. The molecular wires in this study can be regarded as consisting of two barriers of variable length (the alkane chains) and a central conjugated core that forms a notch in the energy profile favouring the conductance across the nanojunction.[46–48] The focus of this work is on the influence of the combined effect of the barriers and the notch on the conductance value and on the attenuation factors **β**.

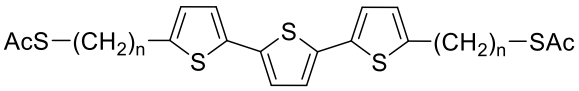

X[T3]X

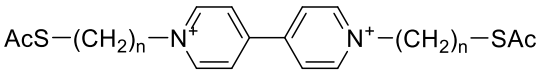

X[V]X

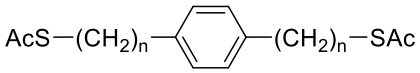

X[Ph]X

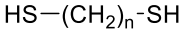

ADT

Figure 2.1 *Structures and labelling of the molecular wires of this study, X indicates the varying sidechain length (nCH2) while the central unit is abbreviated between brackets. The values of n and X ranged between 1 and 6. The counter ion for X[V]X was* $2PF_6^-$.

The series of molecules showed in Figure 2.1 were chosen to have a wide range of aromaticity ranging from the viologen salts, electron withdrawing and poorly

conjugated, to the electron rich and well-conjugated α-tertiophenes.. As previously mentioned, the molecular wires possess a conjugated core, alkane chains of variable length (1 to 6 CH_2 atoms) at opposite sides of the core, terminated with sulfur-based contacts. Those molecular wires are not fully conjugated and for this reason the conductance measurements were performed using the STM-I(s) technique. The measurements have been carried out on single molecules using a sub monolayer of the wires on a gold surface as substrate and a gold tip.

Each series of molecules has been analysed and the most probable conductance values were plotted as natural logarithm of the conductance (ln(G)) vs. length (as expressed both in terms of distance in Ångstrom and as a function of the number of CH_2 units in each alkyl chain). The β' attenuation was then obtained from a linear fitting of all the conductance points for each series as shown in Figure . The standard deviation was used as error.

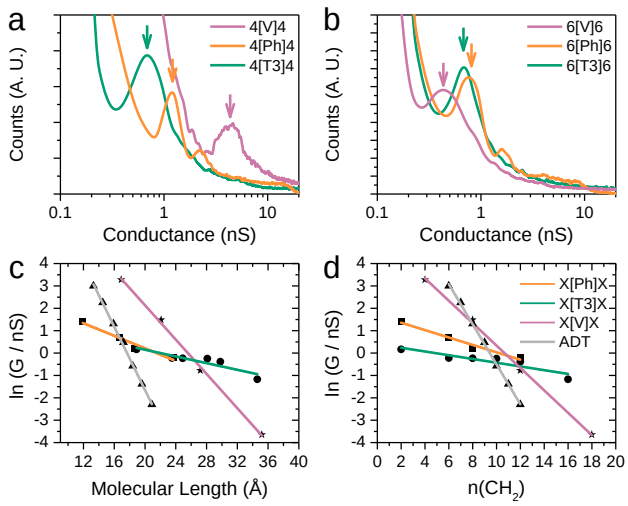

Figure 2.2 *Comparison of conductance histograms for (a) 4[X]4 and (b) 6[X]6. ln(G) vs. length plots and linear fitting of measured data with (c) molecular length expressed in Å and (d) in total number of methylene units in the sidechains. Molecular length is calculated as distance between two gold atoms tethered to the sulfur ends of the molecules in their lowest energy (all trans) conformation, using Wavefun Spartan® '14. All data was recorded at 300 mV tip–substrate bias. Reproduced from Ref.* [49] *with permission from the Royal Society of Chemistry.*

The data for the four series of molecules was calculated for the terthiophene and viologen while the data for the phenyl and the ADT wires was obtained from the literature values[42].

The analysis showed the lowest conductance decay for the α-terthiophene series with **β** = 0.06 ± 0.01 $Å^{-1}$ (0.07 ± 0.01 per total methylene unit) followed by the phenyl series with **β** = 0.14 ± 0.02 $Å^{-1}$ (or 0.17 ± 0.03 per total methylene unit) and by the viologen with **β** = 0.39 ± 0.01 $Å^{-1}$ (or 0.52 ± 0.01 per total methylene unit). The ADT series showed the highest **β** = 0.84 ± 0.01 $Å^{-1}$.

In the present study, for clarity the coefficient **β** should be considered as **β'** since instead of having a series of repetitive structures (as the previous oligophenylene dithiols) we will maintain the central unit of the molecular wire (benzene ring, terthiophene, viologen) and only the alkane part will be variated.

The experimental results have been confirmed by some density functional theory – non-equilibrium Green's function (DFT-NEGF) theoretical calculations to predict the charge transport across the nanojunctions. In addition the optimal geometry was calculated using SIESTA implementation of density functional theory and the GOLLUM code gave an approximation of the conductance value at room temperature to better match the experimental condition used for the conductance measurements.[49–51]The DFT predictions usually underestimate the conductance G of the molecule; in this work the values of conductance G are presented over a range of E_F with a value of $E_F = 0$

In Figure 2.3 are presented the calculations for the four series of molecules: ADTX, X[T3]X, X[Ph]X, X[V]X. The X stands in case of the ADTX for the number of methylene groups in total, while for the other three stands for the number of methylene groups on each side of the core. As shown in Figure 2.3**a,** the calculations predict in the ADTX series two resonances or interference effects, respectively termed Gs and Cs, that are gateway states and coupling states respectively. The resonance at around -1 eV in the HOMO-LUMO gap was previously identified as a Au-S or gateway state in theoretical studies. [16,44,52] The second resonance at the Fermi level (Cs) is much sharper and according to our calculation is due to the interplay between the two gateway states located one at each end of the molecular wire. As shown in Figure(**b**, **c**, **d**) the coupling states are more prominent in the calculations and this is because of the positive interference of the conjugated core. It is also evident that the series of molecular wires having a more conjugated core (α-terthiophene) possesses a

much higher Cs than the others and accordingly the ADTX series shows a very moderate Cs. Finally, in Figure 2.3 **e** and **f** are reported the local density of states plots calculated for the 6[Ph]6 wire showing respectively the coupling states at -0.15 eV and the gateway states at -1.11 eV in the nanojunction.

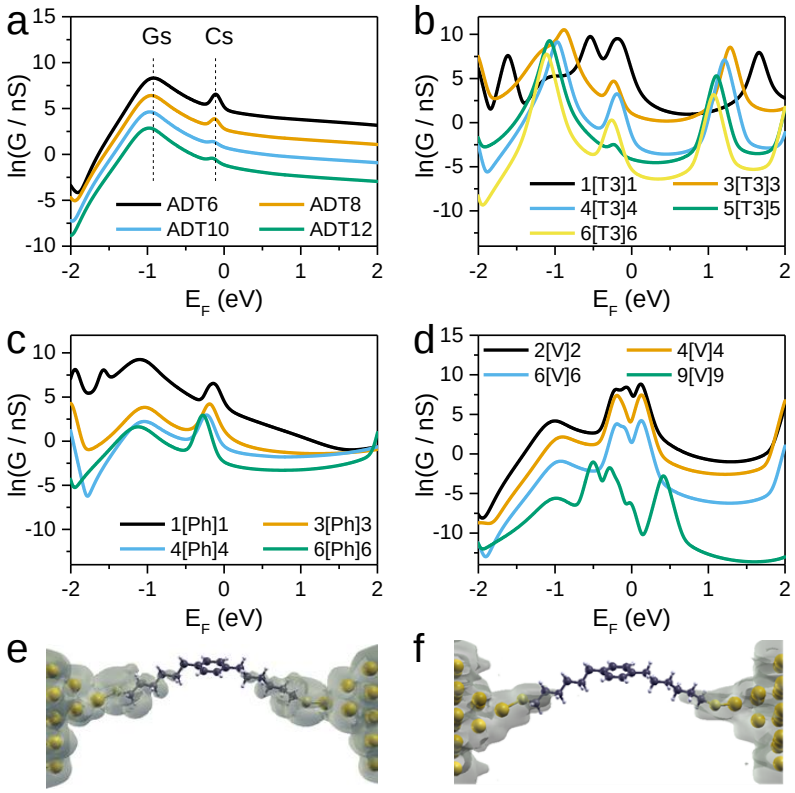

Figure 2.3 *Conductance calculations at room temperature of (a) ADT, (b) X[T3]X, (c) X[Ph]X, and (d) X[V]X vs. Fermi energy for alkyl chains with different numbers of CH2 groups. EF = 0 corresponds to the DFT-predicted Fermi energy, Gs and Cs stand for Gateway and Couplings states. LDOS at −0.15 eV (e) showing Cs, and at −1.11 eV (f) showing Gs for 6[Ph]6. Reproduced from Ref.* [49] *with permission from the Royal Society of Chemistry*

The experimental results obtained were compared with the theoretical calculation for the same series of molecular wires obtained from the DFT-predicted Fermi energy. As shown in Figure the attenuation factor **β'** experimentally obtained reflected well the calculated values for each series of wires.

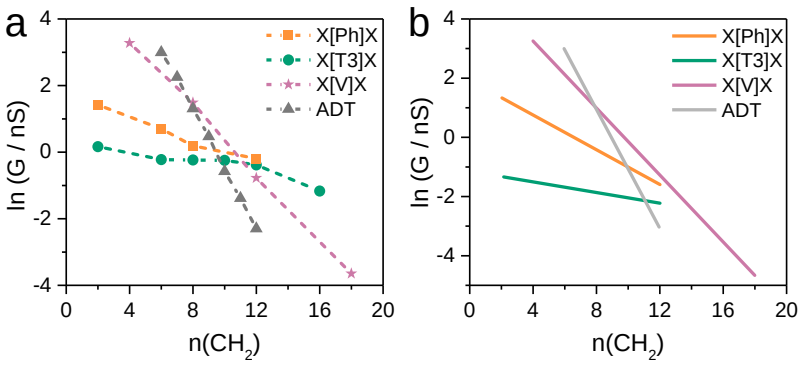

Figure 2.4 *Comparison of experimental (a) and calculated (b) natural logarithm of conductance versus the number of methylene units in the side chains for the four series of molecular wires considered in this study. Reproduced from Ref.* [49] *with permission from the Royal Society of Chemistry*

In addition, from the plots of the conductance values against the length of the alkane chains it is clear that the attenuation factors **β'** for the three molecules with the conjugated cores are much lower than the ADT series. This is happening because of the influence of the gateway states and coupling states that is stronger in the X[Ph]X and X[T3]X series due to the higher level of conjugation and still present although less pronounced in the X[V]X series that possess a slightly higher β' value.

Table 2.1: comparison of the attenuation factors **β'** expressed in methylene units

Series of molecular wires	Theoretical **β'**	Experimental **β'**
X[T3]X	0.086	0.07 ± 0.02
X[Ph]X	0.20	0.17 ± 0.02
X[V]X	0.56	0.52 ± 0.02
ADT	0.93	0.66 / 0.76

As shown in Table 2.1 the exact values calculated did not differ very much from the experimental data showing that the contributions of the Au-S contacts can in fact influence the attenuation factor β and not only the pre-exponential factor **A.**

In this thesis the first series of molecular wires (with thiols as contact group) was synthesized, and conductance measurements were carried out using the STM-based

I(s) technique, by other researchers (Andrea Vezzoli, Carly Brooke,[42] Harry M. O'Brien, Laurent Bouffier). All the theoretical calculations were carried out at the University of Lancaster by Colin Lambert's group (Sara Sangtarash, Hatef Sadeghi and Iain Grace).

In this thesis are reported the synthesis of a new series of molecular wires having methyl thioethers as contact groups and their conductance measurements using the STM I(s) and STM-BJ techniques to prove the existence of the gateway states in these DBT molecular wires.

2.2 Methods

The molecular wires used in this study (1[Ph]1-SMe, 3[Ph]3-SMe, 4[Ph]4-SMe, 5[Ph]5-SMe, 6[Ph]6-SMe), excluding the other series of molecule above mentioned that were prepared and measured previously, were synthesised, purified and characterised using common synthetic laboratory techniques (see chapter5 for more information on the syntheses). The conductance measurements of these molecules were carried out using the STM-I(s) technique for all the molecules and the 1[Ph]1-SMe wire was also measured with the STM-BJ technique to validate the values obtained using a different method and to check the accuracy of one of the measurements. The experiment was carried out using a freshly cut Au tip (from Goodfellows Cambridge Ltd) and a 1 x 1 cm Au-on-glass slide (Arrandee GmbH). The I(s) technique was performed to observe single molecules junctions and measure their conductance; the technique was previously described in the introduction; the following experimental conditions were applied here.

The samples for STM-I(s) analysis were prepared by immersion of a flame-annealed gold slide in a dilute (10^{-4} M) solution of the molecular wire (in CH_2Cl_2) for 90 seconds, to obtain a sub-monolayer coverage. The slide was then washed thoroughly with ethanol and dried with inert gas before being connected to the STM sample holder. The STM tip was then approached until a setpoint current was established, and then

the I(s) method described previously was used to obtain molecular conductance data.

For a more detailed description of the STM I(s) technique please go to Chapter 6.

2.3 Results

To demonstrate in an alternative way that these resonances effects due to the interplay between gold and thiol contacts really exist and play a crucial role for the factor **β'** an additional experiment was designed. A series of molecular wires (X[Ph]X-SMe) with a phenyl ring as central core, alkane chains and methyl sulfide as contacts was synthesized in order to test the existence of these gateway states and coupling states, by suppressing them. The methyl sulfide contact group as previously mentioned differs from the thiol group in the way it interacts with the gold electrodes; the thiol group binds covalently to the gold electrode while the methyl sulphide group binds only though the S lone pair with a weaker coordinative bond. According to calculations the coordinative bond between gold and sulphur should avoid the formation of the gateway states giving significantly higher values of **β'**.

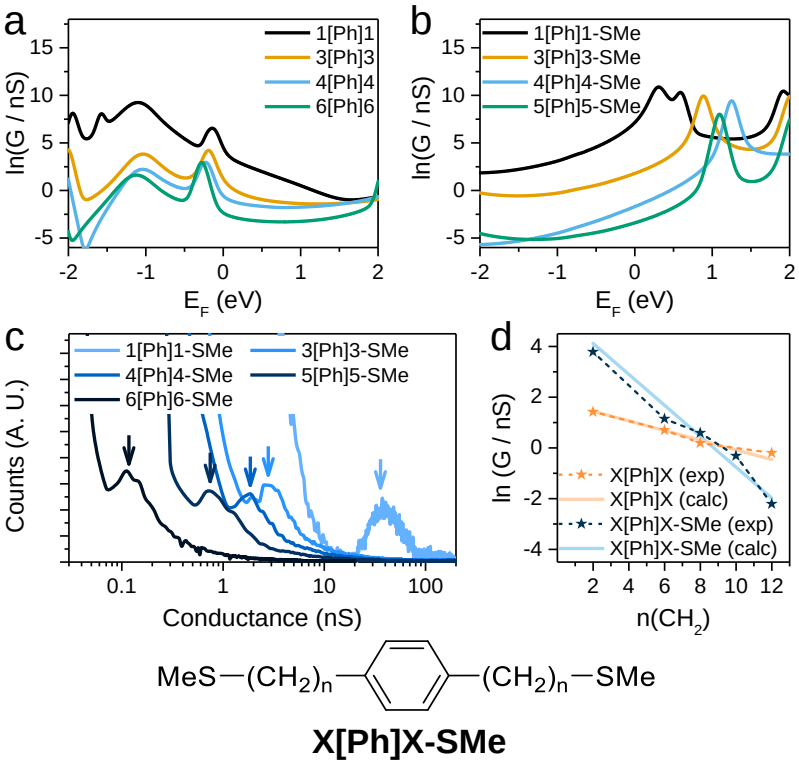

Figure 2.5 *Calculated DFT conductance of (a) Au-X[Ph]X-Au and (b) Au-X[Ph]XSMe-Au at room temperature. (c) Experimental X[Ph]X-SMe conductance histograms. Data is displayed on a logarithmic scale, bin size 0.01 nS. Histograms are normalised to the total number of I(z) scans selected (607 for 1[Ph]1-SMe, 656 for 3[Ph]3-SMe, 501 for 4[Ph]4-SMe, 566 for 5[Ph]5-SMe and 513 for 6[Ph]6-SMe). (d) Experimental and calculated conductance for X[Ph]X (orange) and X[Ph]X-SMe (blue) vs. number of CH2 units. Below is added the structure of the new series of wires X[Ph]X-SMe. Reproduced from Ref.* [49] *with permission from the Royal Society of Chemistry*

As shown in Figure 2.5 the comparison between the DFT calculations for the phenyl-based series with thiol contacts and thioether contacts have clearly different behaviours. The new series (Figure 2.5 b) does not possess the sharp interference at -1 and at 0 E_F typical of the gateway states and couplings states previously mentioned and its profile is completely different. The conductance measurements of the series X[Ph]X-SMe are displayed in Figure 2.5 c and the trend of conductance values observed match very well the theoretical findings. The plot in Figure 2.5 d shows the interpolation of conductance measurements and the behaviour predicted from the DFT calculations. It is certainly clear that the two series of molecules possess different slopes both in the experimental and theoretical data confirming that the experimental data for the conductance of the new wires (X[Ph]X-SMe) lies very near to the predicted behaviour demonstrating both theoretically and experimentally that the attenuation factor **β'** is actually influenced by the contact groups. The **β'** for the series X[Ph]X-SMe is 0.56 ± 0.05 per methylene unit which is more than two times the attenuation of the previously measured X[Ph]X series (**β'** = 0.20 per methylene unit). This series of molecular wires was measured using the STM-I(s) technique but since the wire 1[Ph]1-SMe showed a very high conductance it was possible to conduct additional measurements with the STM-BJ technique to compare the two methods. The two techniques (Figure 2.6) confirmed the same conductance of 44 nS for this molecule.

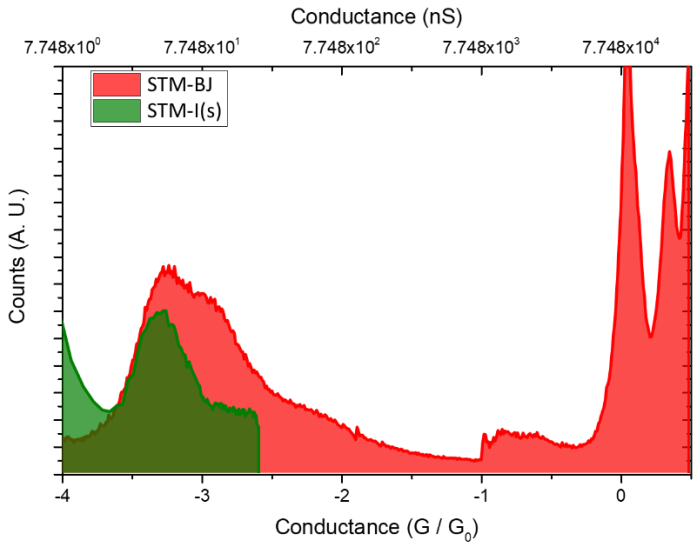

Figure 2.6 *Comparison between conductance histogram compiled with unselected STM-BJ (red) and STM-I(s) (green) data. Both techniques gave the same conductance value, 44 nS (5.6 ×10^{-4} G_0)*

Figure 2.6 shows the superposition of the I(s) technique and the BJ. From the figure it is clear that the molecular peak at *5.6 ×10^{-4} G_0* (or 44 nS) is the same. The two histograms look slightly different to each other because of the technique used: the I(s) technique the analysis window is much narrower than the one recorded with the BJ technique. In addition, the BJ technique possess some typical sharp peaks at the beginning of the histogram that represent multiple quantum of conductance (i.e. contact with 1 gold atom at G_0, and multiple gold atoms thereafter). Similar peaks cannot be shown with the I(s) simply because this technique does not contact the gold surface and the traces are focused in a smaller area of conductance.

2.4 Conclusion

In conclusion, in this first project the main goal was to give a better understanding on the electron transport through double tunnelling barrier molecules, and to understand the effect of the contact groups on the conductance decay β. It was found that the latter is profoundly affected by the presence of interferences effects (Couplings states and Gateway states), located at the Au-S interface. This explains why the conductance of the molecular wires analysed in this study, alkane chains with a conjugated core, showed an attenuation factor much lower when compared with simple alkane wires of the same length. The series of wires with a phenyl core

(X[Ph]X) showed in fact a β′ = 0.20 (per metilene unit) or 0.18 $Å^{-1}$ that is much lower that the attenuation factor of the alkanedithiols (β = 0.9 (per metilene unit) or 0.9 $Å^{-1}$).

Theoretical DFT supported the effect of these interfacial interferences, and a "smoking gun" control experiment was designed to unambiguously confirm it, by using non-covalent contacts to the electrode which are designed to suppress the interference features. The theoretical calculations predicted that the series of wires with methylthioether contacts would possess an attenuation factor much higher than the molecule with thiol contacts. This was experimentally confirmed by the X[Ph]X-SMe series with an attenuation factor much higher: β′ = 0.50 $Å^{-1}$.

The outcome of this large collaborative effort led to a publication in Nanoscale at beginning of 2018.[49]

Chapter 3: Testing quantum interference effects in 4H-cyclopenta[2,1-b:3,4-b']dithiophene-based molecular wires

3.1 Introduction and aim of the project

The understanding of the electron transport in a nanojunction is a fundamental step for the advancement of molecular electronics. In order to investigate interferences effects arising from functional groups outside the conduction pathway, two series of bridged bithiophenes have been synthesized and studied using the STM Break Junction technique. In our case we decided to introduce some different moieties or functional groups orthogonal to the conductance pathway in order to test how these affect the behaviour of a molecular wire. In this study we worked on the synthesis and the analysis of the electrical properties of molecular wires based on series of 4H-cyclopenta[2,1-b:3,4-b']dithiophene with methylthioether contacts in position 2,6. We introduced in each molecule different bridges in position 4 in order to tune and modify the conductance of the wires (Figure 3.1).

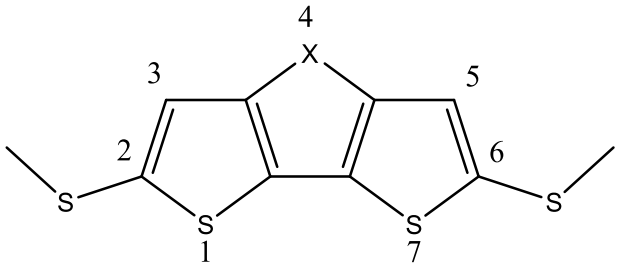

X = $SiPh_2$, $GePh_2$, CPh_2, CO, COCO, CMe_2

Figure 3.1 *General structure of the wires of this study the numbers are added to clarify the position of the contacts*

In this work we decided to study these modified bithiophenes because of the feasibility of the syntheses: bithiophenes have a well-known reactivity and a small band-gap, some positions are more reactive than others due to charge delocalization and this feature was perfect for reaching our bridged target molecules. In addition, thiophene-based molecular wires have been previously synthesised and effectively used in single molecule conductance thanks to their strong conjugation. In addition terthiophene-based wires[49], some bithiophene-based wires[53] and other oligothiophene-based wires[54,55] have also been reported, and this provides some points of comparison for our study of functionalised fused bithiophenes.

In this work two parallel series of molecules have been studied in order to investigate the possibility of quantum interference from functionalities orthogonal to the conduction pathway using two different approaches both backed with transmission studies and DFT calculations carried out by our collaborators at Lancaster University (Mohsin Al-Khaykanee, Khalid Ali Ismael and Colin Lambert performed the DFT calculations).

The electrons involved in the charge transport in a nanojunction prefer to be transported through a conjugated path. The first project involved variation of the heteroatom bridge X (Figure 3.2). The addition of three different atoms would create three different degree of strain in the planar base of the wires and potentially increase or decrease the conductance profile. Another factor that must be considered is the different inductive effects created by different bridge atoms that could affect the wire properties and thus their conductance.

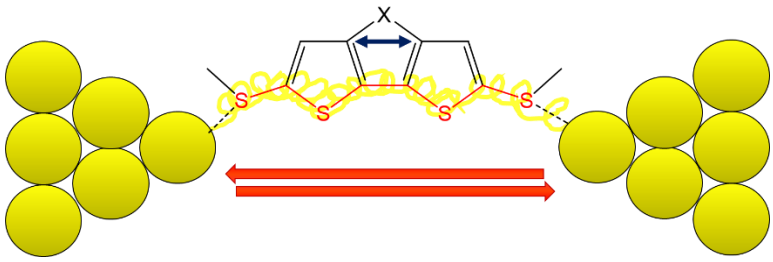

Figure 3.2 *Bithiophene-base molecule in the nanojunction (X = $SiPh_2$, $GePh_2$, CPh_2, CO, COCO, CMe_2), in yellow there is an idea of the hypotheszed primary conductance pathway.*

In the second group of molecules, 'X' consisted of oligocarbonyl groups in order to investigate the interferences effects induced by one or more carbonyls orthogonal to the conductance path (Figure 3.2). Transport calculations suggested that one (or more) carbonyls in a bridged bithiophene could induce a strong interference effect owing to the presence of cross-conjugation. Theoretical calculations predicted a number of Fano resonances equal to the number of carbonyl present in the wire. The introduction of a Fano resonance in this type of molecule is predicted to be very likely near the E_F and this would translate into a direct boost or decrease of the transmission curve of the wire and thus in a modification of the electronic behaviour of the wire. In this series a molecular wire without carbonyl was also synthesized as

control experiment to better understand the effects in play. A similar project was developed also by Andrea Vezzoli in our group and executed in parallel with bridged bipyridines.[56] He observed some interferences and that in addition with the strong theoretical calculations increased the interest to this study.

These projects have been studied in parallel and led to different outcomes. Both the projects were experimentally challenging firstly from the synthetic point of view and secondly in terms of the conductance study. Due to some experimental difficulties encountered, see results section, a more limited study was executed on the first project while in the second project (carbonyl interferences in bithiophenes) due to a better resolution of the data in the STM measurements a more profound study was done using additional STM-based techniques to reach a higher understanding of the behaviour of these molecular wires in a Au nanojunction.

3.2.1 Heteroatoms bridges in planar bithiophenes-based molecular wires

Initially the ideal molecules for this study were three: a bithiophene bridged with $SiPh_2$, $GePh_2$ and CPh_2 (Figure 3.3). The choice of these heteroatoms was due to the fact that all these molecules possess different sizes that might affect the strain of the molecule; another factor was the ready availability of the starting materials used for the synthesis and finally, the fact that related molecules have been synthesised previously by other groups[57–59] giving the syntheses a good chance of success. The synthesis of the first two is described in the synthetic section and it involves a three-step synthesis from the commercially available bithiophene. The synthesis of similar molecules (without the MeS contact groups) was previously reported[60] and an adaptation of the synthetic pathway was successful for the synthesis of the third molecular wire for this project. A detailed description of the synthesis can be found in Chapter 5. In this case the last three steps of the synthesis were carried out in collaboration with a Year 3 student (Emma Jones) during her bachelor project in 2017.

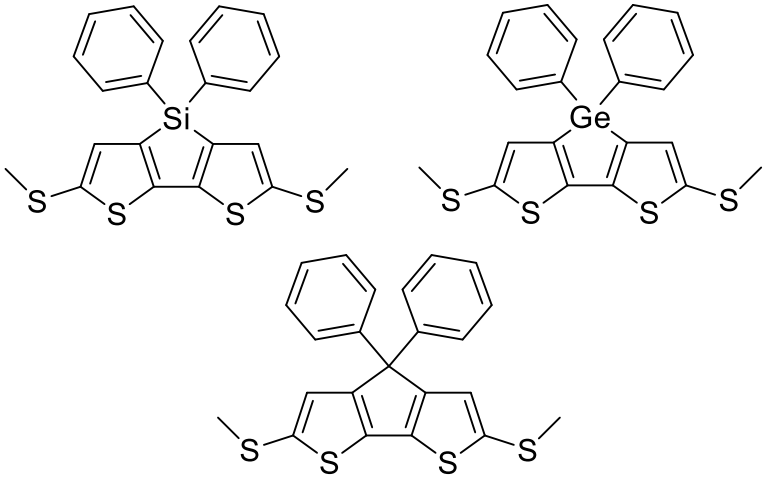

Figure 3.3 *The series of bithiophene-bridged molecular wires used in this study*

3.2.2 Measurements and results

The measurements of the three wires have been performed with the STM-BJ technique (check Chapter 6 for a detailed description of the method).

Interestingly, all these molecules produced noisy histograms in which peaks were difficult to spot due to the high noise level or inefficient junction formation, or some combination of these factors. Conductance measurements were tried using a range of conditions to find the optimum for obtaining better-defined peaks in the histograms. We varied the concentration of the solution used in the measurements and the solvent system employed, but little effect was found in either case; the measurements were still very noisy, and it was impossible to determine a reliable conductance value. These factors were varied to determine if aggregation or π-stacking of the molecular wires might be responsible for the broad ill-defined histograms. Additionally, other researchers in the group obtained similar results with these molecules.

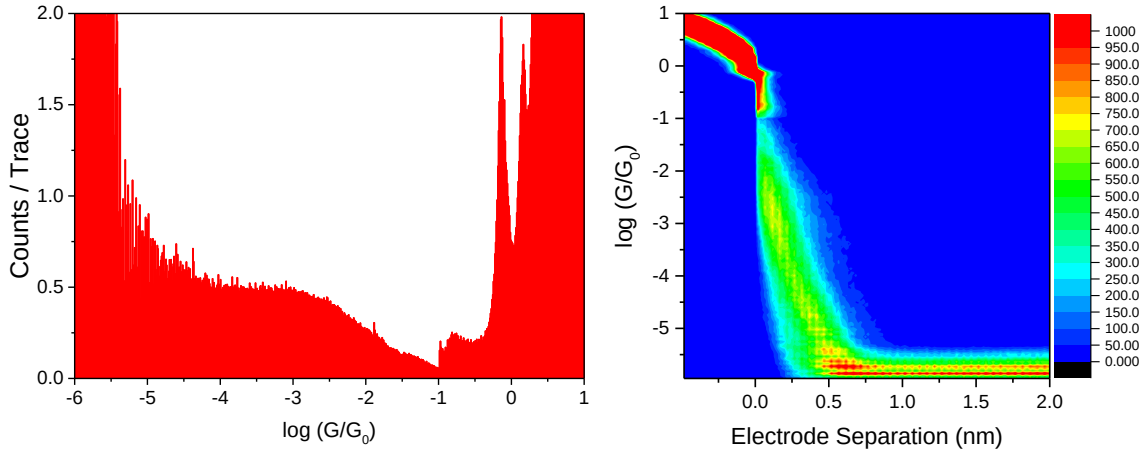

Figure 3.4 *Histogram and 2D plot of a measurement of the* ***TGePh$_2$T*** *wire with evidence of high noise level and low hit probability. A shoulder that might be an indication of the molecular conductance peak is evident at around 10^{-3} G_0. The measurement was performed with bias 100mV, and using 1mM solution of the wire in mesytilene.*

In Figure 3.4 is shown a histogram and the 2D plot for a measurement of the wire TGePh$_2$T in mesitylene at 100 mV (concentration 1mM in mesytilene). From the image, we can rule out contamination of the gold surface since in this case a G_0 peak is clearly visible; in addition is also visible $2G_0$. If the Au-Au junction is clean, so should be the nanojunction with the molecule. This result indicates that the issue is a very low hit rate of the wire. At around 10^{-3} G_0 in the conductance histogram, it is possible to make out a broad peak. The hit rate shown on the left corresponding to this peak is very low when compared with more conventional measurements (here the peak is around 0.5 counts/traces while more commonly, the value would be about 4 times higher) and in addition, it is also partially obscured by the noise level. This last part might influence the value of the conductance, for this reason new ways of reducing the noise or obtaining a higher ratio should be tried.

An alternative that turned out to be a better solution, was to create a sub monolayer of the wire on the gold surface (as in the typical STM-I(s) sample preparation) and to perform the STM-BJ measurements on the substrate in air, without any solvent. This method provided more acceptable histograms of the molecular wires as shown in Figure 3.5. The histograms clearly show a peak around $10^{-2.7}$ G_0 for both the molecules and possibly a second one near 10^{-5} G_0 that is partially obscured by the noise level which could be a different type of nanojunction. The second hypothesis is

supported by the 2D plot on the right (Figure 3.5) that clearly shows the presence of an elongated junction or two kind of conductance values: a higher at $10^{-2.7}$ G_0 and a lower one at 10^{-5} G_0. This might be due to the presence of the secondary pathway or due to a different geometry involving other parts of the wire.

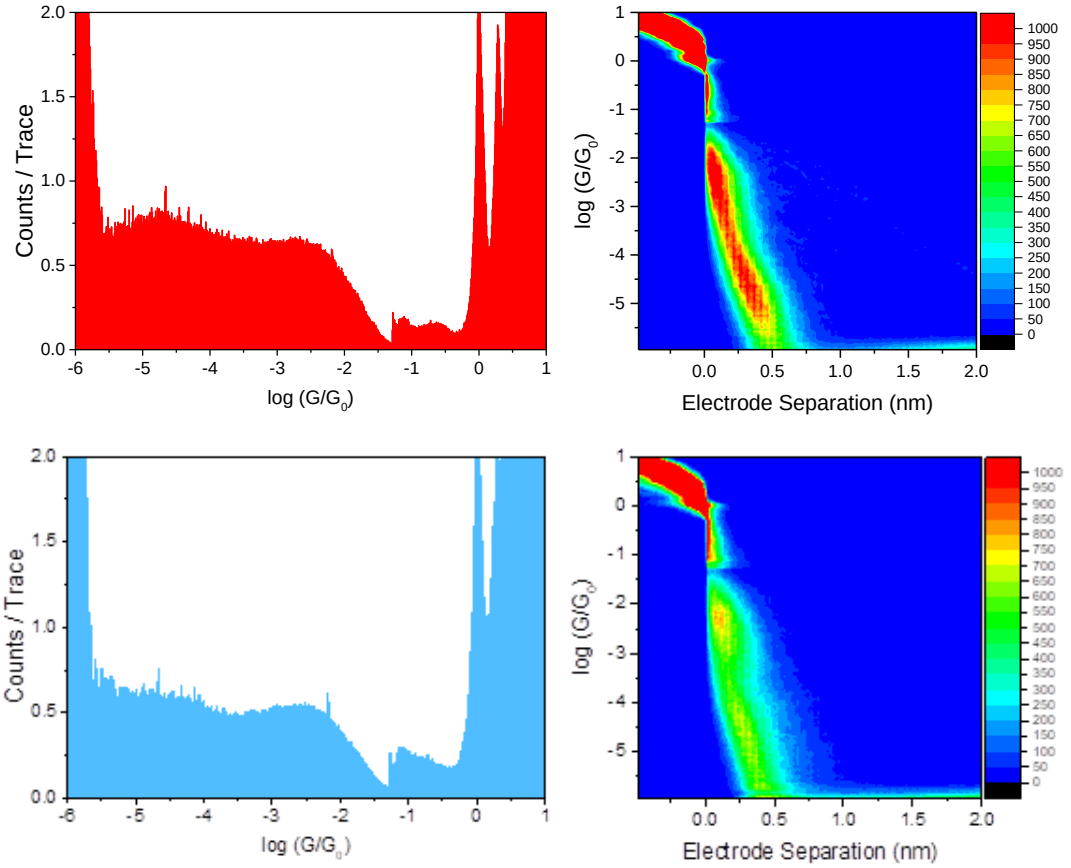

Figure 3.5 *At the top (in red) the measurement of the* ***TGePh$_2$T*** *wire in air at 200 mV and in the bottom (light blue)* ***TCPh$_2$T*** *in air at 200 mV.*

In the histograms shown above, once again the G_0 peak and (in the case of the germanium-based wire, also 2 G_0) is evident. This means that a clean substrate was present and that the relatively high noise level was not due to substrate contamination. In addition, both the 2D histograms suggest the presence of two different contributions, although the data is not perfectly clear. To clarify the situation, a manual selection of the single traces was performed to reach a better point of view on the understanding of the behaviour and the conductance values of these molecules.

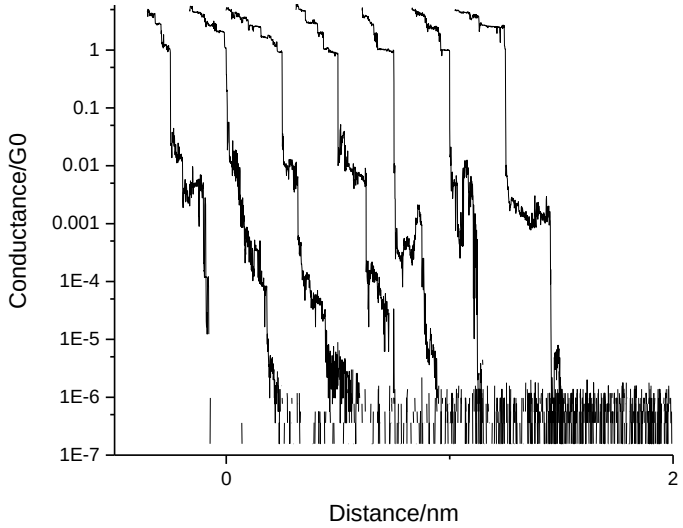

Figure 3.6 *Single traces of $TGePh_2T$; there is a lot of variability in the traces, some show a high and a low conductance while others just high conductance.*

In the usual data analysis for the STM-BJ measurements, all the recorded data is directly elaborated without selection of single traces, so a different approach was used (for a more detailed description please go to chapter 6). A short routine in Labview (software for data analysis) was developed in our group in order to manually select the single traces before the final elaboration. This gave more control over traces with high noise that could statistically hide single molecular junctions in case of low hit-rate. Since a full STM-BJ study contains on average around 5000 traces the manual selection was time consuming since every scan had to be handpicked in order to discard noisy traces and to collect typical nanojunction plateaux. So far a software able to autonomously select the data for this propose has not been created yet, despite some interesting attempts previously reported in the literature for different systems.[61]

Despite the unusual manual selection, the single trace study led to some interesting results: in Figure 3.6 are shown some examples of single traces for $TGePh_2T$. The most common trace was unusual and is so far unexplained, (the 2nd, 3rd and 4th traces in Figure 3.6). The 'plateaus' are unusually elongated with a decreasing conductance; since there is no defined step down in conductance, it could not be considered a

proper plateau but since the decay of conductance with distance is clearly slow, this indicates that there is some sort of interaction with the molecule. The second most common trace was the tunnelling decay without molecule or with some gas molecule trapped and no molecular junction formation (1st trace in Figure 3.6). About 10 % of the traces contained at least one clear plateau somewhere in the conductance decay. The data selection was made in order to save only the traces with a clear step or plateau; for this reason, the traces with the long decay were discarded as well as the traces without the wire. The sum of the single traces gave a much sharper peak with conductance comparable to the first low peak observed in the unselected data. The 2D plot confirmed the presence of a clear short junction (Figure 3.7) consistent with the data shown in the histogram.

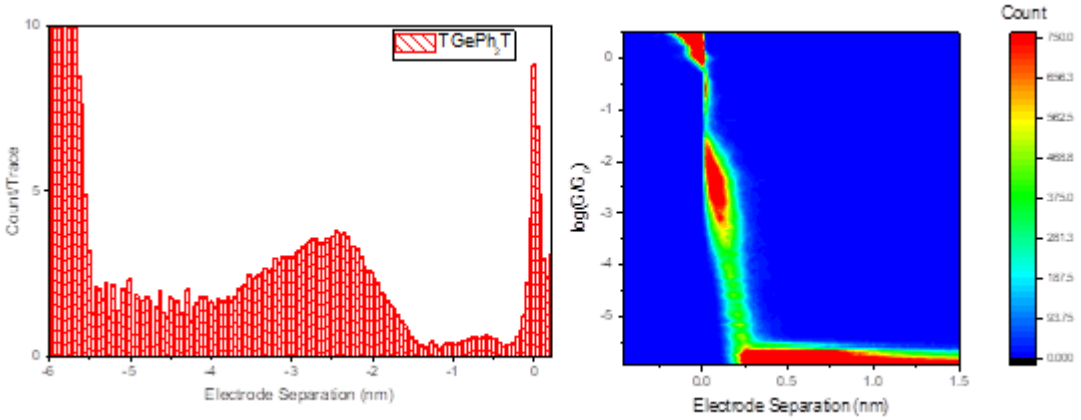

Figure 3.7 TGePh₂T *measurements at 200 mV after the data selection and the relative 2D plot*

During the data selection only, the traces containing a visible plateau (*ca*. 10 %) have been selected. Only a few contained a clear and relatively long molecular junction. Similar results were obtained with the other two molecular wires (only the data for the **TGePh₂T** are discussed in detail here as an example). An important detail was uncovered by studying the selected data: that the first broad peak seen in the unselected data is in fact a good representation of the conductance of the molecular wire since the conductance value recovered from the selected data is the same; the peak is just clearer. Similar results were observed with the **TCPh₂T** wire; the **TSiPh₂T** wire gave a slightly sharper peak but still quite noisy.

Considering these results, we decided to step back and to use the unselected data, even if noisy, to compare the conductance of the three molecules in order to keep all the information gathered with the measurements. In the data selection, a lot of elongated plateaux were deleted and not including most of the traces would not give an accurate statistical analysis of the conductance of the molecule. Figure 3.8 shows the comparison between the three molecular wires. There is a first conductance peak around 10^{-3} G_0 that was confirmed from the correspondent peak discovered in the selected histogram and a second one half hidden in the noise level around $10^{-4.75}$ G_0. What is clear is that the three molecular wires show very similar conductance values; for this reason, we can conclude that changing the bridge atom had little influence on the conductance of the molecule.

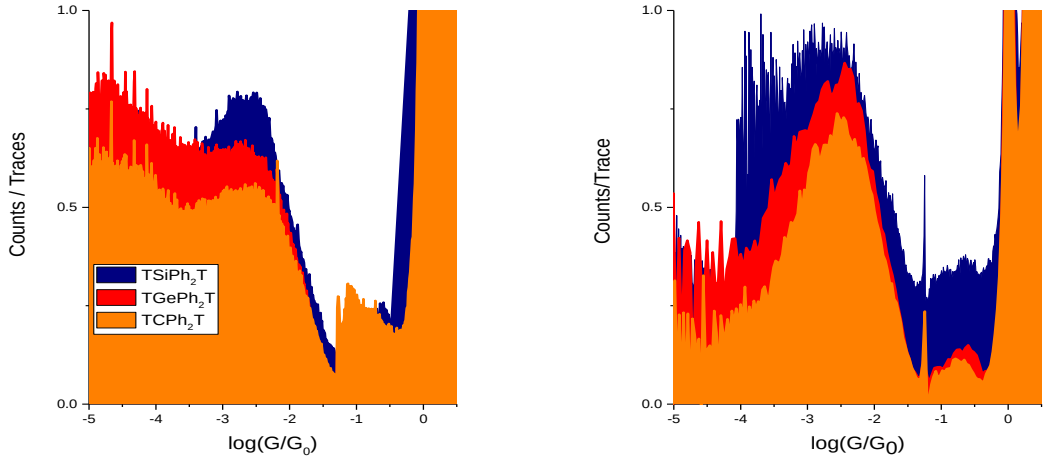

Figure 3.8 *Comparison of the conductance measurements of* ***TGePh₂T****,* ***TSiPh₂T*** *and* ***TCPh₂T*** *molecular wires, using the STM-BJ technique. On the left the non-selected histograms and on the right the histograms from the selected traces.*

The primary peak was most probably the result of the electron transport through the contact groups from one thioether end to the other thioether. This fact is in

accordance with the conductance of a similar wire: the dimethylthio-bithiophene. This simpler wire has only a main peak at $10^{-2.7}G_0$ and is very similar to the results

obtained. Since the conductance of the wires of this study is slightly lower than a simple dimethylthio-bithiophene this might imply that the bridges are influencing negatively the conductance by adding some negative quantum interference.

An additional but important observation is that the histograms also show a secondary peak near the noise level. A simple explanation for the reason behind this second peak could be that a different pathway through the molecule have been used to transport current. A benzene ring is usually not used as contact group but sometimes some organic compounds might conduct also through an aryl group.[56,62] A benzene ring might bind to the gold though the π system. The secondary peak for this reason seems to be due to the addition pathways provided by the two benzene rings in the molecule. The low conductance might be due to the weak binding of the benzene to the gold and also to the fact that it includes a non-conjugated pathway that is always less conductive than a conjugated one.

In summary, the primary peak is due to the electron transport between the two sulfur atoms and the secondary peak might be due to the transport from one sulfur to one benzene ring, and the high level of noise and the low count of nanojunction formation can be explained as result of a combination of the two mechanisms.

3.2.3 Calculations

As briefly explained above, the conductance through the target molecules have been studied with some calculations. Figure 3.9 reports the zero-temperature transmission coefficients T(E) of the three molecules used in this study.

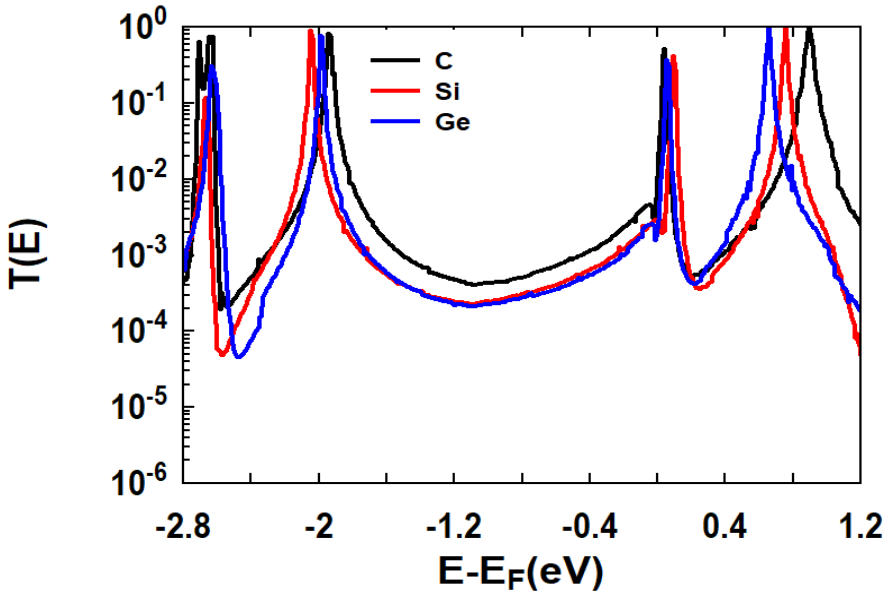

Figure 3.9 *Transmission curves for the three molecular wires of this study: the legend identifies the three wires by their bridge atom.*

From the transmission curves is it possible to estimate the behaviour of the molecules; in this case there are not many differences between the wires and both the silicon- and the germanium-bridged wires show similar profiles, while the other shows a slightly higher conductance. Generally, the area near $E_F = 0$ approximates the behaviour of the molecule during an STM measurement, and in this case the carbon bridge wire is therefore predicted to show a higher conductance, is it also true that the calculation is done at 0 K and the measurements are done at room temperature so there is room for discrepancy. The experimental results showed a very similar conductance profile for the three molecules including the conductance value; on the other hand, the peaks shown were very broad and noisy, taking in account these facts we can conclude that the theoretical results are within the range of the conductance measured.

Unfortunately, the effect of the bridge atoms did not interfere much with the conductance pathway but added to the molecule additional pathways (the two phenyl rings) for the charge transport. If the secondary peaks of the molecules are compared, there might be a change in conductance due to the presence of different heteroatoms but unfortunately due to the low conductance (merging with the noise level) the resolution of the second peaks is not possible.

In conclusion from this project a new series of molecules have been synthesised and measured, their structure-property relations have been investigated and even if the main goals of this study haven't been perfectly met, the theoretical calculations compared to the experimental data gave an overall good match.

3.3.1 Interferences effects in ketone-bridges planar 2,2'-bithiophenes-based molecular wires

The second project involved the study of the effects of exocyclic carbonyl groups in fused 2,2'-bithiophene-based molecular wires. A molecule with a simple CMe_2 bridge has also been prepared as a reference compound. According to theoretical calculations (run by our collaborators at Lancaster University) the quantum interference effects from C=O moieties should be stronger than the ones tested in the previous study and thus be more likely to have a visible effect on the conductance of the junctions. In addition, even if a carbonyl group is added not in the primary conductance pathway it might also change the electron density of the molecule resulting again in a more visible difference in conductance.

The syntheses of the three molecular wires were challenging and are described in detail in Chapter 5. The first compound, **TKT**, was most intensively studied; the second, **TDKT,** as explained in chapter 5 and 6 was more difficult to study and for this reason was examined in less detail. The last wire made was the reference molecule **$TCMe_2T$**; the structures of the molecular wires are shown in Figure 3.10.

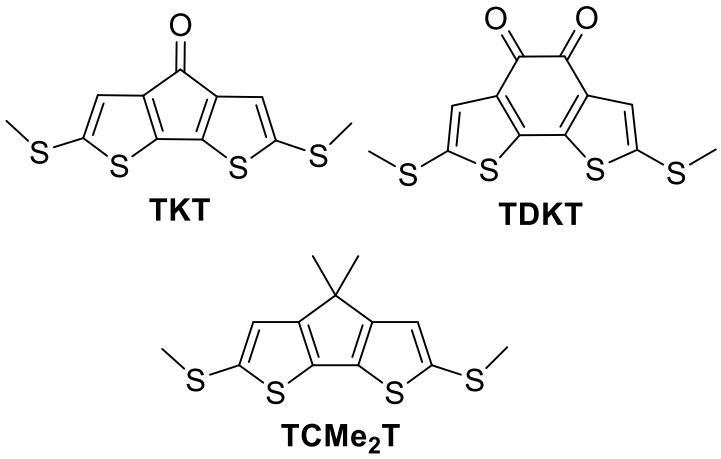

Figure 3.10 *Target molecular wires carbonyl bridged (**TKT** and **TDKT**) and the control wire without carbonyl (**TCMe$_2$T**)*

This molecule was chosen to provide a good reference experiment. This wire maintains the similar planar structure of the other two, possesses the same contact groups and the only difference is the bridge: it has a CMe_2 group instead of one or two carbonyl groups. At the beginning of the study a 2,2'-bithiophene bridged with an even simpler CH_2 group was the first choice but due to the acidity of the hydrogens the reactions were giving low yields and impure compounds. Compound **TCMe$_2$T** was synthesised without any problem, quickly, and with high purity.

The behaviour of the wires during the conductance measurements were much less noisy than those of the $–XPh_2$-bridged molecules (X = C, Ge, Si), and this led to a closer investigation of these molecules. For this project more detailed techniques have been used to obtain a greater understanding of the structure-property relations of these systems.

3.3.2 Initial theoretical calculations

According to some theoretical calculations the presence of one carbonyl as bridge of a bithiophene-based molecular wire creates a Fano resonance in the transmission profile. An additional carbonyl can provide an additional Fano resonance. The

position of these resonances according to the calculations sits between the HOMO and the LUMO and should be near the Fermi level of the molecule. Figure 3.11 shows the calculated transmission curves for the **TKT** and the reference wire **TCMe$_2$T**. To better investigate the Fano resonance effects the wire **TKT** was studied at different biases (voltage applied). Usually the study, of a wire at different bias can provide more information on the area around the Fermi energy of the electrodes. Any change in conductance (increment or decrement) might be considered as a direct result of the Fano resonance. The Fermi energy of the electrodes is calculated at 0 Kelvin and for this reason is usually an approximation since the measurements are executed at room temperature. Furthermore, the calculation on the wire **TDKT** predicts behaviour similar to the single carbonyl-wire: the presence of two carbonyls results in the addition of two separated Fano resonances in the transmission curve between the LUMO and HOMO of the wire. This wire has the second Fano resonance even closer to the Fermi energy of the electrodes making more probable the observation of interferences effects in the conductance profile of that wire.

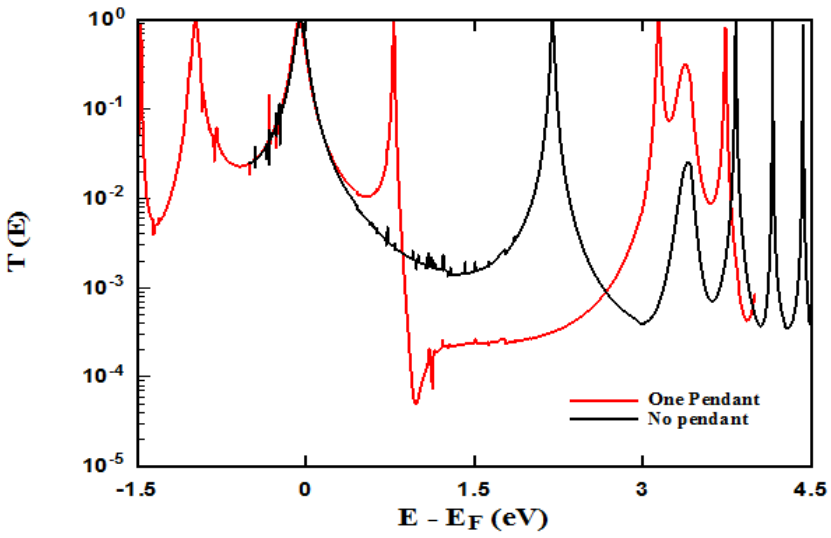

Figure 3.11 *Transmission curve for the **TKT** (one pendant (carbonyl moiety)) in red and **TCMe$_2$T** (no pendant) in black. The Fano resonances is the sharp resonance at 1.2 eV, the HOMO of the wire is around 0 eV and the LUMO is at 1.8 eV.*

Unfortunately, these theoretical calculations were wrongly calculated on a thiol-based series of molecular wires, these mistakes were discovered after the

experimental studies because of the non-matching results (that will be shortly presented); the recalculated transmission curves for these molecules are still under revision and will provide a better fit for the experiment data.

3.3.3 STM Measurements and results

The conductance of the three molecular wires was measured with the STM-BJ technique and their histograms showed clearly some different behaviour, as seen in Figure 3.12. As predicted, the **TCMe$_2$T** wire is slightly more conductive followed by the **TKT**, and by the **TDKT** that registered the lowest conductance of the series. In addition to the value of conductance also the shape of the peaks is slightly different; the three wires show relatively less noisy histograms if compared with the wires from the previous project resulting in higher counts/trace and cleaner peaks. The measurement of the **TKT** and **TCMe$_2$T** wires was performed without any problems but the **TDKT** wire due to its low solubility had to be measured several times before managing to obtain good data. The reason behind the difficulties encountered in the measurements of the **TDKT** apart from the low solubility are not fully clear so far. The main result arising from the comparison of the three wires is that they show clearly different conductance values with the following trend: **TCMe$_2$T > TKT > TDKT**. It is also important to notice that the peaks of the histograms are still quite broad.

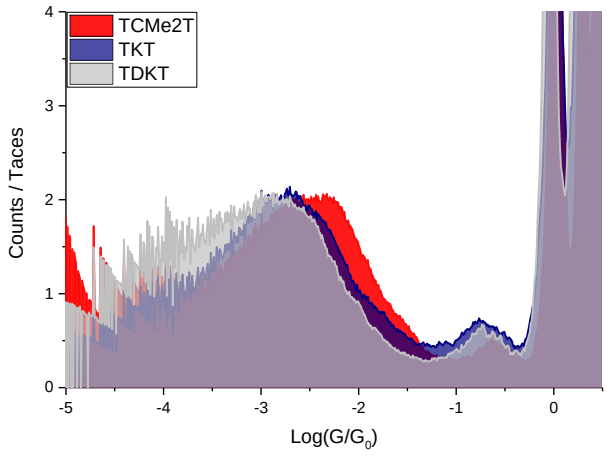

Figure 3.12 *Comparison of the STM-BJ measurements of the three wires of this study*

The reason for the difference in conductance can be attributed to some factors, the increasing electron-withdrawing effect of the bridges, and/or to the effects of the predicted Fano resonances near the Fermi level of the electrodes that interferes negatively with the conductance profile of the molecules with carbonyls. If the Fano resonances are the cause of the different values the conductance of the molecules at different bias should show a negative differential resistance effect (NDR) at a certain voltage. This means that the system with one or two carbonyls must show a consequent increase and a decrease in conductance at a certain bias range.

To better explain the cause of the wires' behaviour at different bias, I/V experiments were performed, and interesting results have been obtained.

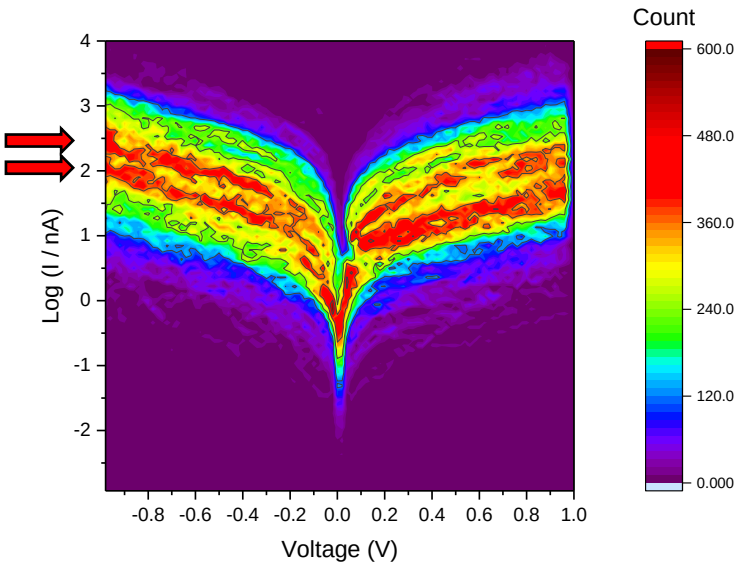

Figure 3.13 *I/V map of* ***TKT*** *between 1 and -1 V. In this image two conductance paths are visible (the two red trails from 2 and 2.5 at -1 V that go to 0 V and then back to 2 and 2.5 at 1 V)*

The I/V experiments were carried out with a STM-BJ set up and a slight modification of the method used: the tip was crashed and retracted as usual in a Break Junction experiment into a gold substrate with the wire. During the retraction the tip was withdrawn in subsequent steps, each of 1 Å (instead of linearly) and kept in position for 100 ms; during this time one I/V scan was performed (between -1 and +1 V in this case) for 90 ms and after this point another 1 Å retraction, and a new I/V scan, was

performed, and so on until junction breakdown. The statistical analysis of the traces was performed on only the traces containing a molecule trapped in the nanojunction during the whole I/V scan. This was evaluated by measuring the conductance of the molecule before and after the I/V in the 10 ms window (5 ms before and 5 after). From the I/V curves of the **TKT,** some interesting features arose from the histogram. As shown in Figure 3.13 the wire has been measured between -1 and +1 V. At high voltages (> 0.3 V and < -0.3 V) two major conductance trails are visible. In addition, the I/V presents values spread across two orders of magnitude (or even three orders of magnitude if the traces with lower count are included), while usual molecules do not show such a wide spread of data. The two trails observed suggested the presence of two conductance pathways or a bi-stability effect of the molecule where the wire possess two main conductance values. Unfortunately, the possible NDR effect cannot be confirmed from the results observed in the I/V measurements. In addition, the presence of the two trails of conductance was observed in both the molecules with and without the carbonyl demonstrating that the observed effect does not depend on the predicted Fano resonances and thus the carbonyl moieties.

Other molecules have been analysed with the I/V technique such as the simple 4,4'-bis(methylthio)-1,1'-biphenyl wire resulting in a much narrower I/V traces and only a single conductance is visible as shown in Figure 3.14.

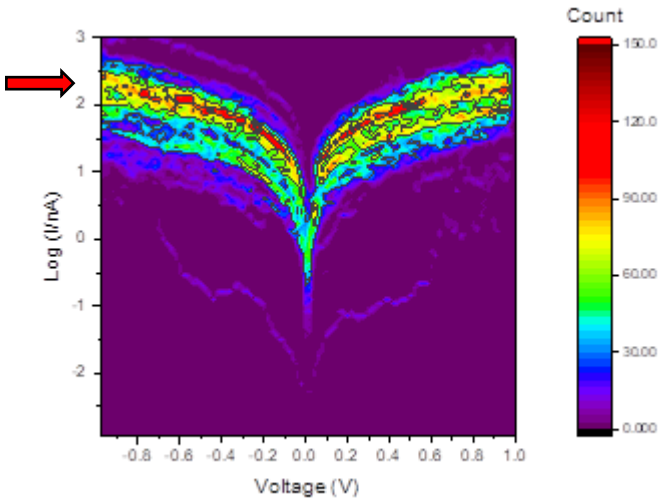

Figure 3.14 *I/V measurements of the 5,5'-bis(methylthio)-2,2'-bithiophene*

Some more investigation on these molecules was needed and for this reason some modulation tests were executed. A CLEAR explanation of this technique can be found in chapter 6. The presence of the bi-stability in the conductance profile of the molecules in the *I/V* curves, and also the large peaks observed in all their STM-BJ measurements, made us consider the fact that the behaviour of the molecules was not strictly connected to the presence of the carbonyl moieties but could be a feature of the backbone of the wires.

The modulation experiments consisted in a technique similar to the STM-BJ. The only difference is that mechanical stress is applied to the molecule during the retraction of the tip by pushing the tip up and down a few angstroms, thus squeezing and stretching the molecule throughout the experiment in order to stress the configuration of the wire with the electrodes. The wires were tested at different biases and using different modulations, all the measurements not shown in this chapter can be found in the appendix of this thesis.

The molecular wires responded very well to these tests, these experiments showed that all the molecular wires can be mechanically switched from a low conductance state to a high one when squeezed between the electrodes. This behaviour was observed in all the three wires and was more accentuated in the **TCMe$_2$T.**

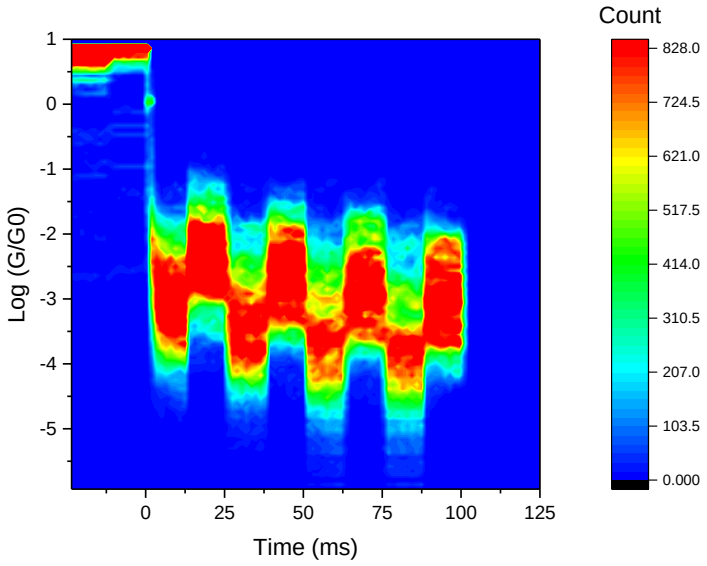

Figure 3.15 *Modulation experiment with* ***TMe$_2$T*** *at 200 mv and 3 Å of modulation (±1.5 Å)*

As shown in Figure 3.15 when a modulation of ± 1.5 Å was applied to **TCMe$_2$T** junctions, a big switch in conductance could be observed. This effect is a proper switch mechanism and a similar behaviour have been seen in molecular wires that possess more than two contacts or related special structural features.[56]

In our case the switch can only be explained if we consider the thiophene ring as a possible weak additional contact. According to this theory the switch is explicable as a simple jump from the thioether contact to the π-system of the thiophene and the consequent jump back. The existence of an additional pathway through the thiophene system can explain the very broad peak observed in the previously discussed STM-BJ measurements of the wires. The combination of the conductance of nanojunctions using both the contacts or a combination of them can result in an enlargement of the peaks and that was what experimentally was observed. In addition to this, although this effect is still under study some preliminary calculations from our theoretician collaborators confirmed this mechanism. A more detailed model will be defined in future to explain the experimental data collected from this study.

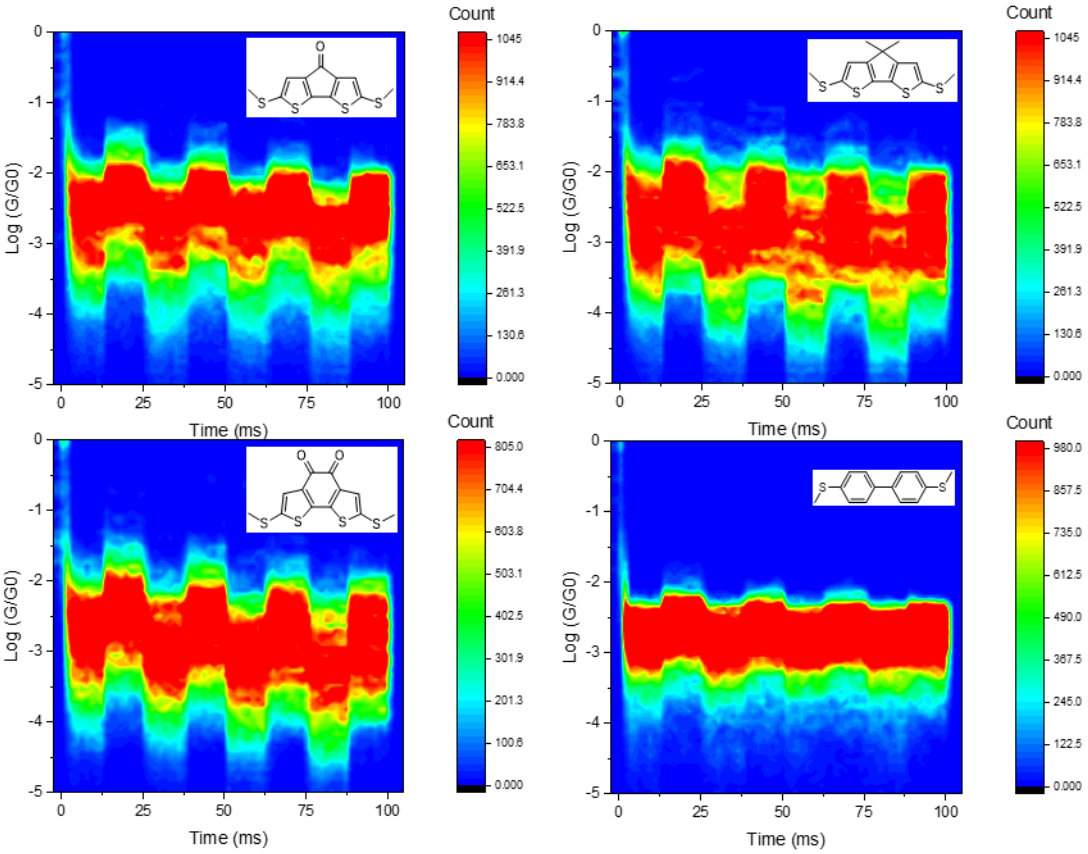

Figure 3.16 *Comparison of the three molecular wires of this study at 200 mV and 2Å of modulation.*

Figure 3.16 compares the modulation tests of the three molecular wires used in this study and an additional one as a control experiment. The wire used as control does not possess a bithiophene base but is a simple biphenyl-based wire; the shape and the structure are similar to the molecules used in this study and for this reason was chosen as control experiment. From the results it was clear that the switching feature was evident only in the bithiophene-based wires and not at all present in the biphenyl-based wire. In addition, the fact that the switching seemed stronger in the **TCMe$_2$T** and less intense in the other two led us to think that the electron withdrawing carbonyl moieties have a negative effect on this phenomenon while the electron-releasing –CMe$_2$ group positively influences this effect. The biphenyl-based wire did not significantly switch during the modulation tests; in order to better understand this phenomenon further molecules were examined to shed more light on the mechanics involved in these experiments.

A 3,3’-bithiophene without contact groups was studied in order to better address the role of the bithiophene as cause of the switching. This molecule was chosen because it is commercially available and because it has the right symmetry for contacting two opposite electrodes; 2,2’-bithiophene was incapable of forming junctions with sufficient hit rate and for this reason was not used.

A possible explanation was a change of contact groups between thioether and the sulfur atom of the thiophene, or the π system of the thiophene. The effect was not observed in the biphenyl-based wire, and the reason could have been the absence of the sulfur atom, or a system not conjugated enough, or a combination of the two effects. Another reason could have been the nature of these planar bithiophene systems. To investigate the involvement of the thiophene and to exclude the planar configuration from the list the 3,3’-bithiophene was measured. Surprisingly it showed a switching effect as well (Figure 3.18), but not as marked as the one observed with **TCMe$_2$T**. The last result showed some switching behaviour in a simple bithiophene molecule resulting in defining the bithiophene unit as primary cause of the switching effect. Even if these effects have been seen in the 3,3’-bithiophene the response to the modulation and the hit-rate were much lower when compared with the other wires **TCMe$_2$T**, **TKT** and **TDKT**. The results from the last tests can be explained by assessing the cause of the switching effect to the π system of bithiophenes, they can actually be used as contacts as well.

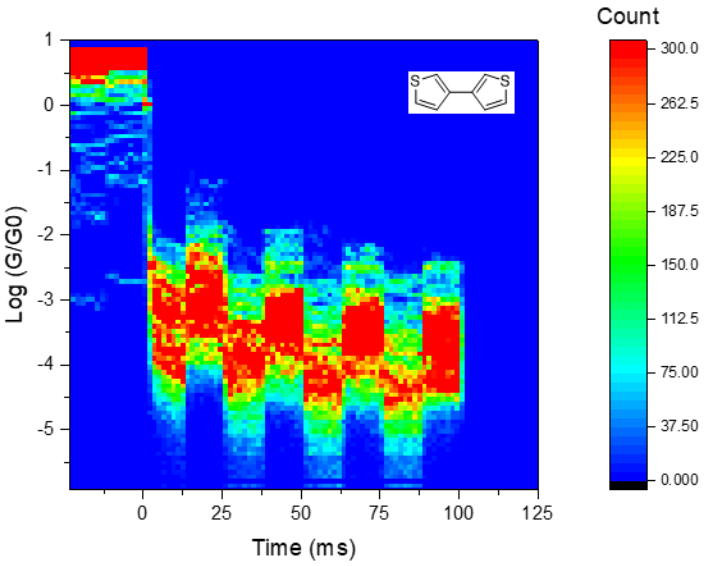

Figure 18 *Modulation test on 3,3'-bithiophene at 200 mV and 3 Å of modulation*

In addition, these results gave important information on the conductance of bithiophenes in a nanojunction. Previously, methylthioether-bithiophene wires were linked to broad peaks[55,63] and that was explained as effect of the 5-fold symmetry of the wire, with our study we demonstrated that the large peak is caused by the interplay between the thiophene π system and the electrodes.

This effect was confirmed from the study of the single traces and can also be addressed to the noise observed in the first part of this chapter on the phenyl-bridged bithiophene wires.

More studies are still ongoing on the strong modulation effect observed with the **TCMe$_2$T** wire in order to better define and put to use its strong switching effect. This molecule showed unprecedented response to junction modulation, and for this reason its uses in molecular electronics could be multiple.

Conclusion

In conclusion this chapter focused on the study of 2,2'-bithiophene-based molecular wires, by synthesising innovative wires and by studying their electrical properties with different techniques. The two studies provided very important clues and shed some light on the behaviour of bithiophenes in a molecular junction. In the first project the presence of the diphenyl groups was strongly interfering with the charge transport by adding extra contacting groups to the wires. In the second project the research of the resonances due to the presence of the carbonyl gave some more results: firstly, the presence of the carbonyl is moderately influencing the wire conductance and secondly the discovery of a switching mechanism present in bithiophenes. The last discovery brought on the table of molecular electronics a new innovative way of switching never reported before. The interplay between thioethers and thiophenes was more understood. Finally, more studies including modulation test will be carried out in order to verify switching mechanisms also on the wires used for the first study. In this case it could be very interesting to find out how the additional phenyl rings will drive the switching mechanisms and what will be the role of the heteroatoms used as bridges.

Methods

The molecular wires used in this study (**TGePh$_2$T**, **TSiPh$_2$T**, **TCPh$_2$T**, **TKT**, **TDKT** and **TCMe$_2$T**), were synthesised, purified and characterised using common synthetic laboratory techniques (see chapter 5). The biphenyl and terthiophene-based wires were synthesised using published procedures.[55,63] The conductance measurements of these molecules were carried out using the STM-BJ technique for all the molecules (see chapter 6). Additional experiments such as *I/V* measurements and modulation tests were also executed on some of them using the STM-BJ set up with some adjustments in order to make the experiments possible. A detailed description of these techniques can be found in Chapter 6, while all the measurements executed on the wires can be found in the Appendix.

Chapter 4: Testing quantum interference in longer thiamethyl-thiophene- and bipyridine-based molecular wires

4.0 Synthesis and measurements of longer molecules

In this chapter the attention is focalized on the synthesis and study of extended molecular wires. The previous studies (Chapter 3) concentrated on the interference effects in small molecules; unfortunately, due to a series of different factors (switching of the wires and noisy or very broad peaks in the conductance histograms), the interference effects are far from being fully understood. Another good reason for looking at extended wires could be that with the expected much smaller conductance values, the presence of a new resonance in the T(E) curve between the HOMO and LUMO resonances might result in a larger factor increase in conductance.

We decided to use two strategies to observe interference effects in a wire: the first consisted of comparing a series of wires with carbonyl groups added outside the conductance pathway as source of cross conjugation. This study differs from the one in the previous chapter with the kind of conjugated core used and the kind of contact used. In this study the central cores are based on fluorene/fluorenone and the contacts are methyl thioethers connected to the cores through a thiophene (Figure 4.1).

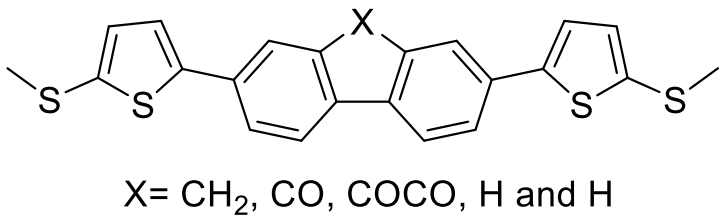

Figure 4.1 *Example of extended wire used in the first study of this chapter (H and H stands for a biphenyl based wire)*

This kind of wire is a simple extended version of the previous study: instead of bridging thiophene-based conjugated cores, commercially-available biphenyl-based and fluorene-based cores are used to investigate the interference effects of carbonyls.

The second study was focused on the comparison of a series of 2,2'-bipyridyl wires complexed with carbonyl-rich metal complexes (such as $Mo(CO)_4$ as example). In this case the number of carbonyl groups is considerably higher (between 3 and 4) but they are coordinated to a metal that is itself coordinated to the molecular wire. According to some preliminary theoretical calculations, the number of carbonyls introduced in a wire would produce an equal number of Fano resonances in the HOMO-LUMO gap. Since metal complexes with a bidentate ligand as molecular wire can be coordinated to up to four carbonyl groups, some stronger effect might be expected.

Previously organometallic complexes used as molecular wires were designed to incorporate the metal ion into the conductance pathway; for examples by using metal-alkyne complexes of ruthenium or platinum[64,65]. This simple but straightforward strategy may produce changes in the conductance of the final wires, but in our case, we did not choose to use this strategy since such complexes would be conformationally flexible, possibly obscuring any interference effects. In our case, we decided to focus our attention on the study of interferences outside the conductance pathway; this strategy should give more information on the influence of different complexes on the conductance of the molecular wires rather than producing a strongly modified wire. Previously, in a similar study carried out by Van der Zant and Coronado[66] it was demonstrated that the complexation of a molecular wires with a ligand moiety in the middle with a metal always resulted in a change in conductance of the wire. The study was concentrated on different contacts groups: ethynyl, thiol and 4-pyridine and the complexation of the wire always resulted in a compression of the HOMO-LUMO gap with increase in conductance for the pyridine-based wire and decrease for the other two. This study demonstrated decrease in conductance in wires with HOMO-based contacts and a boost in conductance in LUMO-based contacts. In our study we focused our attention towards the development of a similar system. We aimed to observe interferences effects created by the presence of metal carbonyls groups in a molecular wire placed outside the conductance pathway.

4.1 Interference effects in extended biphenyl-based molecular wires with 2-(methylthio)thiophene-based contacts

This first study is based on the interferences created by the presence of carbonyls in a conjugated core as additional pathway.

In the previous study the bithiophene based wires showed very little differences in conductance values and the interferences effects were difficult to address; in addition, the conductance peaks obtained in the STM-BJ were very broad. In order to overcome all those drawbacks, we chose to create a series of wires with some slight modifications. The first was the extension of the wires: experimentally we are aware that longer wires might create cleaner traces and cleaner traces means sharper peaks and thus more precise values of conductance for the molecular wires. Unfortunately using a quaterthiophene as a wire for this study was not possible due to the very low solubility of the quaterthiophene itself. The presence of four thiophene could bring the switching mechanism back in play and on top of this adding even one carbonyl would most probably create solubility issues resulting in poor measurement with the STM-BJ technique. In this case we decided to use a biphenyl-based core and methylthioether-thiophenes as contact group in order to avoid the low solubility issues. An additional benefit was the possibility to use common organometallic couplings to connect commercially available bridged cores (such as dibrominated fluorene, fluorenone, biphenyl and phenathrene-8,9-dione) to the methylthioether-thiophene contacts.

The targets molecules for this project are shown in Figure 4.2. A molecule with one carbonyl, fluorenone based, one with two carbonyl (phenanthrene-dione-based) and two control wires (fluorene and biphenyl-based) were synthesised in order to have a wider overlook on the interference effects.

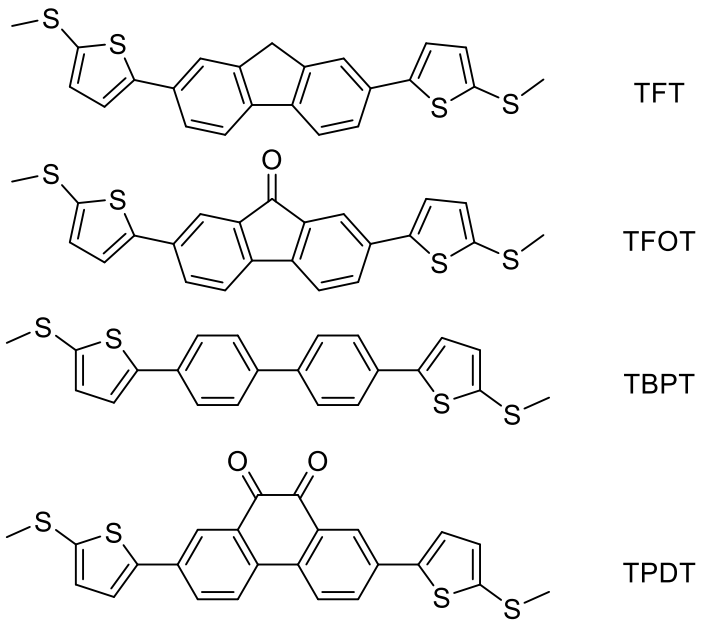

Figure 4.2 *First series of extended wires with biphenyl-based core and methylthioether-thiophene-based contacts*

The syntheses were straightforward for most of the wires and the final products were obtained after a simple Stille coupling, excluding the **TPDT** that was eventually obtained in very low yield and quantity. This was purified but unfortunately due to its extremely low solubility, it was impossible to execute any conductance measurements.

The series of wires have been designed in order to have a carbonyl group as a source of cross conjugation in one molecule (**TFOT**) and a couple of control wires to be used as comparison. The first is the **TFT** and possesses the same number of phenyl rings in the core (two) but does not have any carbonyl groups.

4.2 STM measurements of the extended molecular wires

The three molecular wires that have been successfully measured showed sharper peaks and a much higher hit-rate and cleaner traces than the ones observed in the measurement of the bithiophene-based series.

The comparison of the wires' conductance profiles in Figure 4.3 did not show many differences and surprisingly at 200 mV bias the conductance of the carbonyl-rich

molecule is higher than the conductance of the other to control experiment and in addition to that the conductance of the **TFT** and the **TBPT** are basically equal. The only difference between the **TFT** and TBPT is that the latter present an even sharper peak that is probably due to the higher symmetry present in this wire and a slightly higher conductance.

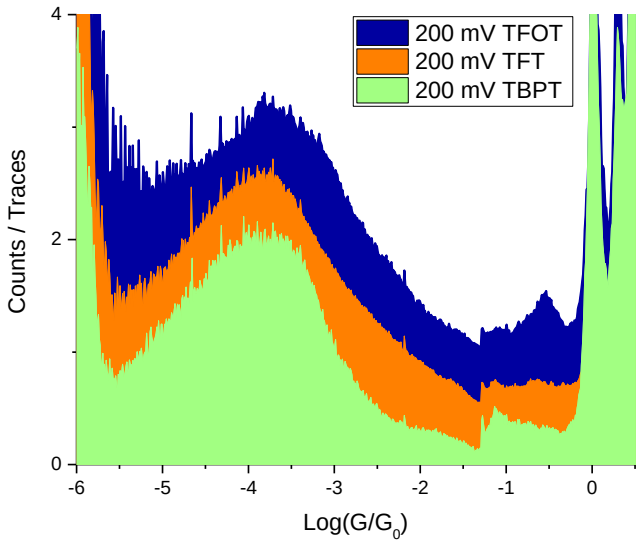

Figure 4.3 *Comparison of the three mws of the study:* ***TFT, TFOT*** *and* ***TBPT***

A possible explanation could be that in this case the carbonyl group was providing a positive conductance boost that could not be achieved in the other two control experiment since they did not have this specific moiety.

The wires have been studied also across different bias (100, 200 and 300 mV) in order to observe any changes in conductance, unfortunately the conductance values obtained with this study were slightly different as shown in Figure 4.4 but within the peak range. This signifies that the interference effects due to the presence of the carbonyl were theoretically overestimated. The effect is in fact too small to be considered statistically significant and the only visible observation in this comparison is the slight decrease in conductance with the increase of the bias voltage. This small effect could be due to different causes including noise from the instrument itself but also interference effects due to the carbonyl.

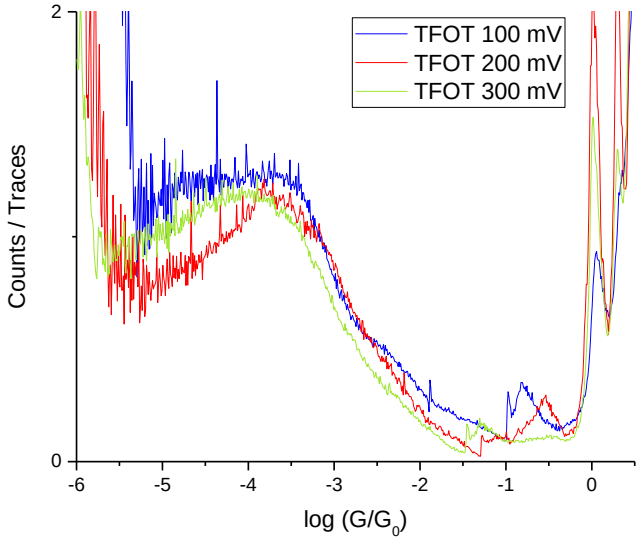

Figure 4.4 *comparison of conductance histograms for the wire* ***TFOT*** *at variable bias (at 100, 200 and 300 mV)*

To further study these wires, some I/V experiments have been executed in order to observe the behaviour of the wires across higher voltages. Only the **TFT** and **TFOT** were measured and they both showed a similar behaviour. In this case the histograms consisted of a single major conductance trail in both the wires. This result is opposed to the one observed for the previous molecular wires based on bithiophenes that showed a double trace in the I/V histogram. In addition, the histograms showed a much smaller data spread probably due to the more elongated structure of these wires that produced cleaner junctions during the experiments. These results clearly show the absence of the switching mechanism observed in the bithiophene-based wires. In this case no switching was present. In fact, only a single trace of conductance was visible with the I/V experiments. Both the molecular wires of this study (**TFT** and **TFOT**) present similar features in the I/V and for this reason the effect of the interferences due to the presence of a carbonyl was very small and not very well expressed with these experiments. An important result arising from these histograms is the total absence of the switching mechanism.

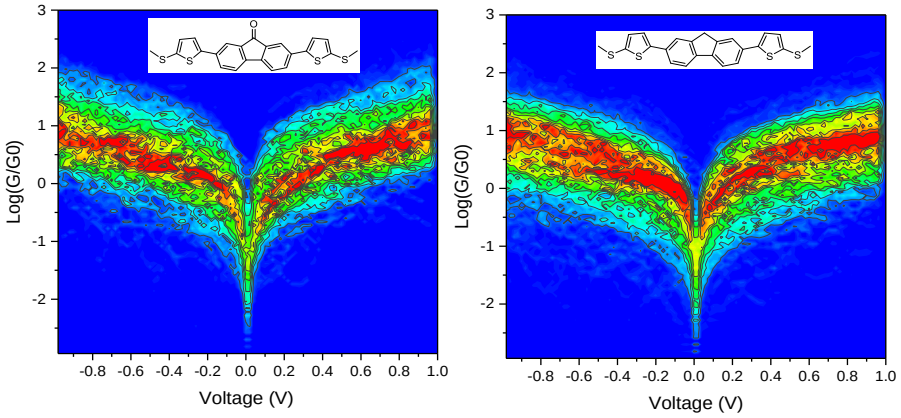

Figure 4.5 *I/V measurements of the* ***TFOT*** *on the left and* ***TFT*** *on the right*

The switching mechanism observed previously involved actively the switch between thioether and the thiophene ring as effective contact to the electrodes, in this case this effect was not observed even though the contacts and the moiety are the same. The probable explanation could be in the different structure of the wires: the ones used for this study possess a higher freedom of rotation, a longer structure and a much less conjugated core. Those characteristics may obviate the switching effect in this set of wires demonstrating that the switching effect observed in the bithiophene-based wires was typical of shorter and fully planar systems.

In conclusion, with these molecules there were some small conductance changes from one molecule to another, but the trend and the sizes of the changes did not definitively prove the existence of quantum interference effects due to carbonyl side-groups. On the other side we cannot prove the contrary; to have a better idea on whether the interference effects are present or not, better calculations are required for these molecules.

The study could provide some interesting tools or techniques or at least some interesting ideas on the tuning of molecular wires; the addition or the substitution of a carbonyl moiety outside the primary conduction pathway can be used in the future for small adjustments of a better-performing molecular wire. This study also provides

more understanding on the behaviour of the thiophene-methylthioether contacts used and together with the previous study on the bridged bithiophenes helped gather information on the switching effect observed. In molecular electronics the introduction of carbonyls and the addition of our contacts could be employed as fine-tuning tool for improving and designing molecular wires.

4.3 2,2’-Bipyridine-based complexes as molecular wires

In this study, a different strategy was adopted to observe interference effects: organometallic complexes were used as source of interferences. The basic principle of this work was similar to the previous studies and was focused on testing whether the conductance of a series of molecular wires was influenced by interference created by metals coordinated with a larger number of carbonyl groups and bonded to the wires outside the conductance pathway. We decided to develop a series of molecular wires based on 2,2’-bipyridine as core. This core was connected to the contacts in position 5,5' to create the wires. Several complexes originating from 2,2’-bipyridine-based molecules[67–69] and with transition metals such as molybdenum, rhenium, tungsten, platinum and palladium have been reported. For this reason, the 2,2'-bipyridine-based core was selected with the idea of creating complexes on a molecular wire. The addition of a metal outside the conduction pathway could provide some interferences to the molecular conductance. In this work, the starting aim was to synthesise 2,2’-bipyridine-based molecular wires and successively coordinate these wires with carbonyl-rich metal complexes to observe and study the differences in conductance due to the influence of complexes with many carbonyls (≥3) on the wires. In the previous study on bridged bithiophenes and longer wires the influence of the carbonyl groups was grasped but not fully understood. With this project the increased number of carbonyl and the addition of metal complexes to a molecular wire could produce a much higher effect that can clearly produce different conductance values. Figure 4.6 shows the first set of molecular wires for this study. The contact group was 4-pyridine and an alkyne was used as spacer; this choice was made in order to have a molecular wire able to transfer charge through the LUMO,

and pyridine usually conducts through the LUMO orbital. This choice was made in order to change the conductance with metal complexes.

Unfortunately, the synthesis of these complexes turned out to be extremely challenging. The starting molecular wires were synthesised without problems but the purification of the two complexes (with, respectively, $ReCl(CO)_3$ and $Mo(CO)_4$ units) was not feasible. The solubility of the starting compound was already low but dropped dramatically after the introduction of the metal centres and for this reason the complete isolation of both the wires was unfruitful. In order to overcome this problem, the solubility of the wires had to be increased, this would result in an easier purification protocol for the wires and to successful measurements. Usually long alkane chains attached to a molecule increase the solubility, but in this case, in order to avoid steric hindrance problems during the measurements due to some alkane chains the contact group was changed. A more soluble contact group such a thioether based wire seemed to be the best solution, since this contact can also favour LUMO-based conductance (depending upon the electron density of the molecular wire).[54] In addition, removing the pyridine contact would simplify the synthesis even more. This is because two wires with pyridine contacts could generate by-products by complexing the metal complexes used in the synthesis of the wires. Changing to a thioether based wire would signify higher yields, purer compounds and easier purification/measurements of the final wires.

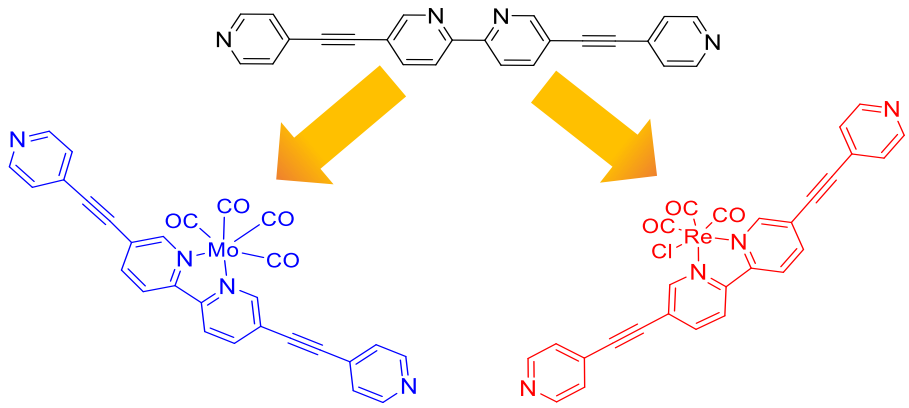

Figure 4.6 *First set of target molecular wires based on a 2,2'-bipyridine core*

Due to time constraints and the availability of an interesting contact group synthesised by Dr Ross Davidson from Durham University, we decided to join our

efforts in studying the interference effects of these wires by collaborating in this interesting project. Dr Davidson synthesised a series of molecular wires based on the 2,2'-bipyridine core with carbonyl-rich metal complexes and 3,3-dimethyl-2,3-dihydrobenzo[b]thiophene as contact group. More wires are still under synthesis and their conductance will be studied after the successful purification and characterization of the wires. Although only four molecular wires have been synthesised so far, enough material was provided to start investigating the interference effects in these complexes. The structures are summarized in Figure 4.7.

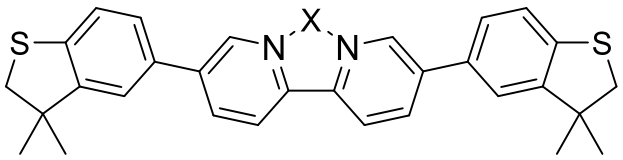

X= $Mo(CO)_4$, $MnBr(CO)_3$, $ReBr(CO)_3$

Figure 4.7 *2,2'-bipyridine-based complexes used in this study as molecular wires (also the precursor wire is included in the study)*

4.4 STM-BJ Measurements

The conductance of the molecular wires was measured with the STM-BJ technique at 300 mV and the resulting histograms (Figure 4.8) showed sharp peaks and some clear differences in conductance for some of the wires. The wire without any metal centre (**BTBipy**) showed a smaller peak and a conductance similar to the wire with the Re as complexed metal. All the other wires showed higher traces and the wire with the Mo complex (**BTBipy-$Mo(CO)_4$**) showed a much lower conductance than the others.

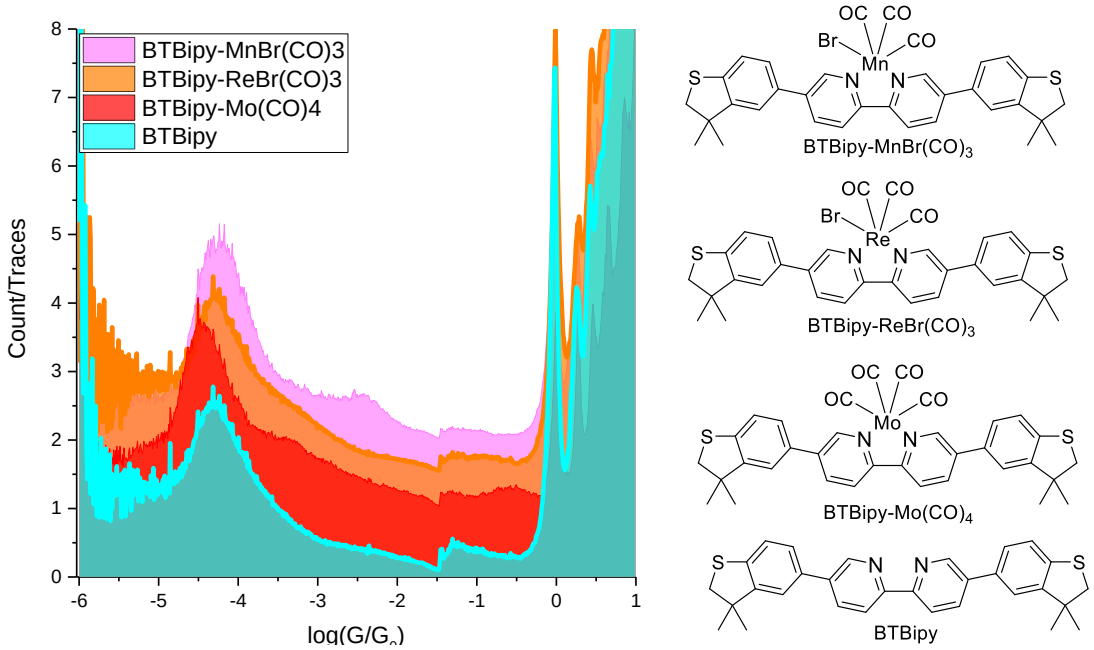

Figure 4.8 *Comparison of the conductance of the 2,2'-bipyridine-based molecular wires at 300 mV*

The wire with the Mn complex showed on the other hand just a wider peak. The comparison of the histograms clearly showed that the metal complexes influenced the conductance of some of the wires, even though the complexes were outside the conductance pathway. The same measurements have been repeated at 200 mV bias but no differences from the measurements at 300 mV were observed. In summary the addition of a complex outside the conductance pathway can influence the ,conductance of the wire itself but this was only observed with the molecular wire with the Mo complex (**BTBipy-Mo(CO)$_4$**). The presence of this carbonyl-rich complex reduced the conductance of the wire significantly but the reasons behind this are still unknown. This wire is the only one with a neutral oxidation state and therefore does not possess a bromine to counterbalance the charge resulting in a more electron withdrawing effect on the bipyridine ligand and finally to the reduced conductance value. Anyway, the non-existing change in conductance of the complexed wires is still unexplained compared with the conductance of the free wire alone since Van der Zant's study[70] reported always a change in conductance with the addition of a complex to a molecular wire.

4.5 Methods

The molecular wires used in the first study (**TFT**, **TFOT**, **TDPT**, **TPDT)** were synthesised, purified and characterised using common synthetic laboratory techniques (see chapter 5). The wires of the second group (**BTBipy-Mo(CO)$_4$, BTBipy-MnBr(CO)$_3$ BTBipy-ReBr(CO)$_3$, BTBipy**) were synthesized by our collaborator Ross Davidson at Durham University. The conductance measurements of all these molecules were carried out using the STM-BJ technique for all the molecules. Additional experiments such as I/V measurements were also executed on some of them using the STM-BJ set up with few adjustments in order to make the experiments possible. The experiment was carried out using the same procedures described in the method section of the previous chapter. The only difference was that for these longer and less soluble molecular wires the STM-BJ measurements have been carried out in a dilute solution (10^{-3}M) of mesitylene/THF 4/1. The wires were dissolved in THF first and then the mesitylene was slowly added.

The *I/V* measurements were executed with the same instrument and methodology described in the method section of the previous chapter.

4.6 Conclusions

These studies were designed to continue investigating interference effects arising from carbonyls outside the conduction pathway. The previous study with bithiophene-based wires could not prove the existence of these interferences since the effects were covered by other behaviours: high noise and switching mechanisms. The aim of these additional studies was to design alternative experiments to observe any kind of effects created by interferences due to carbonyl groups.

The first study shown a very small interference effect due to the carbonyl addition and at the same time despite having the same contact group (2-(methylthio)thiophene) did not show any switching effect. The last fact is very important because provide useful information on the importance of the molecular wire structure. With the first series of wires we also demonstrated that the switching

between methyl thioether and thiophene is not exclusively due to the presence of these two moieties. In the previous chapter we observed the switch between these two moieties and in this study we did not. This fact confirms that the effect observed is particular to bithiophene-like molecular wires.

The second study used a different strategy and 2,2'-bipyridine complexes to observe interference effects in molecular nanojunction. Even though preliminary theoretical calculations predicted the existence of a number of Fano resonances near the Fermi level of the electrodes the experimental data did not show clear results. The behaviour of the wires used in this study was very unexpected for two reasons: the first is that did not match the preliminary theoretical calculations and the second is that two out of three complexes did possess the same conductance of the free wire. The presence of carbonyls outside the conducting pathway as part of a metal complex attached to the wire did interfere with the conductance of the wire in one case out of three while in the other cases the conductance matched the one of the free wire. Unfortunately, the reasons of this difference in behaviour are still unknown; more detailed DFT calculations will be executed in order to provide a better explanation of the observed data. In addition, the syntheses of more wires with different metals are under development. The jointed efforts of theoretical calculations and more molecular wires analysed will provide a wider understanding of the interference effect of the carbonyls and the complexes in a molecular wire.

Chapter 5: Synthesis of the Molecular wires

5.0 General introduction

Throughout this thesis, molecules were synthesised using standard preparative chemistry techniques. All the molecular wires were analysed shortly after synthesis and were stored in the fridge or freezer in order to avoid degradation. In cases where the STM analyses were carried out after an appreciable time following synthesis, the purity was re-checked via NMR spectroscopy and elemental analysis.

All moisture- or oxygen-sensitive reactions were performed under Ar or N_2, in oven dried or flame dried glassware using dry solvents. All reagents including molecular sieves were purchased from Sigma-Aldrich (Merck), and all the solvents were purchased from Fisher except where otherwise stated and used as received unless otherwise stated.

When the following solvents: THF, toluene, Et_2O, CH_2Cl_2, EtOH were used for moisture/oxygen sensitive reactions, these solvents were dried over activated molecular sieves (3 or 4 Ångstrom) for at least 48 hours using 20 to 25% m/v, following the published guidelines.[71] *N*-bromosuccinimide (NBS) and *N*-iodosuccinimide (NIS) were recrystallised from boiling H_2O and dried overnight under vacuum in the presence of silica gel before use. PPh_3, tri(*o*-tolyl)phosphine and 1,2-*bis*(diphenyl)phosphine (DPPE) were recrystallised from boiling 95% ethanol, dried in vacuum and stored under Ar. *n*-Butyllithium was titrated against benzylbenzamide. This compound was purchased from Sigma-Aldrich in both 25 mL and 100 mL sure-seal® flasks, with nominal concentration of 1.6 M in hexanes. Palladium(0) tetrakis(triphenylphosphine), 2,2'-bithiophene, 5-bromo-2-iodopyridine, bromobenzeneboronic acid, 4-bromopyridine hydrochloride, tin(IV) chloride, 4*H*-cyclopenta[1,2-*b*:5,4-*b'*]dithiophene, 2,7-dibromophenanthrene-9,10-dione, (trimethylsilyl)acetylene and pyridine-4-boronic acid hydrate were purchased from Fluorochem. 2-Isopropoxy-4,4,5,5-tetramethyl-1,3,2-dioxaborolane, tri(*o*-tolyl)phosphine, 9,10-phenanthrenequinone and 4*H*-Cyclopenta[1,2-*b*:3,4-*b*']dithiophene were purchased from TCI. 1,4-Diiodobenzene and 2,2'-bithiophene were purchased also from Manchester Organics. Iron(III) chloride was purchased from Alfa Aesar. 2,7-Diiodophenanthrene-9,10-dione was synthesised according to

the published procedure.[72]

Thin layer chromatography was performed using Merck Silica Gel 60 F-254 plates, and flash column chromatography with Sigma-Aldrich technical grade silica (230-400 mesh, pore size 60 Å).

Proton and ^{13}C NMR spectra were recorded using a Bruker Avance 400 Ultrashield spectrometer and referenced to internal TMS. Mass spectra were recorded using a Carlo Erba 8000 Trio-1000 quadrupole spectrometer in CI positive ion mode (NH_3). High resolution mass spectra were recorded using an Agilent Q-TOF 7200 GC/MS or a Waters Micromass LCT TOF spectrometer.

The series of molecules X[Ph]X, X[T3]X, and X[V]X used in chapter 2 were previously synthesised and the alkanedithiols used were purchased from Sigma-Aldrich.

This chapter will firstly discuss the synthetic strategies used for the preparation of the molecular wires and secondly will be reported the experimental part with all the procedures and molecule characterization.

5.1 Synthesis of X(Ph)X-SMe series

1[Ph]1-SMe was prepared by methylation of the corresponding thiol using iodomethane in basic conditions (Scheme 5.1).

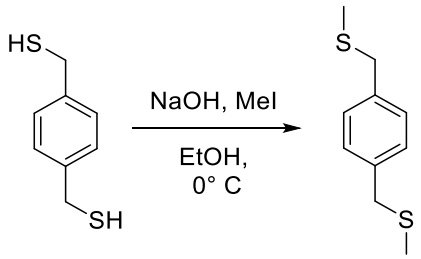

Scheme 5.1: Synthesis of **1[Ph]1-SMe**

The preparations of **3[Ph]3-SMe** and **4[Ph]4-SMe** were complicated by unexpected experimental difficulties.

Sonogashira coupling between 1,4-diiodobenzene and, respectively, propargyl alcohol and 3-butyn-1-ol was first attempted. A common side-reaction of this

coupling is the Glaser oxidative homocoupling of the alkyne (Scheme 5.2) and since the alkynes in the reaction were used in excess, this by-product was created in significant quantity in both the reactions. The two products and the two by-products had similar solubilities and Rf values making purification by the usual means (chromatography or recrystallization) impractical. The reactions were repeated reducing the equivalents of CuI but the results was still a mixture of compounds difficult to resolve.

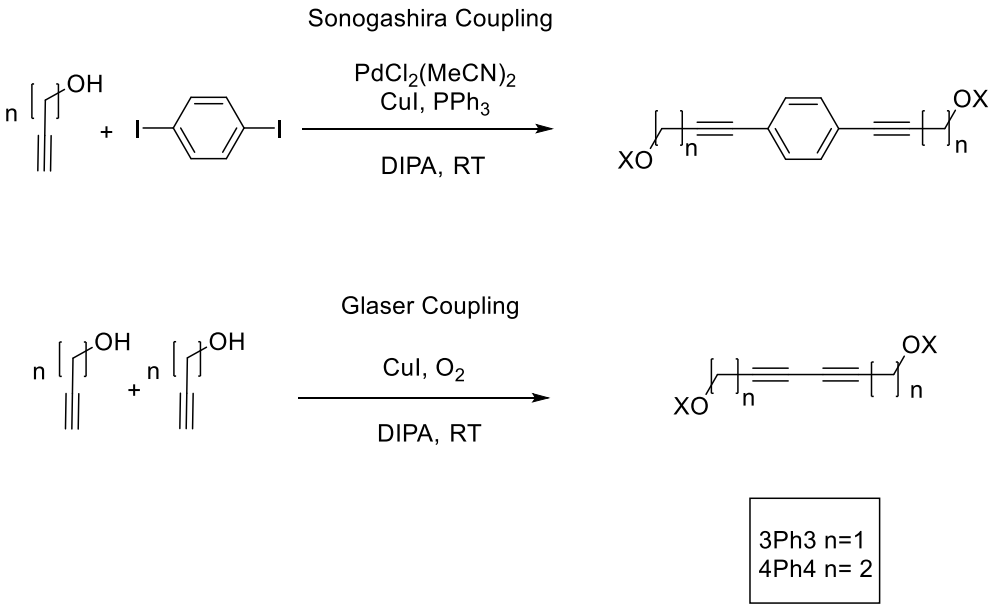

Scheme 5.2: Sonogashira coupling (upper) and Glaser coupling (lower**)**

Although in an earlier synthesis of the 6Ph6 family of molecules we had eliminated the Glaser by-products by hydrogenation of both di-ynes followed by chromatography,[73] this was unsatisfactory for other X[Ph]X molecules, so a protecting group strategy was decided upon. Benzyl propargyl ether was commercially available and used as supplied, and 3-butyn-1-ol was protected as a THP ether under acid condition with 3,4-dihydro-2H-pyran. The products of both of the subsequent Sonogashira couplings were easily purified. The choice of these specific protecting groups was not casual. In a synthesis adding a protecting group usually means adding two steps: protection and deprotection. However, since the chosen synthesis includes a hydrogenation step, protecting groups unstable under hydrogenation conditions were chosen. The two pure products were then hydrogenated and also conveniently deprotected in the subsequent catalytic

hydrogenation. In order to afford the target compounds the hydroxyl group was substituted with a more reactive function. For the 4[Ph]4-SMe synthesis an Appel reaction gave the bromoalkane derivative, but in low yields. For this reason, in the 3[Ph]3-SMe synthesis activation with TsCl was preferred to the bromination. Finally, a nucleophilic displacement with sodium thiomethoxide afforded the target compounds in high yields (Scheme 5.3).

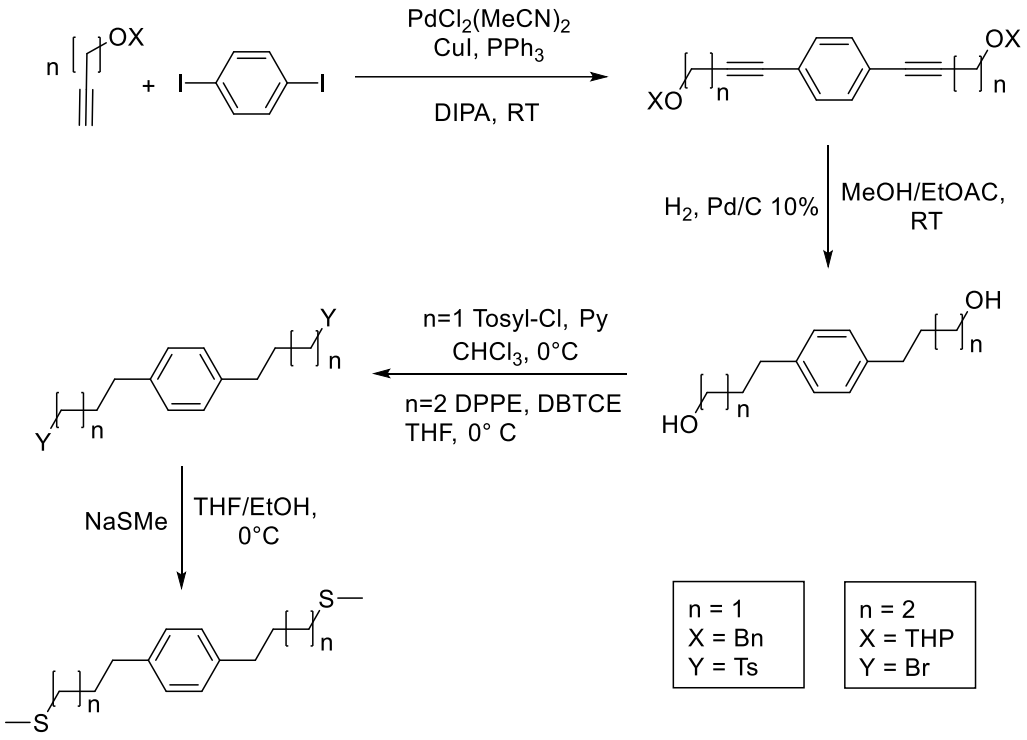

Scheme 5.3: Synthesis of **3[Ph]3-SMe** and **4[Ph]4-SMe**

5[Ph]5-SMe was prepared by an initial Sonogashira cross-coupling of 1,4-diiodobenzene with commercially-available 5-chloro-1-pentyne, hydrogenation of the alkynyl groups and subsequent reaction with KSAc gave the corresponding thioacetic acid ester. Methylation with iodomethane in basic conditions led to the title compound using the same conditions as for 1[Ph]1-SMe (Scheme 5.4). In this case, preparation of the intermediate di-thioacetate was selected since conductance measurements on the di-thiol 5[Ph]5 were also desired, in order to complete the X[Ph]X set of measurements.

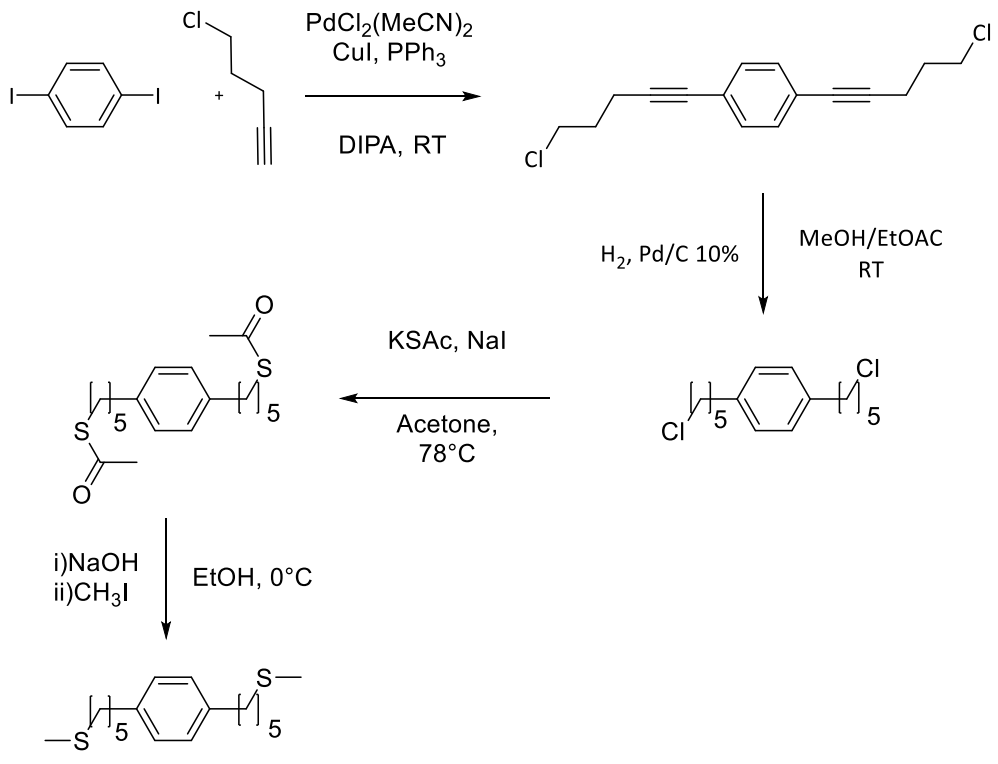

Scheme 5.4: Synthesis of **5[Ph]5-SMe**

6[Ph]6-SMe was prepared by treating 1,4-bis(5-chlorohexyl)benzene[46] with sodium thiomethoxide in a mixture of THF and ethanol under the same conditions used for 3[Ph]3-Me and 4[Ph]4-SMe (Scheme 5.5).

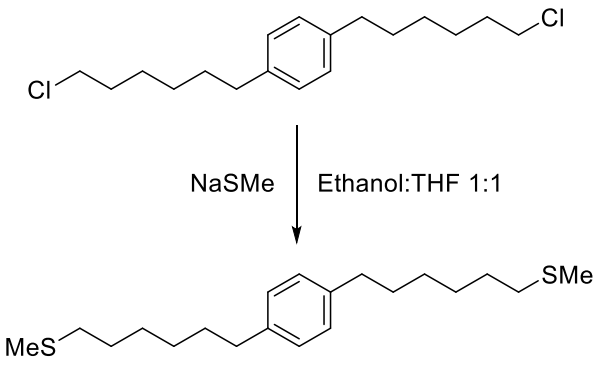

Scheme 5.5 Synthesis of **6[Ph]6-SMe**

5.1.0 Additional molecules

An additional molecular wire: 2Ph2 was required for a project in collaboration with the University of Bristol[12,74] for formation of close-packed SAMs on GaAs substrates, for this reason its synthesis is included in this thesis.

Since 2,2'-(1,4-phenylene)diacetic acid is commercially available, a different approach was used for the synthesis of 2Ph2. Reduction of the carboxylic acids to alcohols was preceded by an esterification step in order to execute a milder reduction with $NaBH_4$, a much milder and safer reagent than the normally-used $LiAlH_4$. The second step was the tosylation of the alcoholic functions using the same conditions as in the synthesis of 3[Ph]3-SMe, and finally the last reaction was a simple nucleophilic displacement with potassium thioacetate to give 2[Ph]2 as the bis(thioacetate) (Scheme 5.6).

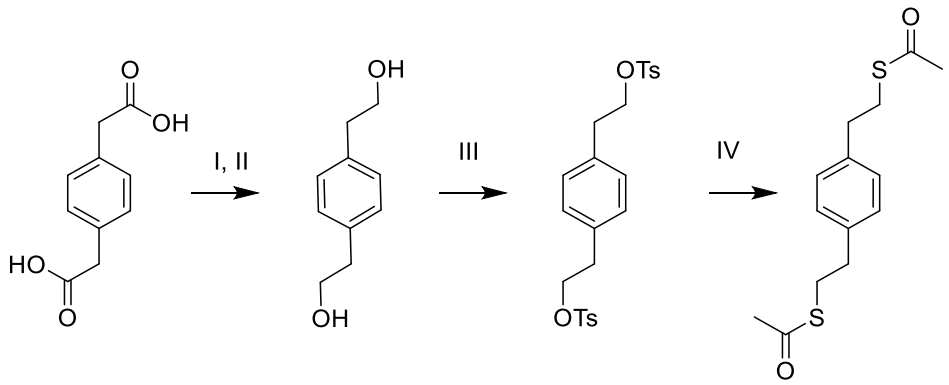

Scheme 5.6 Synthetic procedure for the preparation of **2[Ph]2.** I) MeOH, H_2SO_4. II) $NaBH_4$, THF. III) TsCl, pyridine, $CHCl_3$. IV) KSAc, NaI, acetone.

5.2 4*H*-cyclopenta[2,1-*b*:3,4-*b'*]dithiophene derivatives

The synthesis of bridged methylthioether-functionalised bithiophenes included the parallel development of molecules bearing both carbonyl related bridges and a series of Ph_2X (X = Group 14 element) bridges.

As mentioned in chapter 3 this project followed the theoretical calculations run by our partner group at Lancaster University. According to their theories the conductance of bridged bithiophenes with different atoms as bridges would vary following the trends observed in their transmissions' curves.

In order to match the theory with the experimental data three molecular wires bridged with different atoms were synthesized (specifically, CPh_2, $SiPh_2$ and $GePh_2$).

The synthesis of the **$GePh_2$ and $SiPh_2$** bridged bithiophenes started from 2,2'-bithiophene, on this molecule a tetra-bromination was executed with simple addition of 4 equivalents of Br_2 in a mixture of acetic acid and chloroform[75]. This procedure gave in good yields the 3,3',5,5'-tetrabromo-2,2'-bithiophene. Despite the fact that there are actually six possible bromination sites the first bromination in position 5, 5' activates the position 3, 3' giving 3,3',5,5'-tetrabromo-2,2'-bithiophene as primary product in good yields. This reaction was carried out several times during the course of three years in multigram scale to provide a good amount of material for the following reaction. The second step was the introduction of the methylthioether-based contact groups via a double selective lithium-halogen exchange with n-buthyllithium in position 5, 5' with subsequent quench with dimethyldisulphide (Scheme 5.7). Halogen-lithium exchange is selective for the 5, 5' positions because these are alpha to the electronegative S atom.

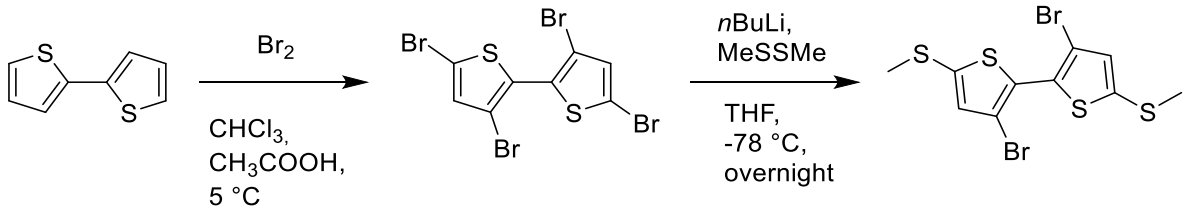

Scheme 5.7 Synthesis of the 3,3'-dibromo-5,5'-bis(methylthio)-2,2'-bithiophene

The final products have been obtained by lithium halogen exchange on 3,3'-dibromo-5,5'-bis(methylthio)-2,2'-bithiophene with nBuLi and subsequent quench with one equivalent of the dichlorodiphenylgermane or in case of the Si derivative with dichlorodiphenylsilane (Scheme 5.8).

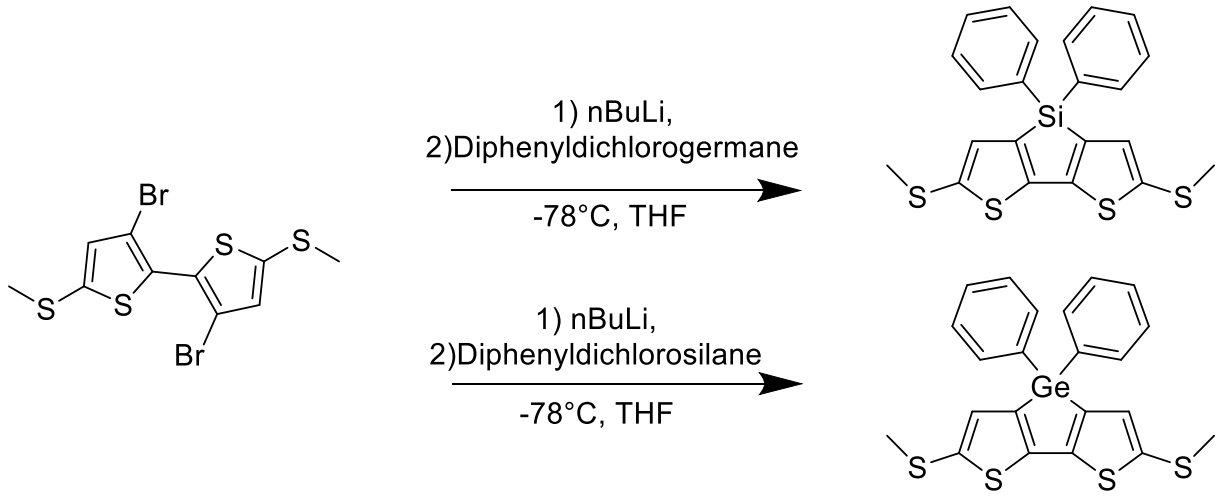

Scheme 5.8 Syntheses of bithiophenes with **$SiPh_2$** and **$GePh_2$** bridges.

The synthesis of the CPh_2 derivative was slightly more challenging. The analogous reaction failed so an alternative pathway was tried. As reported by Nemoto on a similar substrate[76] a good idea was to perform a nucleophilic attack on a benzophenone derivative and a subsequent dehydration to close the ring.

The reported procedure was carried out on a substrate without the methyl thioether contacts and unsubstituted in positions 3,3'. The synthetic procedure chosen for this target (Scheme 5.8) began with the tri-bromination of the 2,2'-bithiophene simply using 3 equivalents of Br_2. The purification of the tribromobithiophene was particularly challenging since care was required to remove by-products (the tetra-

and dibromo-derivatives). However, the second step was the insertion of the contacts via double lithiation and quench with MeSSMe, the third step was another lithium-halogen exchange and treatment with 1 equivalent of benzophenone. Finally, dehydration with tin tetrachloride closed the ring (Scheme 5.9).

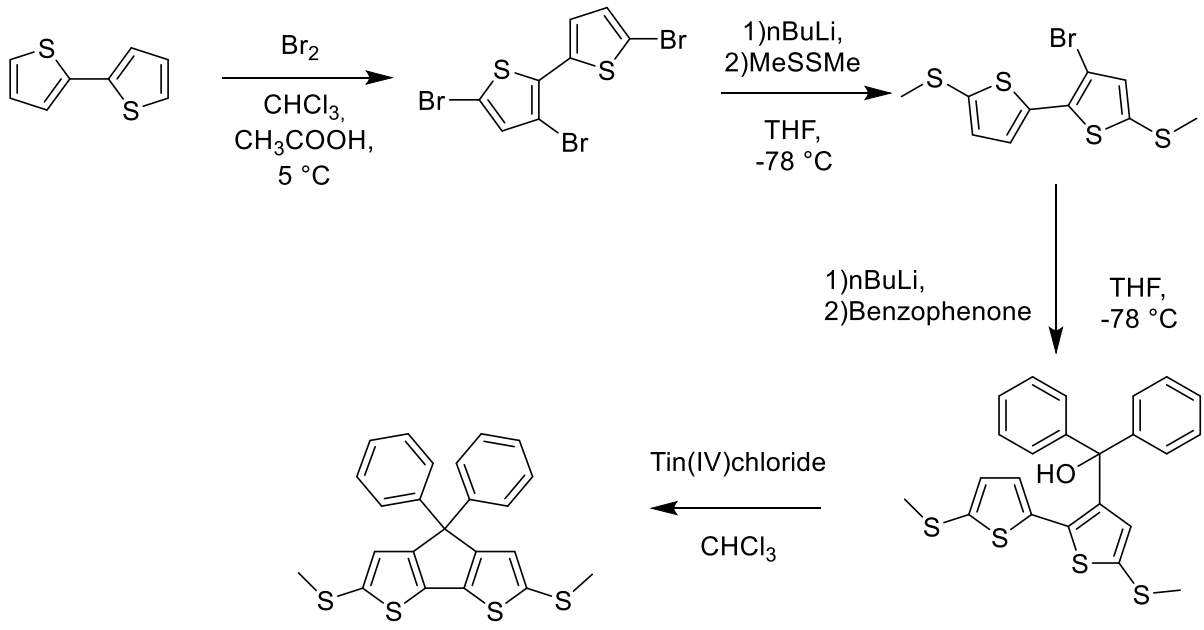

Scheme 5.9 Synthesis of bithiophene **CPh_2** bridged

5.3 Carbonyl-bridged bithiophene-based molecular wires

The carbonyl bridged bithiophenes study was very challenging and several routes were tried before a satisfactory synthesis of the final molecular wires was achieved.

The synthesis of the **TKT** started from the same starting material used for the $GePh_2$ and $SiPh_2$ bridged wire: the 3,3'-dibromo-5,5'-bis(methylthio)-2,2'-bithiophene and used pretty much a similar ring closure mechanism. In this case the last step was the introduction of the carbonyl to bridge the bithiophene and was achieved by a lithium-halogen exchange between n-butyllithium and the bromine groups in position 3, 3' and subsequent quench with dimethylcarbamyl chloride as a source of carbonyl (Scheme 5.10). This step required careful workup at –60°C in order to obtain the molecular wire in good yields and was an adaptation of the procedure used by Getmanenko in a 2011 study to successfully synthesize similar compounds.[77]

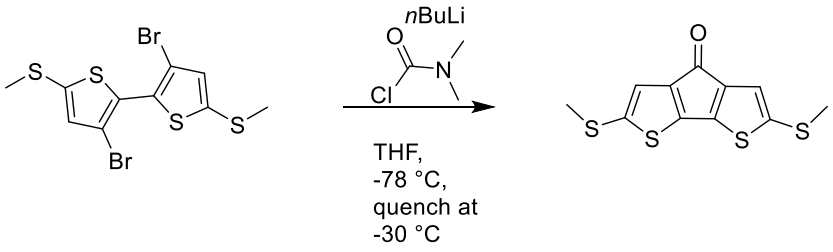

Scheme 5.10 Synthesis of **TKT** from the 3,3'-dibromo-5,5'-bis(methylthio)-2,2'-bithiophene.

Although 4*H*-cyclopenta[2,1-b:3,4-b']dithiophen-4-one is commercially available, this molecule is unsuitable for lithiation; for this reason on this substrate only reactions of bromination and couplings have been successfully achieved.[78] The need for the contact groups and their addition necessitated the insertion of the carbonyl in the last step.

The synthesis of **TDKT** was very similar with the one described above and was achieved after much trial and error. Firstly a double lithium-halogen exchange on the molecule 3,3'-dibromo-5,5'-bis(methylthio)-2,2'-bithiophene with subsequent quench with diethyl oxalate or 1,4-dimethyl-2,3-piperazinedione were tried since similar bithiophenes have been previously reported,[77] unfortunately the presence of the thiomethyl moieties may change the behaviour of the molecule, since in our case such reactions failed producing many side products and not the target molecule. For this reason, an alternative milder approach was tried: an initial lithium-halogen exchange followed by transmetallation with LiBr and CuBr followed by the addition of oxalyl chloride. This reaction (shown in Scheme **5.11**5.11) led to the formation of the desired product, but its subsequent purification was extremely difficult. Although the compound possessed a good R_f value on TLC (0.3 with 1/1 DCM/ethyl acetate), flash chromatography on SiO_2 failed, with complete retention of the compound. Also, several recrystallizations were tried but no pure compound was successfully separated. Eventually a small sample of pure product was obtained using preparative TLC. Due to the difficulties encountered in the purification steps the final compound was recovered in very low yield: 7 %. Fortunately, the 25 mg recovered were more than enough for the characterization and for conductance measurements.

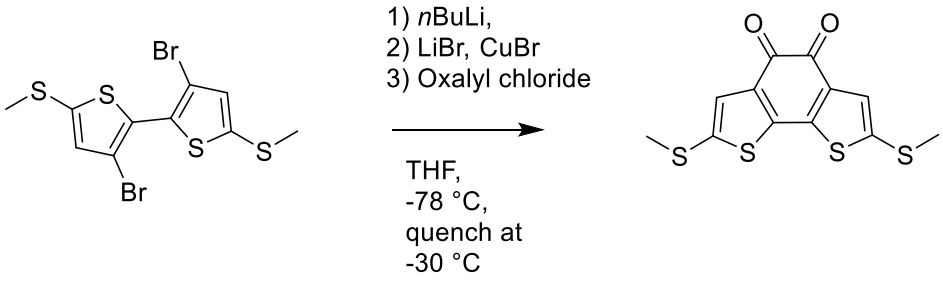

Scheme 5.11 Synthesis of **TDKT** from 3,3'-dibromo-5,5'-bis(methylthio)-2,2'-bithiophene.

To complete the study a bridged bithiophene without carbonyls was synthesized to be compared with the two molecules previously measured. Initially the target molecule was a simple methylene-bridged bithiophene. This molecular wire has been previously reported by Venkataraman and Campos in 2013[63] in low yields. They obtained the molecule 2,6-bis(methylthio)-4*H*-cyclopenta[2,1-*b*:3,4-*b*']dithiophene starting from 2,6-dibromo-4*H*-cyclopenta[2,1-*b*:3,4-*b*']dithiophene with a very quick lithium-halogen exchange and the subsequent quench with dimethyl disulfide as shown in Scheme 5.12. Unfortunately, due to the excessive cost of the starting material the synthesis from its precursor was tried. The initial bromination of 4H-cyclopenta[2,1-b:3,4-b']dithiophene using $FeCl_3$ and Br_2 was tried three times but only a very low amount of product (2,6-dibromo-4H-cyclopenta[2,1-b:3,4-b']dithiophene) was obtained. Furthermore, when the second step was tried in the same reported conditions the reactions never gave the desired product but always mono-substituted cyclopentadithiophenes in low yields. This was mainly due to the short period of time used for the lithiation and also for the presence of hydrogens in position 4. Lithium-halogen exchange is done using *n*-BuLi which is a very strong base that can react with the weakly-acidic protons of the molecule in position 4 reducing dramatically the yields and leading to byproducts.

Since the previous route failed we focused our attention towards the synthesis of another molecule without acidic protons in position 4: the **TCMe$_2$T**. The better way to avoid the presence of acid protons was to substitute them with something else

less reactive but not very bulky such as a couple of methyl groups. The same starting material, the 4*H*-cyclopenta[2,1-b:3,4-b']dithiophene was then easily methylated in position 4 using KOH and MeI in DMSO using a common and previously reported procedure[79] and the positions 2 and 6 were brominated in the next step using NBS in DMF.[79] The bromination in this case was successful. In the previous attempts, the use of NBS as brominating agent was not considered because the position 4 could have been brominated as well from this reagent leading to the formation of by-products. The final reaction was then a classic lithium-halogen exchange with subsequent quench with dimethyl disulfide. Since no acidic protons were present in the molecule a spot to spot reaction occurred leading only to the formation of the desired product in good yields (Scheme 5.12).

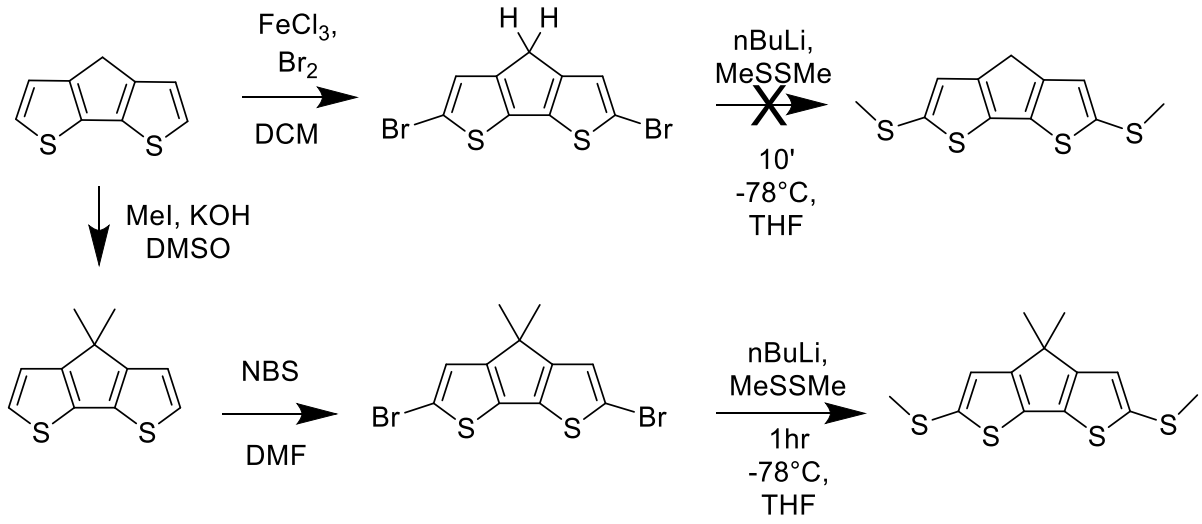

Scheme 5.12 First synthetic route tried and effective synthesis of **TCMe2T**

5.4 Synthesis of longer molecular wires with 2-(methylthio)thiophene contacts and carbonyl moieties

After observing interesting effects in the conductance of bithiophene-based molecular wires we focused our attention towards longer molecular wires containing carbonyl groups and 2-(methylthio)thiophene contacts. This decision was made because the STM-BJ measurements carried out on the previously mentioned molecular wires were quite noisy, often longer molecules gives cleaner histograms, in addition to that longer wire with lower conductance values might be more influenced by interferences effects (that it also the aim of this thesis). A longer molecular wire could also be slightly easier to synthesize using coupling chemistry (Stille or Suzuki) to attach a series of conjugated cores with the 2-(methylthio)thiophene contacts. A combination of the two reasons and increasing interest about the interference effects of the carbonyl group led the creation of this project. In this project four molecular wires have been synthesized to better study the interference effects: a molecular wire with one carbonyl moiety as central core (fluorenone-based), another one with two carbonyls (9,10-phenantrenequinone-based), and two control experiments: one bridged by a CH_2 group (fluorene-based) and another one with no bridge at all but otherwise analogous to the other molecules (biphenyl-based). The choice of the central cores as biphenyl-based instead of bithiophene-based was made because of the availability of the starting materials and for the solubility of the final product: bithiophene-based cores would have yielded quaterthiophenes molecules not very soluble in most solvents. The low solubility is an important drawback for both purification of the compounds and their measurements with the STM-BJ technique that is usually performed in solution (usually mesitylene).

As shown in Scheme 5.13 the fluorene-based molecular wire was synthesised by a Stille coupling between 2,7-dibromo-9*H*-fluorene and trimethyl(5-(methylthio)thiophen-2-yl)stannane in DMF and the same procedure was tried with the fluorenone-based (2,7-dibromo-9H-fluoren-9-one) and with the biphenyl-based core (4,4'-diiodo-1,1'-biphenyl). The Stille reaction did not work on the 2,7-

diiodophenanthrene-9,10-dione so an alternative Suzuki coupling was tried and successfully executed using 4,4,5,5-tetramethyl-2-(5-(methylthio)thiophen-2-yl)-1,3,2-dioxaborolane to provide the contacts.

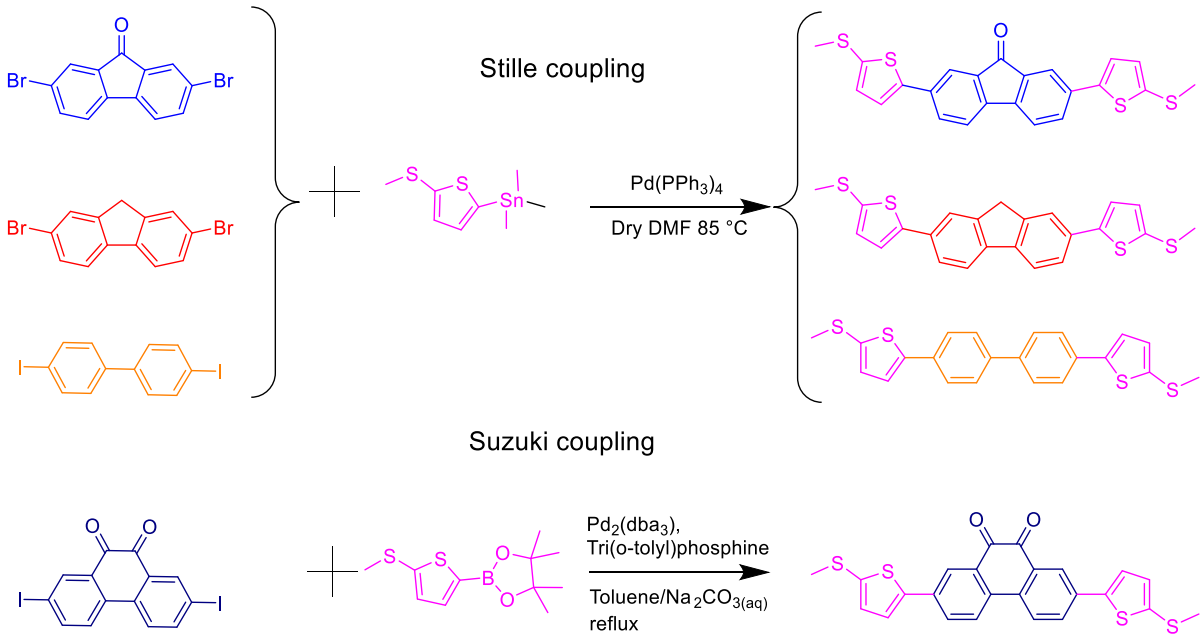

Scheme 5.13 Synthesis of the series of longer molecular wires with methylthiothiophene contacts

As observed from the TDKT molecular wire the presence of a diketone moiety lowers the solubility and makes the purification process more challenging, and this was also observed in the phenanthrene-9,10-dione-based wire. Finally, is important to state that some of the reported yields for these compounds are quite low. This because firstly the main aim of the synthesis is to provide a pure final compound, so the optimization of the reactions is not of primary interest, secondly in order to test a molecular wire's conductance only few milligrams are needed, for these reasons the reactions that produced very low yields but enough pure material to be used for characterization and conductance measurements were not repeated.

5.5 2,2’-Bipyridine-based complexes as molecular wires

This project focused on the study of interferences effects on a molecular wire based from 2,2’-bipyridine. The 2,2’bipyridine can effectively coordinate in complexes of metals such as Mo, Re, W and many more. In this project we focused our attention on the potential difference in conductance of some molecular wires based on 2,2’bipyridine with and without complexation to metals.

The conductance study of inorganic complexes have been discussed previously in several works[80] in each of them the inorganic complex was in the middle of the conductance pathway of the molecular wires, in our study we synthesised molecular wires having inorganic complexes outside the conductance pathway. The main goal is to test whether such complexation can result in quantum interference effects in the conductance of the molecules and, if so, whether this can be tuned by altering the complexes attached to the molecular wire.

To interfere with the molecular wire we focused our attention towards metal complexes with several carbonyls groups in them such as $Mo(CO)_6$, $ReCl(CO)_5$ or $ReCl(CO)_5$ since the presence of carbonyls could induce Fano resonances in the transmission function of the molecular wire.

The choice of the contact group was not simple: at the beginning was tried 4-ethynylpyridine in order optimise the molecular wire for LUMO-based transport. Later, 3,3-dimethyl-2,3-dihydrobenzo[b]thiophene contacts were also tried thanks to a collaboration with a research group at University of Durham.

During the development of this project several drawbacks limited our results. Firstly the 2,2’-bipyridine-based molecular wires possessed very low solubility in the majority of solvents used for STM-BJ measurements, and in many other solvents, complicating attempts to make complexes with this system. Complexation reaction were attempted using $[ReCl(CO)_5]$ and $[Mo(CO)_6]$, however, the products were even less soluble than the starting material, making the purification processes ineffective and complicating subsequent analyses. As matter of fact the complex between 5,5'-bis(pyridin-4-ylethynyl)-2,2'-bipyridine and $[Mo(CO)_6]$ could not be separated from

the starting material and the complex made using [$ReCl(CO)_5$] was so insoluble that was impossible to obtain any clear peaks in the ^{1}H-NMR spectrum.

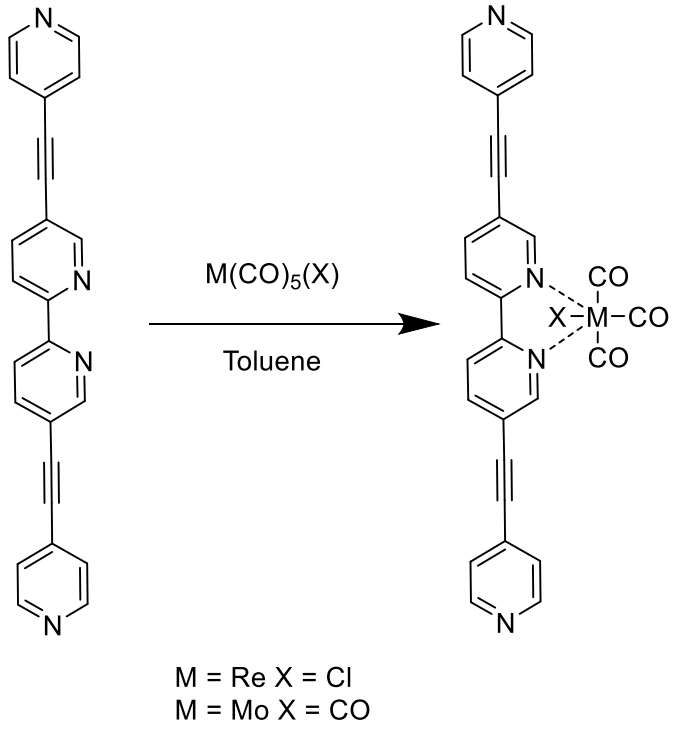

Scheme 5.14 Complexation reaction on 5,5'-bis(pyridin-4-ylethynyl)-2,2'-bipyridine

To overcome those problems only one option was available: increasing the solubility of the wires. One possibility was the introduction of chains in the core of the molecule (2,2'-bipyridine) or changing contact group with something more soluble. At the University of Durham, a group of collaborators developed an interesting and very soluble contact group: the 3,3-dimethyl-2,3-dihydrobenzo[b]thiophene; we decided to join our efforts and create a molecular wire based on the complex's core, 2,2'-bipyridine, with this relatively innovative contact group. Even with this relatively more solubilising group, only three complexes were successfully purified and measured and not without difficulties.

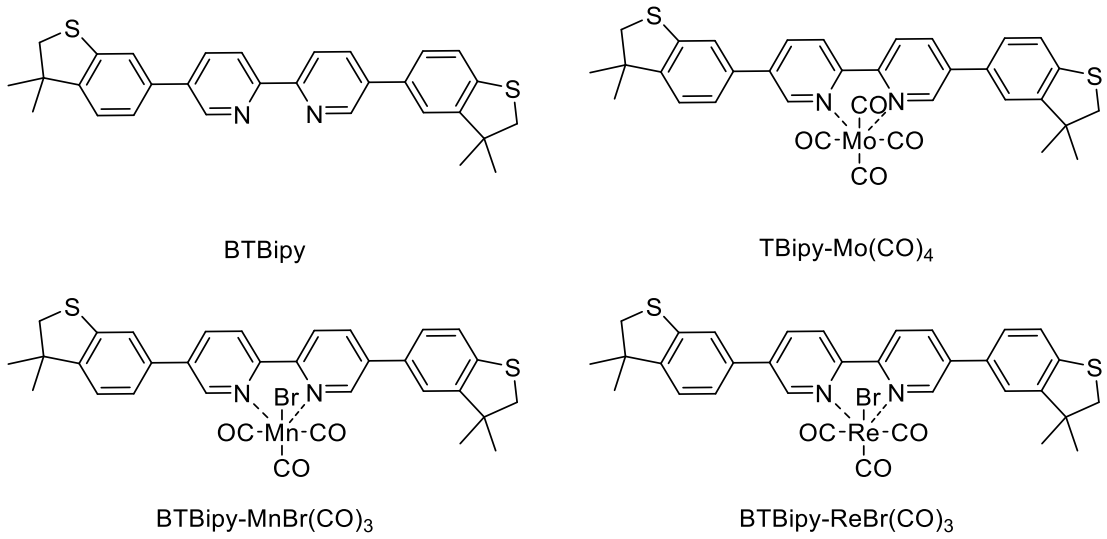

Figure 5.15 Alternative Bipy-based molecular wires

The synthesis of the wire with 4-ethynylpyridine contacts have been previously reported by Xu, Chaojie et al.[81] and involved two subsequent Sonogashira coupling reactions on the 5,5'-dibromo-2,2'-bipyridine. The first was between 5,5'-dibromo-2,2'-bipyridine and ethynyltrimethylsilane and then the second with 4-iodopyridine.

We decided to do a first reaction between ethynyltrimethylsilane and 4-bromopyridine (cheaper than the iodo derivative) and then a Sonogashira between 4-ethynilpyridine and 5,5'-dibromo-2,2'-bipyridine as shown in Scheme 5.15 as alternative solution.

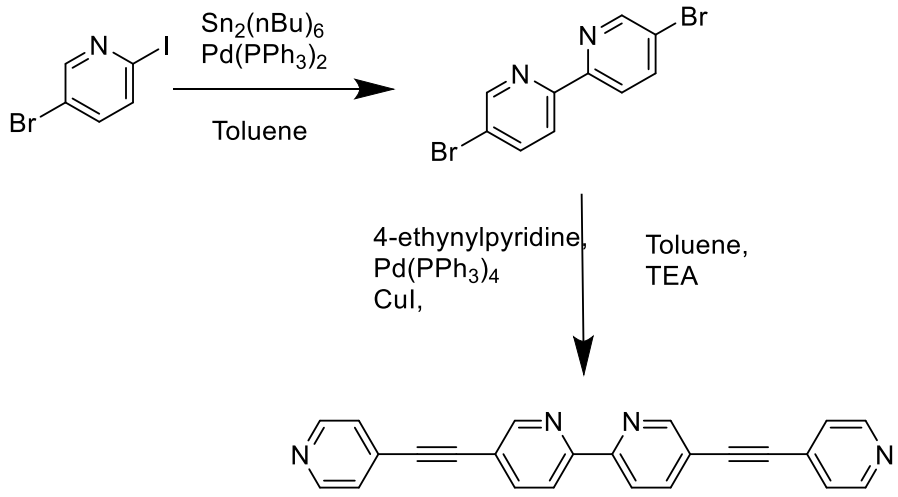

Scheme 5.16: Alternative synthesis of the 5,5'-bis(pyridin-4-ylethynyl)-2,2'-bipyridine

5.1.1: 1,4-bis((methylthio)methyl)benzene, 1[Ph]1-SMe

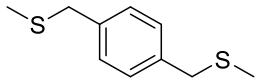

To a solution of sodium hydroxide (282 mg, 7.1 mmol) in ethanol (20 mL) was added 1,4-phenylenedimethanethiol (200 mg, 1.17 mmol) while cooling in an ice bath. The resulting suspension was stirred for 10 minutes at 0 ˚C and then iodomethane (0.147 mL, 2.35 mmol) was added. After stirring overnight, the resulting suspension was quenched with NH_4Cl (aq. sat., 15 mL). The mixture was concentrated under vacuum and then extracted with CH_2Cl_2 (3 x 50 mL). The combined organic phases were washed with brine (50 mL), dried over $MgSO_4$, filtered and the solvent removed under vacuum. Purification by column chromatography on silica (2 % EtOAc in hexanes) afforded the title compound as white crystals (190 mg, 82 %).

Found C = 60.18, H = 7.14, S = 32.22 %. $C_{10}H_{14}S_2$ requires C = 60.55, H = 7.11, S = 32.33 %. ^{1}H NMR (400 MHz, $CDCl_3$) δ: 7.25 (s, 4H, Ph), 3.66 (s, 4H, CH_2), 2.01 (s, 6H, CH_3). ^{13}C NMR (100 MHz, $CDCl_3$) δ: 136.98, 128.98, 36.16, 14.97. *m/z* (HRMS, CI, NH_3) 216.0884 $[M+NH_4]^+$. $C_{10}H_{18}NS_2$ calc. 216.0881.

5.1.2: 1,4-bis(3-(benzyloxy)prop-1-yn-1-yl)benzene

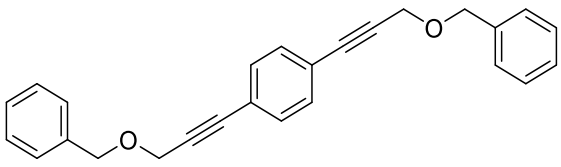

1,4-diiodobenzene (2.00 g, 6.06 mmol), $[PdCl_2(MeCN)_2]$ (80 mg, 0.30 mmol), triphenylphosphine (240 mg, 0.92 mmol) and CuI (116 mg, 0.60 mmol) were mixed in DIPA (80 ml) and the resulting suspension was degassed by bubbling Ar through for 50 minutes. Benzyl 2-propynyl ether (2.22 g, 15.15 mmol) was added, and the resulting suspension was stirred for 24 hours under Ar atmosphere at room temperature. The solvent was then removed *in vacuo*, the solid was picked up in

CH_2Cl_2 and the suspension was filtered. After further removal of the solvent, the crude product was purified by flash chromatography on silica (15% EtOAc in hexanes) and recrystallized from hexanes:CH_2Cl_2 (95:5) to give the title compound as a pale yellow solid (2.01 g, 89 %).

^{1}H NMR (400 MHz, $CDCl_3$,) δ: 7.38 (s, 4H, Ph), 7.37 (m, 10H, Ph), 4.67 (s, 4H, CH_2) 4.40 (s, 4H, CH_2). ^{13}C NMR (100 MHz, $CDCl_3$) δ: 137.4, 131.7, 128.5, 128.2, 127.9, 122.8, 87.0, 86.0, 71.8, 57.9.*m/z* 389.2 $[M+Na]^+$.

5.1.3: 3,3'-(1,4-phenylene)bis(propan-1-ol)

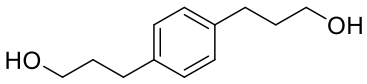

1,4-bis(3-(benzyloxy)prop-1-yn-1-yl)benzene (2.00 g, 5.46 mmol) was subjected to catalytic hydrogenation (25 mL EtOAc, 25 mL MeOH, 300 mg Pd/C 10 %, H_2 atmosphere, 52 h, room temperature). The resulting solution was filtered through a bed of celite and the solvent was removed *in vacuo* to give the title compound as white solid (1.00 g, 94 %).

Found C = 73.69, H = 9.31 %. $C_{12}H_{18}O_2$ requires C = 74.19, H = 9.34 %. ^{1}H NMR (400 MHz, $CDCl_3$) δ: 7.12 (s, 4H, Ph), 3.68 (t, 4H, J = 6.4 Hz, CH_2), 2.68 (t, 4H, J = 8 Hz, CH_2) 1.88 (m, J = 6.4Hz, 4H, CH_2) ^{13}C NMR (100 MHz, $CDCl_3$) δ: 139.38, 128.56, 62.37, 34.22, 31.65. *m/z* (HRMS, CI, CH_4) 177.1281. $C_{12}H_{17}O$ calc. 177.1279.

5.1.4: 1,4-phenylenebis(propane-3,1-diyl) bis(4-methylbenzenesulfonate)

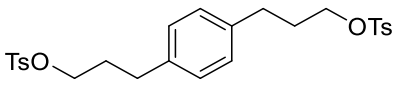

To a solution of 3,3'-(1,4-phenylene)bis(propan-1-ol) (0.30 g, 1.54 mmol) in chloroform (15 mL) pyridine (0.5 mL, 6.2 mmol) was added followed by p-toluenesulfonyl chloride (0.90 g, 4.63 mmol) while cooling in an ice bath. After stirring overnight, diethyl ether (40 mL) and water (15 mL) were added to the mixture

and the layers were separated. The combined organics were washed successively with HCl (2N, 20 mL), $NaHCO_3$ (5%, 20 mL), and brine (25 mL), dried over $MgSO_4$ and concentrated. The crude product was purified by flash column chromatography on silica (25 % EtOAc in hexanes) to give the title compound as white solid (600 mg, 77 %).

^{1}H NMR (400 MHz, $CDCl_3$) δ: 7.80 (d, 4H, J = 8.0 Hz, Ph), 7.49 (d, 4H, J = 8.0 Hz, Ph), 6.99 (s, 4H Ph) 4.03 (t, 4H, J = 5.6 Hz, CH_2), 2.59 (t, 4H, J = 8.0 Hz, CH_2), 2.47 (s, 6H, CH_3), 1.91 (m, 4H). *m/z* 525.1 $[M+Na]^+$.

5.1.5: 1,4-bis(3-(methylthio)propyl)benzene, 3[Ph]3-SMe

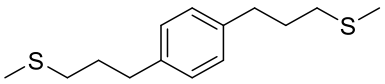

To a solution of sodium thiomethoxide (0.22 g, 3.1 mmol) in dry ethanol (15 mL) under Ar, 1,4-phenylenebis(propane-3,1-diyl) bis(4-methylbenzenesulfonate) (0.26 g, 0.52 mmol) dissolved in dry THF (15 mL) was added. After stirring for three hours the resulting suspension was quenched with water (25 mL) and the aqueous layer was extracted with diethyl ether (3x 30 mL). The combined organic portions were washed successively with brine (2 x 25 mL) and water (2 x 25mL) and dried over $MgSO_4$. The solvent was removed in vacuo and the crude product was purified by flash column chromatography on silica (4% EtOAc in hexanes as eluent) followed by a crystallization with hexanes to give the title compound as colorless oil, (120 mg 90 %).

Found C = 67.12, H = 8.86, S = 24.37 %. $C_{14}H_{22}S_2$ requires C = 66.08, H = 8.71, S = 25.20 %. ^{1}H NMR (400 MHz, $CDCl_3$) δ: 7.11 (s, 4H, Ph), 2.69 (t, 4H, J = 7.6 Hz, CH_2), 2.51 (t, 4H, J = 7.6 Hz, CH_2) 2.10 (s, 6H, CH_3), 1.90 (m, 4H, CH_2) ^{13}C NMR (100 MHz, $CDCl_3$) δ: 139.11, 128.49, 34.34, 33.64, 30.70, 15.47. *m/z* 255.1245 $[M+H]^+$, $C_{14}H_{23}S_2$ calc. 255.1241.

5.1.6: 1,4-bis(4-((tetrahydro-2H-pyran-2-yl)oxy)but-1-yn-1-yl)benzene

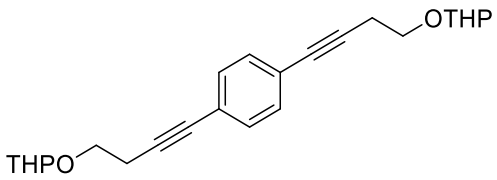

1,4 diiodobenzene (1.60 g, 4.85 mmol), [$PdCl_2(MeCN)_2$] (63 mg, 0.24 mmol), triphenylphosphine (190 mg, 0.73 mmol) and CuI (92 mg, 0.48 mmol) were mixed in DIPA (80 ml) and the resulting suspension was degassed by bubbling argon through for 50 minutes. After this time, 2-(but-3-yn-1-yloxy)tetrahydro-2H-pyran (1.9 ml, 12.12 mmol), was added, and the resulting suspension was stirred for 24 hours under argon atmosphere at room temperature. The solvent was then removed *in vacuo*, the solid was picked up in CH_2Cl_2 and the suspension was filtered. After further removal of the solvent, the crude product was purified by flash chromatography on silica (10 % EtOAc in hexanes) and recrystallized from hexanes:CH_2Cl_2 (95:5) to give the title compound as pale yellow solid (1.2 g, 65 % yield).

^{1}H NMR (400 MHz, $CDCl_3$) δ: 7.30 (s, 4H, Ph.) 4.69, (t, 2H, J = 3.2, CH), 3.91 (m, 4H, CH_2), 3.58 (m, 4H, CH_2), 2.71 (m, 4H, CH_2), 1.85 (m, 4H, CH_2) 1.74 (m, 4H, CH_2), 1.61 (m, 4H, CH_2).^{13}C NMR (100 MHz, $CDCl_3$) δ: 131.65, 123.00, 98.77, 88.71, 81.21, 65.53, 62.12, 30.36, 25.34, 21.12, 19.11. *m/z* 405.2 $[M+Na]^+$.

5.1.7: 4,4'-(1,4-phenylene)bis(butan-1-ol)

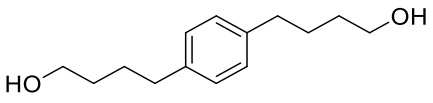

1,4-bis(4-((tetrahydro-2H-pyran-2-yl)oxy)but-1-yn-1-yl)benzene (1.00 g, 3.14 mmol) was subjected to catalytic hydrogenation (25 mL EtOAc, 25 mL MeOH, 100 mg Pd/C 10 %, H_2 atmosphere, 48 h, room temperature). The resulting solution was filtered

through a bed of celite and the solvent was removed *in vacuo* to give the title compound as white solid (0.55 g, 94 %).

^{1}H NMR (400 MHz, CD_3OD) δ: 7.08 (s, 4H, Ph), 3.55 (t, 4H, J = 6.4 Hz, CH_2), 2.59 (t, 4H, J = 8 Hz, CH_2) 1.65 (m, 4H, CH_2) 1.56 (m, 4H, CH_2). ^{13}C NMR (100 MHz, $CDCl_3$) δ: 139.60, 127.93, 61.42, 34.89, 31.81, 27.62. *m/z* 240.0 $[M+NH_4]^+$, 223.3 $[M+H]^+$.

5.1.8: 1,4-bis(4-bromobutyl)benzene

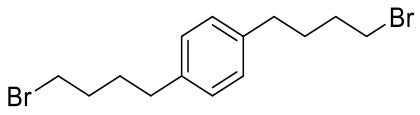

To a solution of DPPE (690 mg, 1.73 mmol) in THF (20 mL) was added 1,2-dibromotetrachloroethane (1.28 g, 3.94 mmol), while cooling in an ice bath and the mixture was left stirring for 15 minutes. 4,4'-(1,4-Phenylene)bis(butan-1-ol) (350 mg, 1.57 mmol) was added and the mixture was allowed to slowly warm to room temperature overnight, whilst stirring. The solvent was evaporated, hexanes (50 mL) and EtOAc (5 mL) were added, the mixture was filtered, and the solvent was then removed *in vacuo*. The crude product was purified by flash chromatography on silica (hexanes) to give the title compound as white crystals (140 mg, 25 %).

^{1}H NMR (400 MHz, $CDCl_3$) δ: 7.10 (s, 4H, Ph), 3.42 (t, 4H, J = 6.8, CH_2), 2.61 (t, 4H, J=7.6, CH_2) 1.89 (m, 4H, CH_2) 1.76 (m, 4H, CH_2). ^{13}C NMR (100 MHz, $CDCl_3$) δ: 141.5, 130.6, 36.7, 35.8, 34.4, 32.1. *m/z* 366.0 $[M+NH_4]^+$.

5.1.9: 1,4-bis(4-(methylthio)butyl)benzene, 4[Ph]4-SMe

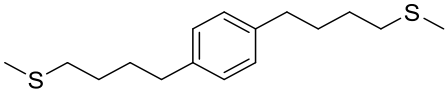

To a solution of sodium thiomethoxide (0.12 g, 1.7 mmol) in dry ethanol (8 mL) under Ar, 1,4-bis(4-bromobutyl)benzene (0.103 g, 0.287 mmol) dissolved in dry THF (7 mL) was added via cannula. After stirring for three hours the resulting suspension was quenched with water (15 mL), and the product was extracted with diethyl ether (3 x 30 mL). The combined organic phases were washed successively with brine (2 x 15 mL) and water (2 x 20mL) and dried over $MgSO_4$. The solvent was removed *in vacuo* and the crude product was purified by flash column chromatography on silica (4% EtOAc in hexanes) and recrystallised from boiling hexanes to give the title compound as white solid that liquefied overnight. (68 mg 83 %).

Found C = 68.69, H = 9.60, S = 20.02 %. $C_{16}H_{26}S_2$ requires C = 68.02, H = 9.28, S = 22.70 %. ^{1}H NMR (400 MHz, $CDCl_3$) δ: 7.09 (s, 4H, Ph.), 2.60 (t, 4H, J = 7.2 Hz, CH_2), 2.50 (t, 4H, J = 7.2, CH_2) 2.09 (s, 6H, CH_3), 1.68 (m, 8H, CH_2) ^{13}C NMR (100 MHz, $CDCl_3$) δ: 139.57, 128.32, 35.07, 34.14, 30.55, 28.74, 15.55. *m/z* (HRMS, CI, CH_4) 283.1553 $[M+H]^+$. $C_{16}H_{27}S_2$ calc. 283.1554.

5.1.10: 1,4-bis(5-chloropent-1-yn-1-yl)benzene

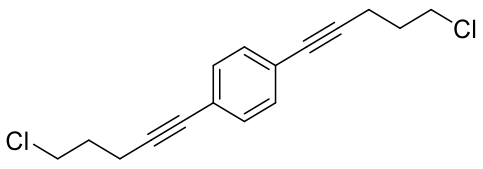

1,4 diiodobenzene (1.50 g, 4.55 mmol), $[PdCl_2(MeCN)_2]$ (0.059 g, 0.23 mmol), triphenylphosphine (179 mg, 0.66 mmol) and CuI (87 mg, 0.45 mmol) were mixed in DIPA (60 ml) and the resulting suspension was degassed by bubbling argon through for 50 minutes. 5-Chloro-1-pentyne (1.2 mL, 11.38 mmol) was added and the resulting suspension was stirred for 24 hours under argon atmosphere at room temperature. The solvent was then removed *in vacuo*, the solid was picked up in CH_2Cl_2 and the suspension was filtered. After further removal of the solvent, the crude product was purified by flash chromatography on silica (0.5 % EtOAc in

hexanes) and recrystallised from hexanes to give the title compound as a pale-yellow solid (830 mg, 66 % yield).

^{1}H NMR (400 MHz, $CDCl_3$) δ: 7.31 (s, 4H, Ph.), 3.71 (t, 4H, J = 6.4, CH_2), 2.62 (t, 4H, J = 6.8, CH_2), 2.06 (q, 4H, J = 6.4, 6.8 Hz, CH_2). ^{13}C NMR (100 MHz, $CDCl_3$) δ: 131.45, 123.02, 89.75, 81.24, 43.73, 31.41, 16.70. *m/z* 304.2 $[M+NH_4]^+$.

5.1.11: 1,4-bis(5-chloropentyl)benzene

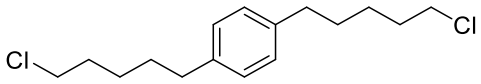

1,4-bis(5-chloropent-1-yn-1-yl)benzene (0.80 g, 2.86 mmol) was subjected to catalytic hydrogenation (25 mL EtOAc, 25 mL MeOH, 130 mg Pd/C 10 %, H_2 atmosphere, 24 h, room temperature). The resulting solution was filtered through a bed of Celite® and the solvent was removed *in vacuo.* The crude product was purified by flash chromatography on silica (10 % EtOAc in hexanes) to give the title compound as a white solid (0.722 g, 88 %).

^{1}H NMR (400 MHz, $CDCl_3$) δ: 7.09 (s, 4H, Ph.), 3.53 (t, 4H, J=6.8, CH_2), 2.59 (t, 4H, J = 8.0, CH_2), 1.80 (m, 4H, CH_2), 1.63 (m, 4H, CH_2), 1.47 (m, 4H, CH_2). ^{13}C NMR (100 MHz, $CDCl_3$) δ: 131.78, 128.13, 45.06, 35.09, 32.28, 30.76, 26.65. *m/z* 304.2 $[M+NH_4]^+$.

5.1.12: *S,S'*-(1,4-phenylenebis(pentane-5,1-diyl)) diethanethioate

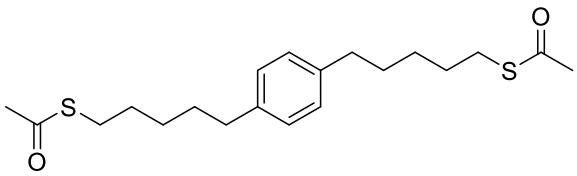

Potassium thioacetate (1 g, 8.8 mmol), sodium iodide (188 mg, 1.26 mmol) and 1,4-bis(5-chloropentyl)benzene (700 mg, 2.48 mmol) were mixed in acetone (70 mL) and

the resulting suspension gently refluxed overnight. The resulting mixture was evaporated and water was added (10 mL), the product was extracted with CH_2Cl_2 (3 X 40 mL), the combined organic portions were washed with brine (20 mL), and dried over $MgSO_4$. The solvent was removed *in vacuo* and the crude product was purified by flash column chromatography on silica (20 % EtOAc in hexanes) and recrystallised from hexanes to give the title compound as orange crystals (478 mg, 54 %).

Found C = 65.37, H = 8.13, S = 17.82 %. $C_{20}H_{30}O_2S_2$ requires C = 65.53, H = 8.25, S = 17.49 %. ^{1}H NMR (400 MHz, $CDCl^3$, TMS) δ: 7.07 (s, 4H, Ph.), 2.86 (t, 4H, J = 7.2, CH_2), 2.56 (t, 4H, J = 7.6, CH_2), 2.32 (s, 6H, CH_3), 1.60 (m, 8H, CH_2), 1.40 (m, 4H, CH_2). ^{13}C NMR (100 MHz, $CDCl^3$) δ: 198.13, 139.70, 128.21, 35.32, 31.02, 30.65, 29.42, 29.05, 28.48. *m/z* (HRMS, CI, NH_3) 367.1775 $[M+H]^+$. $C_{20}H_{31}O_2S_2$ calc. 367.1765.

5.1.13: 1,4-bis(5-(methylthio)pentyl)benzene, 5[Ph]5-SMe

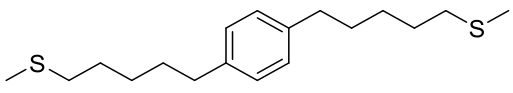

To a solution of *S,S'*-(1,4-phenylenebis(pentane-5,1-diyl)) diethanethioate (180 mg, 0.51 mmol) in ethanol (5 mL) was added a solution of sodium hydroxide (100 mg, 255 mmol) in ethanol (6 mL) while cooling in an ice bath. The suspension was stirred for 15 minutes at 0° C before iodomethane (0.063 mL, 1.02 mmol) in ethanol (0.6 mL) was added. After stirring overnight, the resulting suspension was quenched with NH_4Cl (aq. sat., 15 mL), and the mixture was extracted with CH_2Cl_2 (3 x 50 mL). The combined organic phases were washed with brine (50 mL), dried over $MgSO_4$, filtered, and the solvent removed under vacuum. Purification by column chromatography on silica (30 % CH_2Cl_2 in hexanes) afforded the title compound as clear oil (130 mg, 86 %).

Found C = 70.87, H = 9.98, S = 20.25 %. $C_{18}H_{30}S_2$ requires C = 65.61, H = 9.74, S = 20.65 %. ^{1}H NMR (400 MHz, $CDCl_3$) δ: 7.08 (s, 4H, Ph.), 2.58 (t, 4H, J = 7.6 Hz, CH_2), 2.49 (t, 4H, J = 7.6 Hz, CH_2), 2.09 (s, 6H, CH_3), 1.63 (m, 8H, CH_2), 1.43 (m, 4H, CH_2). ^{13}C

NMR (100 MHz, $CDCl_3$) δ: 128.28, 39.85, 35.43, 34.25, 31.17, 29.12, 28.53. *m/z* (HRMS, CI, CH_4) 311.1873 $[M+H]^+$. $C_{18}H_{31}S_2$ calc. 311.1867.

5.1.14: 1,4-bis(6-(methylthio)hexyl)benzene, 6[Ph]6-SMe

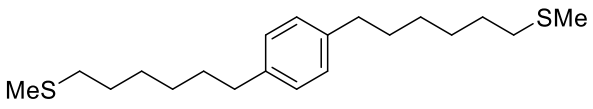

To a solution of sodium thiomethoxide (1.32 g, 18.8 mmol) in ethanol (25 mL) was added dropwise a solution of 1,4-bis(chlorohexyl)benzene[46] (0.987 g, 3.14 mmol) in THF (20 mL). The resulting solution was stirred at room temperature for 16 hours, during which time a white precipitate appeared. The suspension was filtered, the filtrate concentrated *in vacuo* to a thick oil, which was extracted in CH_2Cl_2 (30 mL) and washed with water (3 x 25 mL) and brine (25 mL). The organic phase was then dried over $MgSO_4$, filtered, and concentrated *in vacuo* to a yellow oil. Column chromatography on silica (20 % CH_2Cl_2 in hexanes) afforded the title compound as clear oil (0.574 g, 54 %).

Found C = 71.42, H = 10.21, S = 18.37 %. $C_{20}H_{34}S_2$ requires C = 70.94, H = 10.12, S = 18.94 %. ^{1}H NMR (400 MHz, $CDCl_3$) δ: 7.08 (s, 4H, Ph.), 2.57 (t, 4H, J = 7.6, CH_2), 2.48 (t, 4H, J = 7.2, CH_2), 2.08 (s, 6H, CH_3), 1.59 (m, 8H, CH_2), 1.48-1.32 (m, 8H, CH_2). ^{13}C NMR (100 MHz, $CDCl_3$) δ: 139.9, 128.3, 35.5, 34.3, 31.4, 29.1, 28.9, 28.7, 15.6. *m/z* (HRMS, CI, CH_4) 339.2183 $[M+H]^+$. $C_{20}H_{35}S_2$ calc. 339.2180.

5.1.16 2,2'-(1,4-phenylene)bis(ethan-1-ol)

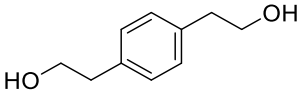

Conc. H_2SO_4 (98 %; 1 mL) was added to a solution of 2,2'-(1,4-phenylene)diacetic acid (3.00 g, 15.45 mmol) in methanol (100 mL). The solution was then refluxed for 16 h, and then allowed to reach room temperature. The solvent was removed in vacuo, the product was extracted into dichloromethane (50 mL) and washed successively

with a saturated solution of Na_2CO_3 (3 x 30 mL), water (30 mL) and brine (30 mL), dried over $MgSO_4$ and concentrated to dryness. The crude product was suspended in THF (100 mL), sodium borohydride (7.0 g, 185.4 mmol) was added portionwise and the mixture was gently refluxed for 15 minutes. After that time methanol (50 mL) was added dropwise during a period of 15 minutes and the reaction was left stirring under reflux for 1 h. The mixture was then cooled to 0 °C, quenched with a saturated solution of NH_4Cl (60 mL) and left stirring for 2 hours. The solvent was removed in vacuo and the solid was extracted into dichloromethane (80 mL) and washed successively with water (50 mL) and brine (50 mL). The organic phase was then dried over $MgSO_4$ and concentrated. The crude product was purified by flash column chromatography on silica (50 % ethyl acetate in hexanes) to give the title compound as a white solid (1.29 g, 50 %).

^{1}H NMR (400 MHz, $CDCl_3$) δ: 7.19 (s, 4H, Ph.), 3.86 (t, 4H, J = 6.8 Hz, CH_2), 2.85 (t, 4H, J = 6.4 Hz, CH_2), 1.45 (s broad, OH). ^{13}C NMR (100 MHz, $CDCl_3$) δ: 136.63, 129.28, 63.69, 38.78. m/z (HRMS, CI, CH_4): 149.0961 $[(M - H_2O) + H]^+$. $C_{10}H_{13}O$ calc. 149.0966.

5.1.17 1,4-phenylenebis(ethane-2,1-diyl) bis(4-methylbenzenesulfonate)

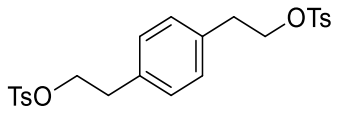

Pyridine (0.89 mL, 10.95 mmol) and tosyl chloride (1.57 g, 8.21 mmol) were added to a solution of 2,2'-(1,4-phenylene)bis(ethan-1-ol) (0.45 g, 2.74 mmol) in chloroform (30 mL) at 0 °C. The resulting suspension was stirred for 20 hours during which time it returned to room temperature. After this time, water (10 mL) and diethyl ether (30 mL) were added, the layers were separated, the organic phase was washed with HCl 2M (20 mL), $NaHCO_3$ (5 %, 20 mL) and brine (30 mL) and dried over $MgSO_4$. After filtration and solvent evaporation, the crude solid was purified by column chromatography on silica (hexanes:ethyl acetate 8:2, followed by ethyl acetate:dichloromethane 1:1) to give the title compound as a white powder (0.50 g, 38 %).

^{1}H NMR (400 MHz, $CDCl_3$) δ: 7.70 (d, 4H, J = 8 Hz, Ph.), 7.30 (d, 4H, J = 8.4 Hz, Ph.), 7.02 (s, 4H, Ph.) 4.18 (t, 4H, J = 6.8 Hz, CH_2), 2.92 (t, 4H, J = 6.8 Hz, CH_2), 2.44 (s, 6H, CH_3). ^{13}C NMR (100 MHz, $CDCl_3$) δ: 144.78, 134.86, 132.92, 129.83, 129.14, 127.86, 70.45, 34.94, 21.66. m/z (HRMS, CI, CH_4): 497.1058 $[M + Na]^+$. $C_{24}H_{26}O_6S_2Na$ calc. 497.1068.

5.1.18 *S*,*S*'-(1,4-phenylenebis(ethane-2,1-diyl)) diethanethioate, 2[Ph]2

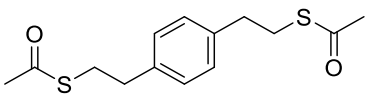

A solution of 1,4-phenylenebis(ethane-2,1-diyl) bis(4-methylbenzenesulfonate) (0.22 g, 0.46 mmol), potassium thioacetate (0.185 g, 1.62 mmol), sodium iodide (0.035 g, 0.23 mmol) in acetone (45 mL) was gently refluxed for 16 hours. After cooling down to room temperature, the solvent was removed in vacuo, the crude solid was extracted into dichloromethane (30 mL) and washed with water (20 mL). The water phase was extracted with dichloromethane (2 x 30 mL), the combined organic phase was washed with brine (20 mL), dried over $MgSO_4$, and the solvent was removed in vacuo. The resulting solid was recrystallized from hexanes to afford the title compound as an off-white solid (0.08 g, 61 %).

$C_{14}H_{18}O_2S_2$ requires: C = 59.54, H = 6.42, S = 22.70 %. Found: C = 59.29, H = 6.34, S = 22.90 %. ^{1}H NMR (400 MHz, $CDCl_3$) δ: 7.16 (s, 4H, Ph), 3.11 (t, 4H, J = 8.4 Hz, CH_2), 2.84 (t, 4H, J = 7.2 Hz, CH_2), 2.33 (s, 6H, CH_3). ^{13}C NMR (100 MHz, $CDCl_3$) δ: 195.75, 138.20, 128.71, 35.41, 30.71, 30.51. m/z (HRMS, CI, CH_4): 305.0641 $[M + Na]^+$. $C_{24}H_{26}O_6S_2Na$ calc. 305.0646.

5.2.1: 3,3’,5,5’-tetrabromo-2,2’-bithiophene

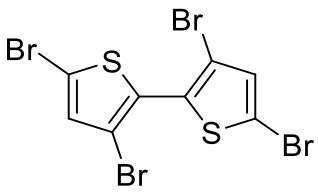

Synthesized by modification of the literature procedure.[82]

A solution of 2,2'-bithiophene (10.0 g, 60.2 mmol) in acetic acid (50 mL) and chloroform (100 mL) was cooled to 0 °C and bromine (16 mL, 300 mmol) was added dropwise over the course of 1 hr. The mixture was then warmed to room temperature and stirred for 2 hours, and then warmed to 60°C for 2 hours. The mixture was then poured into 300 mL of ice-cooled methanol and filtered. The resulting solid was recrystallized four times from ethanol and triturated in hexanes once to afford 14.2 g (49 %) of an off-white solid.

^{1}H NMR (400 MHz, $CDCl_3$) δ:7.05 (s, 2H). ^{13}C NMR (100 MHz, $CDCl_3$) δ 133.00, 129.55, 114.83, 112.13.

5.2.2: 3,3'-dibromo-5,5'-bis(methylthio)-2,2'-bithiophene

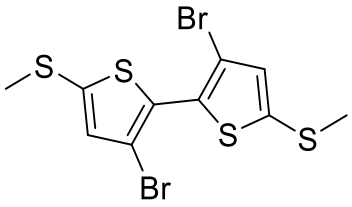

To a solution of 3,3',5,5'-tetrabromo-2,2'-bithiophene (4.22 g, 8.8 mmol) in dry THF (115 mL) under Ar atmosphere that was cooled to -78 °C and *n*-butyllithium (11mL, 17.5 mmol, 1.60 M in Hexanes) was added dropwise while stirring. The resulting yellow solution was stirred for 45 minutes and dimethyl disulfide (1.7 mL, 18.4 mmol) was added dropwise. The mixture was left to reach rt with stirring overnight. The solvent was then removed *via vacuum* and the crude material was taken up into DCM (50 mL) and washed with water (2x25 ml) and brine (25 mL). The organic layer was

then dried over $MgSO_4$ and the solvent was evaporated *via vacuum* to give an orange oil that was purified by precipitation in DCM/hexanes at –61°C to give the title compound as a pale-yellow solid (2.51 g 69 %).

^{1}H NMR (400 MHz, $CDCl_3$) δ: 6.97 (s, 2H, Th), 2.54 (s, 6H, CH_3). ^{13}C NMR (100 MHz, $CDCl_3$) δ: 140.32, 132.28, 129.62, 111.64, 20.95.

5.2.3 2,6-bis(methylthio)-4,4-diphenyl-4*H*-silolo[3,2-*b*:4,5-*b'*]dithiophene, TSiPh$_2$T

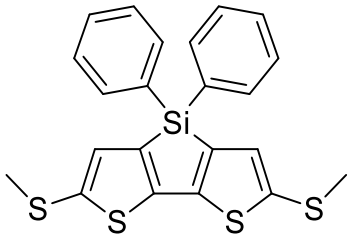

To a solution of 3,3'-dibromo-5,5'-bis(methylthio)-2,2'-bithiophene (0.5 g, 1.2 mmol) in dry THF (35 mL) at -78 °C *n*-butyllithium (2 mL, 2.6 mmol, 1.35 M in Hexanes) was added dropwise whilst stirring. The resulting yellow solution was stirred for 45 minutes at that temperature and dichlorodiphenylsilane (0.66 g, 2.6 mmol) was added in one portion. The mixture was immediately heated to 40 °C and stirred for 3 hours. After this time, the reaction flask was open ad water (50 mL) was added and the product extracted with diethyl ether (3 x 35 mL). The combined organic fractions were dried over $MgSO_4$, filtered, the solvent removed *via vacuum* to give a clear oil that was purified by column chromatography (SiO_2, 25 % CH_2Cl_2 in hexanes) to give the title compound as bright yellow solid (0.186 g, 36 %).

Found: C = 60.59, H = 4.48, S = 28.59. $C_{22}H_{18}S_4Si$ requires C = 60.23, H = 4.24, S = 29.23. ^{1}H NMR (400 MHz, $CDCl_3$): 7.65-7.55 (m, 4H, Ph), 7.45-7.35 (m, 8H, Ph), 7.20 (s, 2H, Th), 2.49 (s, 6H, CH_3) ppm. ^{13}C NMR (100 MHz, $CDCl_3$): 152.1, 139.7, 138.5, 135.4, 134.8, 134.4, 130.5, 128.3, 22.4. *m/z* (HRMS, CI, CH_4) 439.0143 $[M + H]^+$, $C_{22}H_{19}S_4Si$ calc. 439.0139.

5.2.4 2,6-bis(methylthio)-4,4-diphenyl-4*H*-germolo[3,2-*b*:4,5-*b'*]dithiophene, $TGePh_2T$

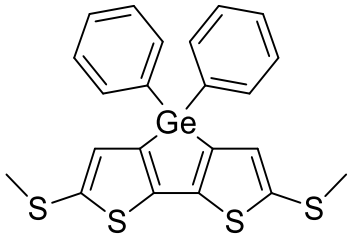

To a solution of 3,3'-dibromo-5,5'-bis(methylthio)-2,2'-bithiophene (0.40 g, 0.961 mmol) in dry THF (30 mL) at -78 °C *n*-butyllithium (0.85 mL, 1.28 mmol, 1.5 M in Hexanes) was added dropwise whilst stirring. The resulting yellow solution was stirred for 30 minutes at that temperature and dichlorodiphenylgermane (0.2 mL, 0.96 mmol) was slowly added. The mixture was stirred overnight. After this time, the solvent was removed, and the solid residues were picked up with DCM (100 mL) and water was added. The organic layer was separated and washed again with water (20 mL) and with brine (20 mL). The organic layer was then dried over $MgSO_4$, filtered, the solvent removed *via vacuum* to give an oil that was purified by column chromatography (SiO_2, 2 % EtOAc in hexanes) to give the title compound as white-yellow solid (0.88 g, 19 %).

Found: C = 54.69, H = 3.81, S = 26.54. $C_{22}H_{18}S_4Ge$ requires C = 54.68, H = 3.75, S = 26.54. ^{1}H NMR (400 MHz, $CDCl_3$): 7.56-7.54 (m, 4H, Ph), 7.42-7.37 (m, 8H, Ph), 7.18 (s, 2H, Th), 2.50 (s, 6H, CH_3) ppm. ^{13}C NMR (100 MHz, $CDCl_3$): 149.8, 140.1, 138.2, 134.6, 134.3, 133.6, 130.0, 128.7, 22.8. *m/z* (HRMS, CI, CH_4) 483.9662 $[M]^+$, $C_{22}H_{18}S_4Ge$ calc. 483.9503.

5.2.5 3,5,5'-tribromo-2,2'-bithiophene

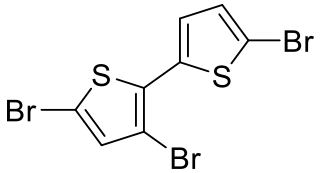

A solution of 2,2'-bithiophene (6.0 g, 36.1 mmol) in acetic acid (30 mL) and chloroform (40 mL) was cooled to 0°C and bromine (5.6 mL, 108 mmol) was added dropwise over the course of 1 hr. The mixture was then warmed to room temperature and stirred 2 hours, and then warmed to 60°C for 2 hours. The mixture was then poured into 100 mL of ice-cooled methanol and filtered. The resulting solid was dissolved in DCM (150 mL) and washed several times with saturated $NaHCO_3$(aq) (4x50mL), the organic layer was then dried over $MgSO_4$, filtered, the solvent removed *via vacuum* to give a green/brown solid that was purified by recrystallized from $CHCl_3$/hexane to afford 7.9 g (54 %) of a yellow solid.

^{1}H NMR (400 MHz, $CDCl_3$) δ: 7.05 (d, J 3.9 Hz, 1H, Th), 7.01 (d, J 3.9 Hz, 1H, Th), 6.89 (s,1H, Th). ^{13}C NMR (100 MHz, $CDCl_3$) δ: 133.7, 132.7, 132.1, 129.0, 126.0, 112.7, 110.4, 106.3.

5.2.6 3-bromo-5,5'-bis(methylthio)-2,2'-bithiophene

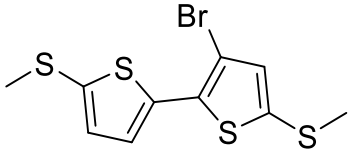

To a solution of 3,5,5'-tribromo-2,2'-bithiophene (3 g, 7.4 mmol) in dry THF (35 mL) under Ar atmosphere that was cooled at -78 °C, *n*-butyllithium (9.3 mL, 14.9 mmol, 1.6 M in Hexanes) was added dropwise while stirring. The resulting dark yellow solution was stirred for 30 minutes and dimethyl disulfide (1.4 mL, 15.6 mmol) was added dropwise. The mixture was left reach rt and stirred overnight. The solvent was then removed *via vacuum* and the orange-brown crude was picked up in EtOAc (150 mL) and washed with water (2x25 ml) and brine (25 mL). The organic layer was then dried over $MgSO_4$ and the solvent evaporated *via vacuum* to give a dark yellow oil that was purified by column chromatography (SiO_2, 100 % hexanes) and by crystallization in DCM and hexanes to give the title compound as a dark yellow solid (0.33 g, 13 %).

^{1}H NMR (400 MHz, $CDCl_3$) δ: 7.18 (d, 1H, J = 3.6 Hz, Th), 7.00 (d, 1H, J = 3.6 Hz, Th), 6.93 (s, 1H, Th), 2.53 (s, 3H, CH_3), 2.51 (s, 3H, CH_3). ^{13}C NMR (100 MHz, $CDCl_3$) δ 139.5, 138.6, 136.8, 135.8, 134.0, 130.6, 126.7, 106.9, 21.8, 21.3. (HRMS, CI, CH_4) 258.9739 $[M - Br + H]^+$, $C_{10}H_{11}S_4$ calc. 258.9743.

5.2.7 (5,5'-bis(methylthio)-[2,2'-bithiophen]-3-yl)diphenylmethanol

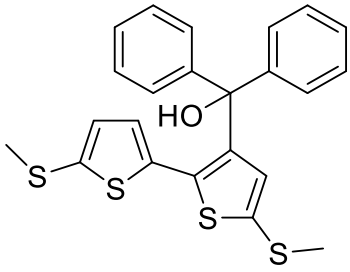

To a solution of 3-bromo-5,5'-bis(methylthio)-2,2'-bithiophene (0.3 g, 0.89 mmol) in dry THF (20 mL) at -78 °C *n*-butyllithium (1.6 M, 0.89 mmol) was added dropwise whilst stirring. The resulting yellow solution was stirred for 120 minutes at that temperature and a solution of benzophenone (0.24 g, 1.33 mmol) in dry THF (4 mL) was slowly added. The mixture was brought to rt and stirred overnight. After this time, the reaction mixture was poured into a saturated solution of ammonium chloride (12.5 mL) and allowed to stir for 5 minutes. The organic layer was then separated, and the aqueous layer was extracted with EtOAc (3x 30 mL). The combined organic layers were then dried over $MgSO_4$, filtered, and the solvent removed *via vacuum* to give a thick dark yellow oil that was purified by column chromatography (SiO_2, 5 % EtOAc in hexanes) to give the title compound as a thick green-yellow oil (0.26 g, 65 %).

^{1}H NMR (400 MHz, $CDCl_3$) δ:7.30 (m, 10H, Ph), 6.77 (d, 1H, J = 3.6 Hz, Th), 6.47 (d, 1H, J = 3.7 Hz, Th), 6.37 (s, 1H, Th), 2.47 (s, 3H, CH_3), 2.44 (s, 3H, CH_3). ^{13}C NMR (100 MHz, $CDCl_3$) δ 146.9, 146.4, 145.6, 139.9, 136.4, 135.7, 134.0, 133.0, 130.3, 128.9, 128.1, 127.5, 80.5, 21.6, 21.4. (HRMS, MeOH) 463.0282 $[M + Na]^+$, $C_{23}H_{20}OS_4Na$ calc. 463.0294.

5.2.8 2,6-bis(methylthio)-4,4-diphenyl-4H-cyclopenta[2,1-b:3,4-b']dithiophene, TCPh$_2$T

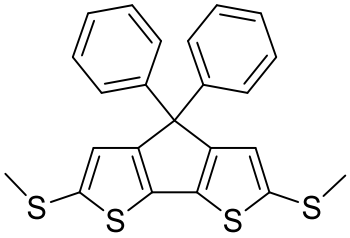

To a solution of (5,5'-bis(methylthio)-[2,2'-bithiophen]-3-yl)diphenylmethanol (0.2 g, 0.45 mmol) dry $CHCl_3$ (15 ml) under Ar atmosphere was slowly added a solution of $SnCl_4$ (0.16 g, 0.62 mmol) in $CHCl_3$ (2 mL), the mixture turned dark immediately and the reaction mixture was left stirring for further 30 mins. The reaction mixture was then poured into a saturated solution of $NaHCO_3$ (12.5 mL) and allowed to stir for 5 minutes. The organic layer was then separated, and the aqueous layer extracted with $CHCl_3$ (3x 30 mL). The combined organic layers were then dried over $MgSO_4$, filtered, and the solvent removed *via vacuum* to give a thick yellow oil that was purified by a short chromatography column (SiO_2, 5 % EtOAc in hexanes) to give the title compound as an orange solid (0.1 g, 52 %).

^{1}H NMR (400 MHz, CD_2Cl_2): 7.31-7.27 (m, 6H, Ph), 7.25-7.21 (m, 4H, Ph), 7.14 (s, 2H, Th), 2.54 (s, 6H, CH_3) ppm. ^{13}C NMR (100 MHz, $CDCl_3$): 156.5, 143.8, 139.1, 138.7, 128.9, 128.7, 128.0, 127.4, 63.4, 23.2. (HRMS, CI, CH_4) 423.0378 $[M + H]^+$, $C_{23}H_{19}S_4$ calc. 423.0369.

5.3.1: 2,6-bis(methylthio)-4*H*-cyclopenta[2,1-*b*:3,4-*b'*]dithiophen-4-one, TKT

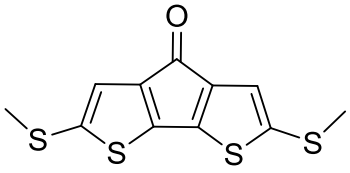

To a solution of 3,3'-dibromo-5,5'-bis(methylthio)-2,2'-bithiophene (600 mg, 1.44 mmol) in dry THF (80 mL) under Ar atmosphere that was cooled at –78 °C *n*-butyllithium (1.8 mL, 2.9 mmol, 1.6 M in Hexanes) was added dropwise while stirring. The resulting dark yellow solution was stirred for 30 minutes and a solution of

carbamoyl chloride (0.14 mL, 1.44 mmol) in THF (1 mL) was added dropwise. The mixture was left stirring at –78 °C for 2.5 hours then warmed to –40 °C and a solution of NH_4Cl_{aq} (10 mL, saturated) was added and the mixture was left reach rt and was stirred overnight. The organic layer was then separated, and the aqueous layer was extracted once with hexanes (20 mL). The organic layers were reunited, dried over $MgSO_4$ and the solvent was evaporated *via vacuum* to give a dark brown oil that was purified by column chromatography on silica (2 % EtOAc in hexanes) and by subsequent crystallization from DCM and hexanes affording the title compound as dark violet crystals (330 mg, 80 %).

Found C = 47.26, H = 3.17, S = 45.00 %. $C_{11}H_8OS_4$ requires C = 46.45, H = 2.84, S = 45.09 %. ^{1}H NMR (400 MHz, $CDCl_3$) δ: 7.02 (s, 2H, Th), 2.48 (s, 6H, CH_3). ^{13}C NMR (100 MHz, $CDCl_3$) δ: 182.25, 150.88, 140.89, 140.54, 126.64, 23.03. *m/z* (HRMS, CI, CH_4) 284.9530 $[M+H]^+$. $C_{11}H_8OS_4$ calc. 283.9458.

5.3.2: 2,7-bis(methylthio)benzo[2,1-b:3,4-b']dithiophene-4,5-dione, TDKT

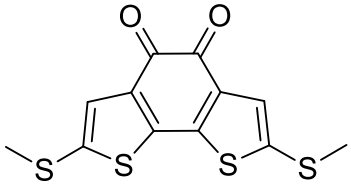

To a flask A *n*-butyllithium (1.6 mL, 2.5 mmol) was added dropwise to dry THF (6 mL) at –78 °C under Ar atmosphere and was stirred for 10 minutes, afterwards a solution of 3,3'-dibromo-5,5'-bis(methylthio)-2,2'-bithiophene (500 mg, 1.2 mmol) in dry THF (5 mL) was added dropwise over 30 minutes and was left stirring at –78 °C for 1 hour. At the same time to another flask B containing dry THF (10 mL) under Ar atmosphere LiBr (208 mg, 2.5 mmol) was added and dissolved, afterwards CuBr (172 mg, 1.2 mmol) was added. The green suspension was left stirring for at least 1 hour and was then cooled –78 °C. Another solution C was prepared containing dry THF (6 mL) and oxalyl chloride (0.1 mL, 1.2 mmol) and was cooled at –78 °C. Afterwards the solution A was cannulated into solution B slowly and dropwise over the course of 1 hour. After

10 minutes more, solution C was cannulated into solution A + B very slowly and dropwise (0.5 mL/minute). The resulting suspension was then left stirring for two hours and was then warmed to RT and quenched with 5 mL of saturated aqueous ammonium chloride. The mixture was stirred for 10 minutes, the organic layer was then separated, and the aqueous layer was extracted with EtOAc (3x50), the organic layers were reunited and washed with water (20 mL) then brine (20 mL), dried over $MgSO_4$ and then evaporated *via vacuum* to give a dark brown oil. At first the purification was tried by a flash column chromatography on silica without success (2% EtOAc in hexanes to 100 % EtOAc. TLC in EtOAc:hexanes 20:90 gave R_f = 0.5 for the title compound). The silica gel from the column was then sonicated with DCM, MeOH and EtOAc (30/20/50) in order to dissolve the compound and the solvent was filtered and evaporated. The obtained dark green oil was then purified by preparative TLC silica on glass (20 % EtOAc in hexanes) and by subsequent crystallization from DCM and hexanes affording the title compound as dark crystals (25 mg, 7 %).
^{1}H NMR (500 MHz, $CDCl_3$) δ: 7.37 (s, 2H, Th), 2.58 (s, 6H, CH_3). ^{13}C NMR (125 MHz, $CDCl_3$) δ: 164.50, 144.00, 140.70, 135.03, 128.93, 21.03. *m/z* (HRMS, CI, NH_3) 312.9476 $[M+H]^+$. $C_{12}H_9O_2S_4$ calc. 312.9485.

5.3.3 4,4-dimethyl-4H-cyclopenta[2,1-b:3,4-b']dithiophene

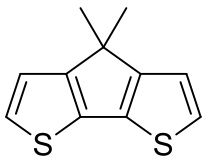

Prepared by modifying a published procedure[60] A suspension of finely ground potassium hydroxide (1.57 g, 28 mmol) and 4H-cyclopenta[2,1-b;3,4-b']dithiophene (1 g, 5.6 mmol) in DMSO (20 mL) was stirred for 1 hour. After this time, methyl iodide (2.39 g, 16 mmol) was added, and the reaction mixture was stirred overnight at room temperature. Water (20 mL) was added to the mixture, and the product was extracted with CH_2Cl_2 (3 x 20 mL). Purification by column chromatography on silica (100% hexanes) gave the title compound as a white solid (1.10 g, 95%).

^{1}H NMR (400 MHz, $CDCl_3$) δ:7.07 (d, 2H, J = 4.8 Hz), 6.91 (d, 2H, J = 4.8 Hz), 1.43 (s, 6H). ^{13}C NMR (100 MHz, $CDCl_3$) δ 160.6, 135.2, 124.8, 120.9, 44.0, 25.1.

5.3.4 2,6-dibromo-4,4-dimethyl-4H-cyclopenta[2,1-b:3,4-b']dithiophene

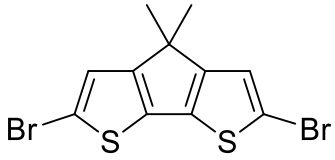

Prepared by modifying a published procedure.[60] To a solution of **1a** (0.50 g, 2.42 mmol) in anhydrous DMF (18 mL), N-bromosuccinimide (0.863 g, 4.85 mmol) was added portionwise in the dark, and the reaction mixture was stirred at room temperature for 1 hour under Ar atmosphere. After this time, the suspension was poured into 10 mL of saturated aqueous sodium thiosulfate, and the product extracted with hexane (3 x 20 mL). The combined organic phases were washed with brine, dried over MgSO4, filtered, and the solvent was removed *in vacuo*. Purification by column chromatography on silica (100 % hexanes) and subsequent recrystallisation from boiling hexane gave the title compound as a white solid (0.397 g, 45%).

^{1}H NMR (400 MHz, $CDCl_3$) δ:7.07 (d, 2H, J = 4.8 Hz), 1.40 (s, 6H). ^{13}C NMR (100 MHz, $CDCl_3$) δ 158.3, 135.1, 124.0, 111.4, 46.4, 24.8.

5.3.5 4,4-dimethyl-2,6-bis(methylthio)-4H-cyclopenta[2,1-b:3,4-b']dithiophene, $TCPh_2T$

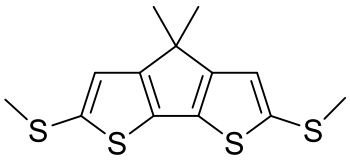

To a solution of 2,6-dibromo-4,4-dimethyl-4*H*-cyclopenta[2,1-*b*:3,4-*b*']dithiophene (247 mg, 0.68 mmol) in dry THF (18 mL) under Ar atmosphere that was cooled to –78 °C, *n*-butyllithium (0.93 mL, 1.49 mmol) was added dropwise while stirring. The resulting yellow solution was stirred for 45 minutes and dimethyl disulfide (0.13 mL, 1.49 mmol) was added dropwise. The mixture was left reach rt and stirred overnight. The solvent was then removed *via vacuum* and the crude product was extracted into DCM (25 mL) and washed with water (2x10 ml) and brine (15 mL). The organic layer was then dried over $MgSO_4$ and the solvent evaporated *via vacuum* to give an off-white solid that was purified by column chromatography on silica (100 % hexanes) and by subsequent crystallization from MeOH affording the title compound as white needle-like crystals (95 mg, 47 %).

Found C = 52.42, H = 4.79, S = 42.46 %. $C_{13}H_{14}S_4$ requires C = 52.31, H = 4.73, S = 42.96 %. ^{1}H NMR (400 MHz, $CDCl_3$) δ:7.27 (s, 2H, Th), 2.50 (s, 6H, SCH_3), 1.41 (s, 6H, $C(CH_3)_2$). ^{13}C NMR (100 MHz, $CDCl_3$) δ 159.54, 137.90, 136.90, 126.49, 45.76, 25,03, 23.37. *m/z* (HRMS, EI, EtOH) 297.9964 $[M+H]^+$. $C_{13}H_{14}S_4$ calc. 297.9978.

5.4.1 2,7-bis(5-(methylthio)thiophen-2-yl)-9*H*-fluorene, TFT

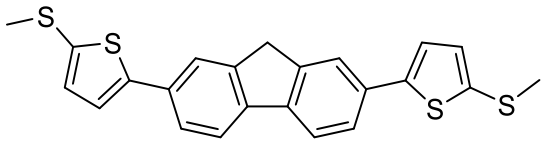

To a solution of 2,7-dibromo-9H-fluorene (550 mg, 1.7 mmol) in dry DMF (15 mL) was degassed for 1 hour with Ar, after that time $Pd(PPh_3)_4$ (170 mg 0.14 mmol) was added and the solution was degassed for further 10 minutes. At the end of this time the trimethyl(5-(methylthio) thiophen-2-yl)stannane (1.0 g, 3.4 mmol) was added via syringe. The solution was then warmed to 85°C for 24 hours. The mixture was then cooled to rt and filtered The solid from the filtration was purified by column chromatography (SiO_2, 30 % DCM in hexanes) and crystallized in a mixture of DCM and hexanes to give the title compound as an off-white solid (0.07 g, 10 %).

Found: C = 65.55, H = 4.40, S = 29.39. $C_{23}H_{18}S_4$ requires C = 65.36, H = 4.29, S = 30.34. ^{1}H NMR (400 MHz, $CDCl_3$) δ: 7.74 (m, 4H, Ph), 7.58 (d, 2H, J = 4.0 Hz, Ph), 7.20 (d, 2H,

J = 3.6 Hz, Th), 7.06 (d, 2H, J = 3.6 Hz, Th), 3.96 (s, 2H, CH_2), 2.54 (s, 6H, CH_3). ^{13}C NMR (100 MHz, $CDCl_3$) δ 147.0, 144.2, 140.8, 136.4, 132.8, 132.1, 124.7, 123.1, 122.2, 120.3, 36.9, 22.2 *m/z* (HRMS, CI, CH_4) 423.0367 $[M+H]^+$. $C_{23}H_{19}S_4$ calc. 423.0369.

5.4.2 2,7-bis(5-(methylthio)thiophen-2-yl)-9*H*-fluoren-9-one, TFOT

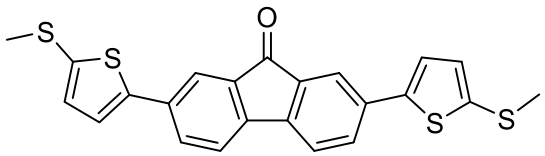

To a solution of 2,7-diiodo-9H-fluoren-9-one (330 mg, 0.76 mmol) in dry DMF (10 mL) was degassed for 1 hour with Ar. After that time $Pd(PPh_3)_4$ (88 mg 0.08 mmol) was added and the solution was degassed for further 10 minutes and heated to 65 °C. Trimethyl(5-(methylthio)thiophen-2-yl)stannane (0.45 g, 1.52 mmol) was added via syringe, and the solution was then warmed to 85 °C for 24 hours. The mixture was then cooled to room temperature and methanol (50 mL) was added. The resulting suspension was filtered, the residue dispersed in chloroform (50 mL), and filtered through a SiO_2 plug, eluting with further 100 mL of chloroform. The solvent was then removed, and the resulting pink solid was recrystallised from boiling methanol to give the title compound as a magenta powder (0.120 g, 36% yield).

^1H NMR (400 MHz, $CDCl_3$) δ: 7.81 (s, 2H, Ph), 7.62 (d, 2H, J = 7.7 Hz, Ph), 7.47 (d, 2H, J = 7.7 Hz, Ph), 7.20 (d, 2H, J = 3.5 Hz, Th), 7.03 (d, 2H, J = 3.5 Hz, Th), 2.54 (s, 6H, CH_3). ^{13}C NMR (100 MHz, $CDCl_3$) δ 193.2, 144.7, 142.8, 137.9, 135.1, 135.0, 131.7, 131.4, 124.0, 121.2, 120.9, 21.9

5.4.3: 4,4'-bis(5-(methylthio)thiophen-2-yl)-1,1'-biphenyl, TBPT

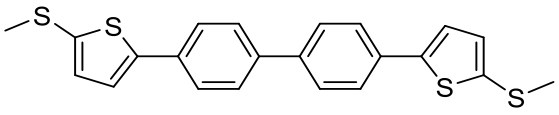

To a solution of 4,4'-diiodo-1,1'-biphenyl (500 mg, 1.2 mmol) in dry DMF (15 mL) was degassed for 1 hour with Ar, after that time $Pd(PPh_3)_4$ (210 mg 0.18 mmol) was added and the solution was degassed for further 10 minutes. At the end of this time the trimethyl(5-(methylthio)thiophen-2-yl)stannane (0.760 g, 2.6 mmol) was added via syringe. The solution was then warmed to 85°C for 36 hours. The mixture was then cooled to rt and filtered The solid from the filtration was purified by column chromatography (SiO_2, 30 % DCM to 100 % in hexanes) and crystallized in a mixture of DCM and hexanes to give the title compound as an orange solid (0.04 g, 8 %).

^{1}H NMR (400 MHz, $CDCl_3$) δ: 7.65 (s, 8H, Ph), 7.22 (d, 2H, J = 3.6 Hz, Th), 7.08 (d, 2H, J = 3.6 Hz, Th), 2.57 (s, 6H, CH_3). ^{13}C NMR (100 MHz, DMSO) δ 143.7, 139.2, 133.8, 128.8, 127.5, 126.6, 126.0, 120.2, , 23.1. *m/z* (HRMS, Cl, CH_4) 411.0374 $[M+H]^+$. $C_{22}H_{19}S_4$ calc. 411.0369.

5.4.4 4,4,5,5-tetramethyl-2-(5-(methylthio)thiophen-2-yl)-1,3,2-dioxaborolane

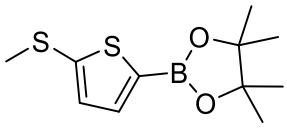

A solution of 2-(methylthio)thiophene (3.0 g, 23 mmol) in dry THF (50 mL) was cooled at -78°C and n-BuLi was slowly added via syringe (17.3 mL, 1.6 M). The mixture was left stirring for 1 hour, and then warmed at room temperature for another hour. The solution was cooled again at -61°C and 2-isopropoxy-4,4,5,5-tetramethyl-1,3,2-dioxaborolane (10.3 mL, 50.7 mmol) was added by a syringe. The resulting mixture was left stirring overnight while slowly reached rt. The solvent was removed via vacuum and the product was picked up with diethyl ether (50 mL) and washed with water (25 ml). The organic layer was then dried over dry $MgSO_4$ and the solvent was removed under reduced pressure to provide the title compound as pale-yellow oil (5 g, 85%).

^{1}H NMR (400 MHz, $CDCl_3$) d 7.48 (d, J = 3.6 Hz, 1H), 7.04 (d, J = 3.6 Hz, 1H), 2.54 (s, 3H), 1.33 (s, 12H). ^{13}C NMR (100 MHz, $CDCl_3$) δ: 145.7, 137.6, 129.5, 84.1, 24.7, 24.9, 20.8.

5.4.5 2,7-bis(5-(methylthio)thiophen-2-yl)phenanthrene-9,10-dione, TPDT

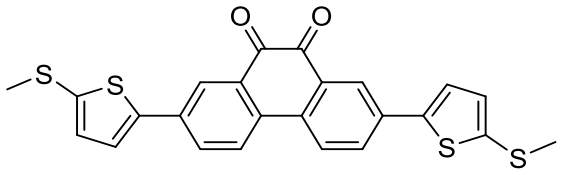

Into a 25 mL two neck flask fitted with a condenser $Pd_2(dba_3)CHCl_3$ (90 mg, 0.10 mmol), 2,7-diiodophenanthrene-9,10-dione (450 mg, 0.98 mmol) and trio-tolylphosphine (60 mg, 0.20 mmol) were added, the apparatus was then evacuated and backfilled with Ar 6 times before the addition of 4,4,5,5-tetramethyl-2-(5-(methylthio)thiophen-2-yl)-1,3,2-dioxaborolane via syringe (500 mg, 1.95 mmol), after that toluene (15 mL) and Na_2CO_3(aq) (1.5 M, 4 mL) were added. The mixture was gently refluxed for 16 hours. The mixture was then cooled to rt and filtrated. The dark solid obtained was crystallized in a mixture of DCM/EtOAc/hexanes to give the title compound as dark violet solid.

^{1}H NMR (400 MHz, $CDCl_3$) δ: 8.25 (s, 2H, Ph), 7.91 (d, 2H, J = 8.4 Hz, Ph), 7.77 (d, 2H, J = 8.4 Hz, Ph), 7.26 (d, 2H, J = 3.6 Hz, Th), 7.00 (d, 2H, J = 3.6 Hz, Th), 2.45 (s, 6H, CH_3). ^{13}C NMR (100 MHz, $CDCl_3$) δ: 143.1, 139.3, 135.3, 134.1, 132.2, 131.4, 131.1, 126.7, 124.8, 124.7, 29.7, 21.7. *m/z* 487.0 $[M+Na]^+$.

5.5.1 5,5'-bis(pyridin-4-ylethynyl)-2,2'-bipyridine

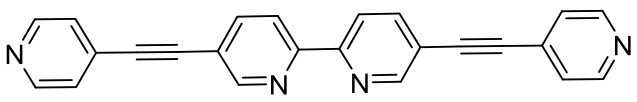

To an oven dried 100 mL round bottom flask fitted with a condenser were added 5,5'-dibromo-2,2'-bipyridine (0.66 g, 3.18 mmol) and CuI (0.09 g, 0.49 mmol), the flask was evacuated and refilled with Ar 4 times.. Dry toluene (66 ml) and NEt_3 (2.5 ml) were added via syringe and the mixture was degassed for 50 min. $Pd(PPh_3)_4$ (0.37 g, 0.32 mmol) was added and the solution degassed further 10 minutes. Finally, a solution of 4-ethynylpyridine* (1.6 g, 15.4 mmol) in dry degassed toluene (5 mL) was added via syringe and the solution was stirred overnight under Ar atmosphere and heated at 60 ℃. The reaction was cooled to rt and the mixture was filtered to obtain the crude product as an orange solid that was filtered through a plug of silica and recrystallized from DCM twice to give the title compound (311 mg 27%).

^{1}H NMR (400 MHz, $CDCl_3$): δ = 8.82 (s, 2H), 8.65 (d, J = 4.8 Hz, 4H), 8.44 (d, J = 6.9Hz, 2H), 7.96 (d, J = 8.1 Hz, 2H), 7.41 (d, J = 5.0 Hz, 2H); ^{13}C NMR (100 MHz, $CDCl_3$): δ = 154.7, 152.0, 149.9, 139.7, 130.6, 125.5, 120.8, 119.6, 90.9, 90.6.

*The deprotection of 4-ethynylpyridine was performed immediately before the Sonogashira reaction. To a MeOH/THF solution (1/1, 44 ml) 4-(trimethylsilylethynyl)pyridine (2.7 g, 15.97 mmol) and Na_2CO_3 (3.8 g, 35.9 mmol) were added and the mixture was stirred under N_2 atmosphere at rt for 30 min. The mixture was filtered through celite and the solvent was removed under vacuum. The dark solid obtained was then dissolved in 5 mL of dry toluene and added to the Sonogashira reaction above.

Chapter 6: STM-Based Measurements

6.0 STM measurements

Here there is a more specific description of the techniques used to better understand the behaviour of the molecular wires studied in this thesis. All the molecular wires used for conductance studies were pure and fully characterized by NMR, CHN, and Accurate mass before any measurement to assure the quality of the data. The measurements were usually carried out in a relatively short time after the synthesis and characterization.

6.1 Sample Preparation

The substrates used for all the measurements were the polycrystalline gold slides were purchased from Arrandee (11x 11 mm gold-on-glass, Arrandee® GmbH, DE – 250 nm Au | 2.5 nm Cr | 0.7 mm borosilicate glass) and they were flame annealed with a butane torch or a Bunsen burner before being used. The annealing was needed because the gold roughness of the slides is too high and could produce high noise due to the uneven surface. This process consisted of heating three times the substrate with the torch at an angle of 45° until glowing red. The process lasts few seconds each time to avoid overheating of the substrate that would produce a bending of the glass underneath the gold layer and therefore an uneven surface. This process (according to the supplier guidelines) produces an atomically flat surface of Au (111) that can be used for STM-BJ and STM-I(s) measurements upon cooling to room temperature.

6.2 Techniques used for Single molecule conductance study

The measurements shown in this thesis were carried out with an STM (Agilent 4500 SPM, Agilent Technologies Inc., USA or an Agilent 5500 SPM, Agilent Technologies Inc., USA) fitted with a freshly cut gold tip (Goodfellow Cambridge Ltd., UK - 99.99+%, 0.25mm), and the substrate (gold slide, Arrandee). The sample preparation with the introduction of the molecular wires varied from technique to technique and will be explained later in more detail.

6.2.1 STM-I(s) sample preparation and measurements

The general description of the STM-I(s) method can be found in the introduction (Chapter 1) and here there will be only a special focus on the working condition used to perform the conductance studies with this technique.

The sample preparation consists in the formation of a sub-monolayer of molecular wires on the gold substrate freshly annealed. This was achieved by immersing the substrate into a 10^{-4} M solution of the molecular wire (typically using ethanol as solvent). The slide containing the molecular wire is then washed with ethanol, dried under Ar and fitted inside the STM on its holder. The I(s) measurements are then carried out in air.

To start the experiment, the tip is approached to the surface and kept on top of the surface at a desired setpoint current and bias voltage. At this point the feedback loop is switched off, the tip is maintained in the same position on the surface and then is moved away and towards the surface at constant speed (10 – 40 nm s^{-1}). The measurement consists in the recording of the current vs distance curve (I = current s = distance or space). During this process the curve should simply describe the exponential decay in conductance if no molecule interacts. If a molecular wire fills the gap between electrodes (tip and substrate) the curve will present a step or plateau, followed by an abrupt decay that represent the nanojunction formation and then its rupture to 0. The experiment then continues and after enough data is collected and manually selected (at least 500 traces) a histogram is created to represent the conductance behaviour of the molecular wire.

6.2.2 The STM-BJ sample preparations and measurements

This technique differs from the STM-I(s) because a contact is made between the electrodes throughout the measurement. The general functioning of this technique is well described in the Introduction (Chapter 1) so here only a few important aspects regarding the sample preparation are discussed.

The sample preparation consists of adding the molecular wire as dilute solution (10^{-3} M) and the measurements are performed in solution. Several solvents can be used such as mesitylene, toluene, trichlorobenzene, ionic liquid, water (with insulated tip), and combination of these with other organic solvents such as THF or methanol. Since the measurements are carried out in solution, the molecular wires must be soluble in the solvent used in order to avoid the presence of solids on the gold surface. The solvent must also be not very volatile to avoid change of concentration or precipitation as a result of its evaporation. Most of the STM-BJ measurement are carried out in solution but it is possible to perform the same technique also on air.

In this thesis the measurements on molecular wires with low conductance (Chapter 2) were carried out with the STM-I(s) technique while the measurements on the bithiophenes and longer wires were performed with the STM-BJ technique. This was for two main reasons: firstly, short and conjugated wires possess higher conductance values that sit perfectly within the working range of the STM-BJ technique while the I(s) can be used for much lower values. Secondly the STM-BJ technique as opposed to the STM-I(s) could potentially be much less biased by the user. In the STM I(s) the single traces are hand-picked and selected by the user, and this might cause systematic errors in the conductance values obtained this way. The BJ on the other hand has a higher noise level but does not need any data selection, giving an unbiased conductance histogram. At the same time the set-up of the BJ can provide more than 5000 traces for a single study as opposed to the 500 traces usually obtained from the STM-I(s). Nonetheless as demonstrated in Chapter 2 when the wire 1Ph1-SMe was measured with both the techniques resulting in the same conductance value we can assume that both of these techniques are useful tools for single molecule conductance studies.

The data analysis for obtaining the conductance values of the molecular wires are here reported in detail.

The output of the STM-break junction apparatus is a multi-columned ASCII table, that consists in values of tip withdrawal z in nm , bias V in volts and junction current I in nanoamperes. Conductance is calculated as a function of $G_0 \approx 77.48\ \mu S$ from the ASCII table using the following relationship

$$G/G_0 = I/VG_0.$$

Traces are fed to an automated sorting algorithm (Labview) that:

- Removes traces where the apparatus couldn't create a fresh nanocontact with conductance higher than a predefined threshold (generally $> 5G_0$)
- Delete traces where the current did not decay at the noise level of the instrument ($\sim 50\,pA$; $10^{-5} - 10^{-6}\,G_0$, depending on the bias used in the measurement [higher bias gives lower noise level]).
- Align all the remaining traces to G_0 *i.e.* defines the 0 of electrode displacement at the point where the atomic contact breaks. Therefore, all events where charge transport occurs through a metallic contact are at negative displacement, and molecular transport occurs at positive displacement; this can help calculating the length of the junction known as break-off distance.

All traces showing clear formation of a nanocontact after the initial gold-gold indentation and a clear decay to the noise level during withdrawal were compiled in histograms and 2d plots without any further selection and modification. The number of traces discarded by the automated algorithm is variable, as it depends on environmental variables (mechanical/acoustic noise, piezo drift/thermalisation, solvent used, etc.) but it is usually lower than 10% of the total number of traces collected.

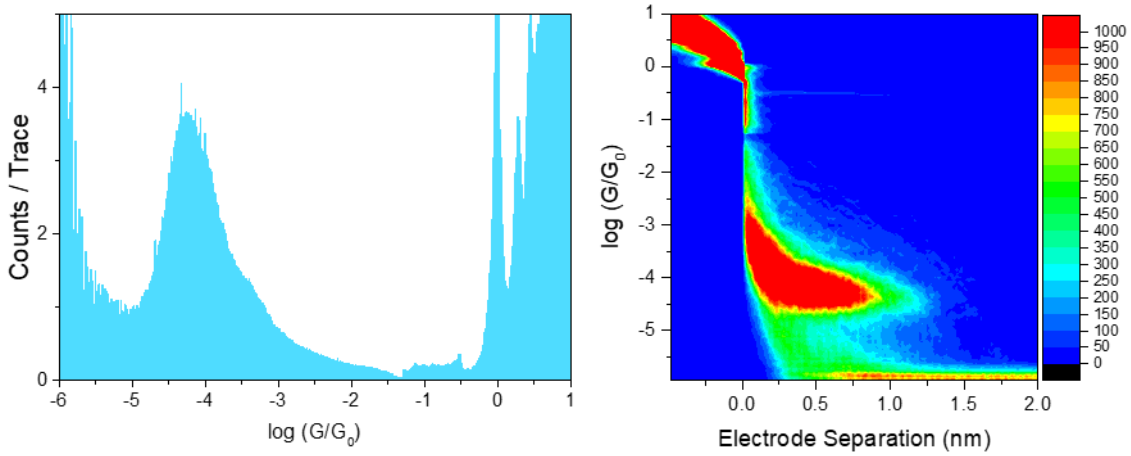

Figure 6.1 *Example of a STM histogram: on the left, only the conductance values are used, on the right the 2d histogram shows the conductance vs the electrode separation.*

As shown in the previous Chapters and in Figure 6.1 Semilog histograms are compiled using the OriginPro data analysis software, using a binsize of 100 bins per decade. Only the conductance values are used in the semilog histograms. 2d maps are compiled using the same software, by calculating a descriptive statistics 100 x 100 matrix of conductance *vs* electrode separation in the range of interest (generally, 0.5 G_0 to 10^{-6} G_0 and -0.5 to 2 nm relative displacement. The counts at each point of the matrix are then plotted as colour gradient heatmap.

6.2.3 The I/V technique.

The I/V technique was used to gather more information on the wires by analysing their conductance across a wider range of bias.

Usually with the STM-BJ is it possible to measure the conductance of a molecule at a defined bias, in this thesis in order to fully study the interference effects on our wires we decided to use the I/V technique.

This method gives a snapshot of the conductance of the wire across a wider bias. The conductance of a molecular wire might be subjected to small changes at a certain bias, this method might provide useful information on the behaviour of a molecular wire.

Few adjustments were made to the STM-BJ set up to perform these experiments such as the introduction of a more flexible logarithmic amplifier and the connection of a dual channel function generator to the system to provide a precise control over both the bias and the tip retraction during the *I/V* measurements.

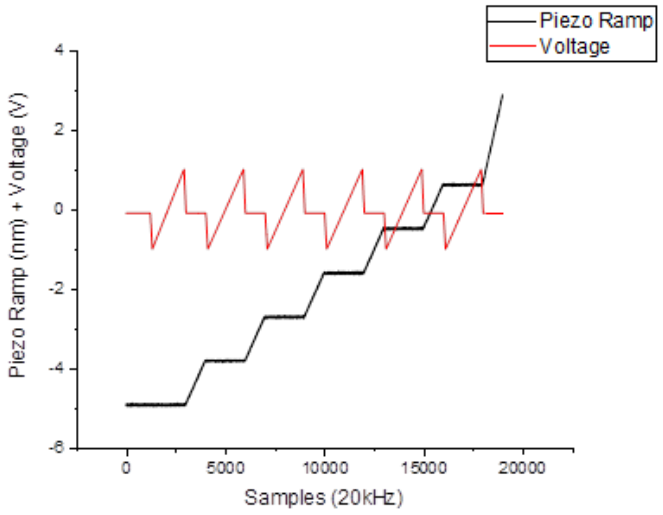

Figure 6.2 *Schematics of an I/V experiment (the black line describes the tip retraction and the red line the applied bias)*

In Figure 6.2 is described the simple mechanism behind a I/V measurement. The black line indicates the piezo ramp and consists of 6 consecutive retractions of the tip of 1 nm each at a certain voltage (100 mV) with a pause between each of them of exactly 100 ms. During each pause the tip was kept steady in position and the *I/V* determination (in red in Figure 6.2) was run in 90 ms centred within the pause allowing the system to return to 100 mV before the next step. The ramp was created in order to statistically trap a molecule at least one time during the retraction. The samples were usually prepared in the same manner as described for the I(s) technique with the only difference being that the dilute solution of the wires was made of EtOH/CH_2Cl_2 1/1 (some measurements were also successfully executed using mesitylene as solvent and performed in solution). The statistical analyses of the measurements were executed by an automated data selection method. Since the high voltage applied to the system often resulted in the breakage of the junction halfway through the measurements, only the traces with the wire trapped in the junction before and after the I/V were saved. This was made possible by the 5 ms windows before and after the measurements. In this time the conductance of the molecule is recorded, and only the traces having a molecule before and after the I/V test were used for the final histogram. If the current dropped after the junction or was higher than G_0 before the start of the I/V the measurement the trace was discarded.

6.2.4 Modulation experiments

The modulation experiments were executed with the same modified system used for the I/V measurements and often the measurements were performed consecutively on the same sample. Similarly, with the previous method the tip retraction consists of roughly 6 consecutive steps of 1 nm each and 100 ms of pause between them. In this case the piezo ramp was created in order to have a modulation pattern of a few Å (from 2 to 4 Å) during the 100 ms pauses between the retractions as shown in Figure 6.3.

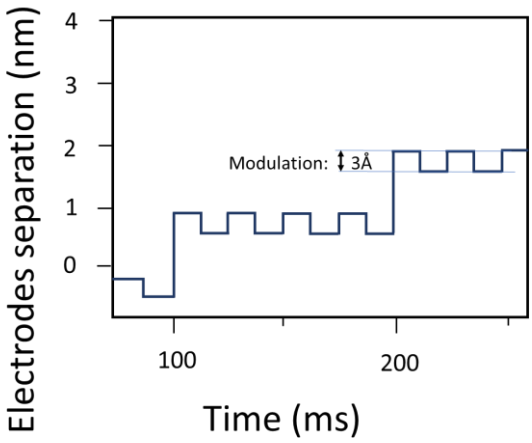

Figure 6.3 *Schematics of a modulation experiment*

As previously mentioned, the statistical analysis of the traces was performed following the same principle of the I/V measurements mentioned before: only the traces with the molecule trapped throughout the measurements were saved and used to create the histograms. This was made possible thanks to an algorithm that selected traces with conductance lower than G_0 before the modulation but higher than the noise level after the modulation.

Chapter 7: Conclusion

7.0 Conclusion

The aims of this thesis were to investigate the structural properties of newly synthesized molecular wires and to test quantum interference effects in single molecule nanojunctions.

The first study was focused on Double Tunnelling Barrier molecular wires. The main aim of that project was to demonstrate the existence of Gateway states and coupling states that were responsible for the suppressed decay of conductance values with the increase of length in these DBT wires. These gateway states were due to the interplay between thiol-based contact groups and the electrodes.

Theoretical calculations predicted that this effect could be switched off by using a different contact group such as the methyl thioether. This work described successfully both the synthesis of these wires and the conductance measurements with the STM-I(s) that lead to the demonstration to the existence of these effect by suppressing them.

The second study was on interference effects in bithiophene-based molecular wires. Two sets of wires have been designed and synthetized in this study: the first was based on heteroatom bridges: theoretical calculations predicted the existence of interferences effects and change in conductance for these molecular wires when bridged by atoms of different size. Three wires were synthetized with CPh_2, $SiPh_2$ and $GePh_2$ bridges. The result of this study was the discovery of strong interaction of the phenyl rings used as side group of the bridging heteroatom with the electrodes used to measure them. In this case some physical interaction prevented the molecules to conduct through the contact group as usual.

The second project of the second study was based on the predicted Fano resonances present in the transmission curves of bithiophenes-based molecular wires with carbonyl bridges. During this study several techniques have been executed in order to define the interferences effects and some of the measurements such as the I/V measurements gave some interesting clues but not full answers. Finally, the

modulation experiments showed an interesting feature arising from the practical results: the molecular wires used in this study and to a good extent also all the other bithiophene-based wires can switch contact group from the standard contacts (thioethers) to a bidentate interaction additionally involving the thiophene ring sulfur. The discovery of this behaviour can be a very useful tool for introducing similar properties to a device. Most importantly this study sheds some light on the conductance of thiophene-based molecular wires finally explaining the characteristic wider histogram when using the STM-BJ for these molecules.

The third project was focused on the interference effects arising from the addition of a carbonyl unit in a molecular wire. This project involved the synthesis and measurements of longer molecular wires in order to observe a higher influence over their conductance that is definitively lower than the wires previously measured. Also, bipyridine based molecular wires able to bind to carbonyl rich metal complexes were studied. These studies provided a lot of information on the behaviour of these wires but not enough clue to clearly pinpoint any underlying interference effect. Certainty future theoretical calculation will be useful tools for providing the right model and could explain the observed results.

In conclusion this work presented the synthesis of several sets of new molecular wires and their study using both STM-I(S) and BJ techniques and also some more peculiar techniques (such as modulations and I/V). Two of the biggest reported results are the demonstration of the existence of the gateway states by suppressing their effects on DBT molecular wires and also the discovery of the switching mechanisms in bithiophene-based molecular wires due to the interplay between thioether-thiophene when in contact with gold.

I hope that the results reported on this thesis might help the design of new molecular wires and that the effects discovered will be the base for future studies.

Appendix: Collection of STM measurements and NMR spectra

A.1 Single-molecule conductance data

Single-molecule conductance data obtained using the STM-*I(s)* technique are presented as 1-dimensional linear histogram (Figure A.1 left) and 2D "density" plots (Figure A.1 right). The x-axis in the linear histogram indicates the conductance and is expressed in nS while the y-axis represents arbitrary counts and they are not shown for clarity. The linear histogram shows the distribution of conductance values recorded during the measurements and the main peak represent the molecule conductance.

The 2D plot represent electrode separation in nm versus conductance expressed in nS, the colour scale goes from blue (low density) to red (high density). This plot gives information on the break-off distance that represent the length of the nanojunction and is also correlated with the linear histogram: the areas with higher density represent the peak present in the linear histogram. The break-off distances are important in order to define the size of the nanojunction and also help pointing out the signal representing the molecular wire.

Here are reported all the measurements that were executed on the molecular wires presented in this thesis accompanied by the condition used.

A.2 1[Ph]1-SMe

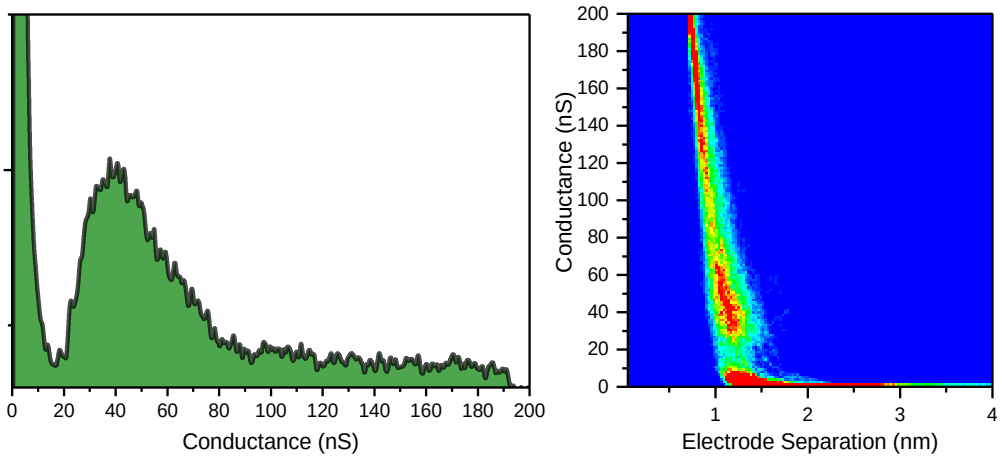

Figure A.1 SMC data (STM-I(s)) for **1[Ph]1-SMe.** 60 nA setpoint, 0.3 V bias.

A.3 3[Ph]3-SMe

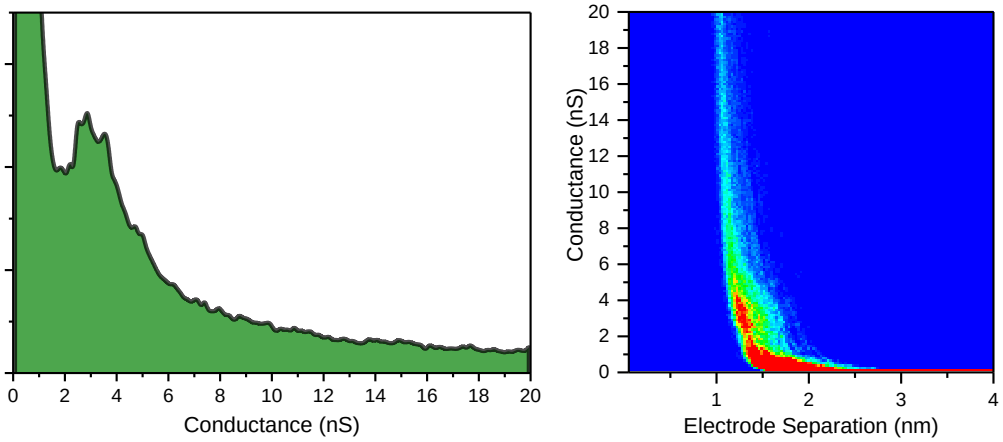

Figure A.2 SMC data (STM-I(s)) for **3[Ph]3-SMe**. 60 nA setpoint, 0.3 V bias.

A.4 4[Ph]4-SMe

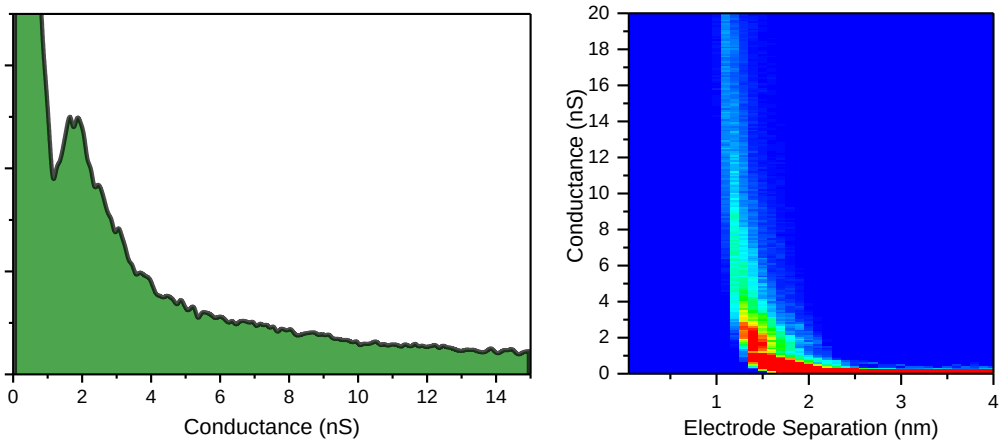

Figure A.3 SMC data (STM-I(s)) for **4[Ph]4-SMe**. 60 nA setpoint, 0.3 V bias.

A.5 5[Ph]5-SMe

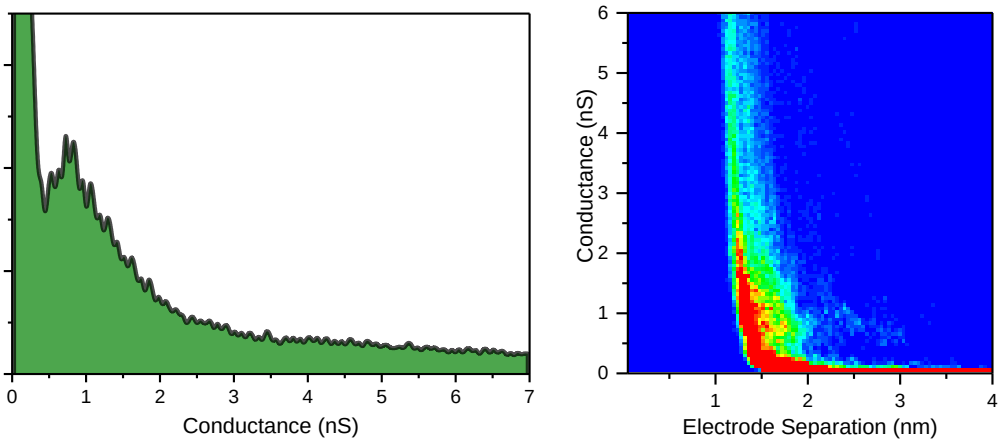

Figure A.4 SMC data (STM-I(s)) for **5[Ph]5-SMe**. 60 nA setpoint, 0.3 V bias.

A.6 6[Ph]6-SMe

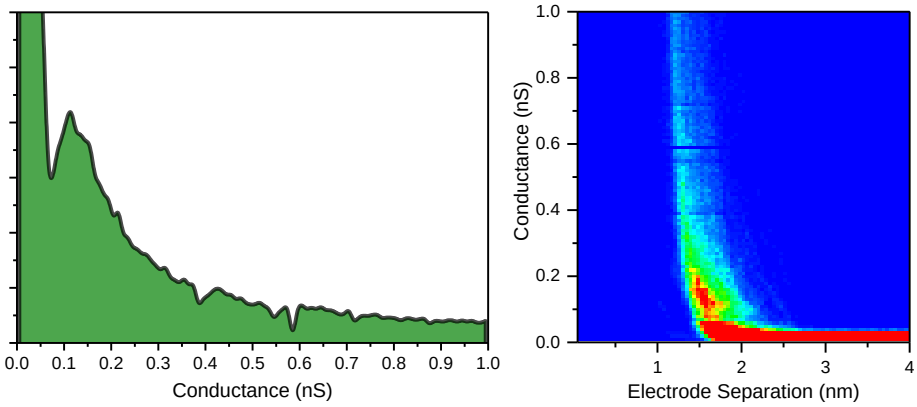

Figure A.5: SMC data (STM-I(s)) for **6[Ph]6-SMe**. 20 nA setpoint, 0.3 V bias.

A.7 $TGePh_2T$

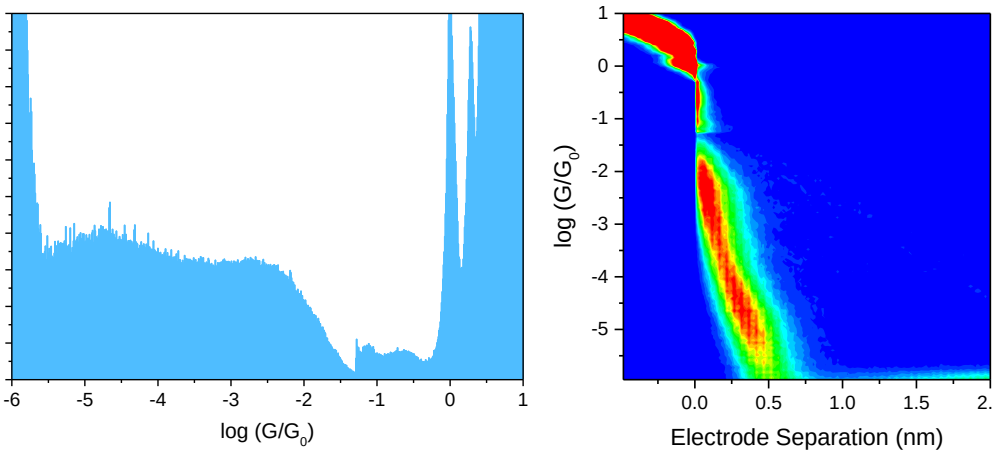

Figure A.6 SMC data (STM-BJ) for **TGePh2T** on air at 200 mV

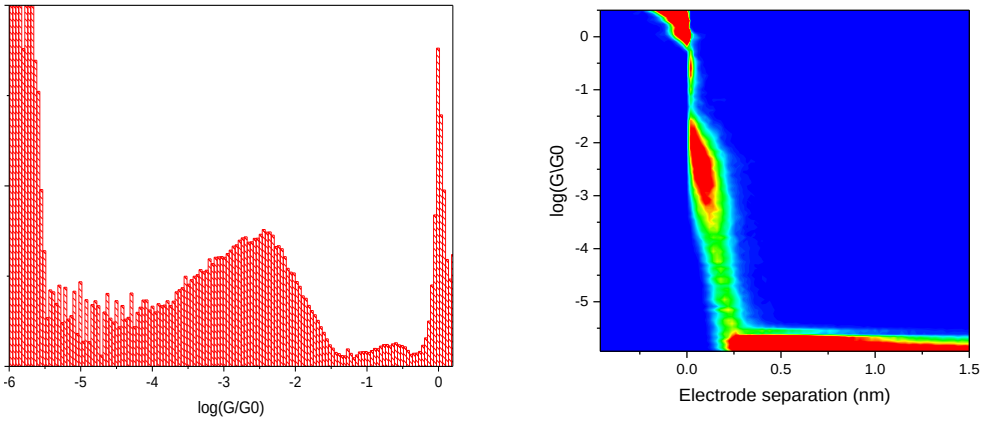

Figure A.7 *SMC selected data (STM-BJ) for* ***TGePh2T*** *on air at 200 mV*

A.8 $TSiPh_2T$

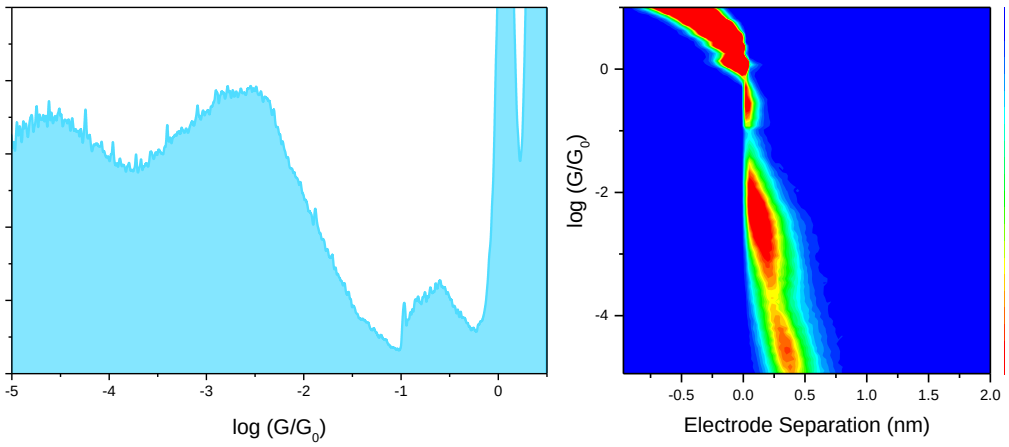

Figure A.8 SMC data (STM-BJ) for **$TSiPh_2T$** in mesytilene at 200 mV

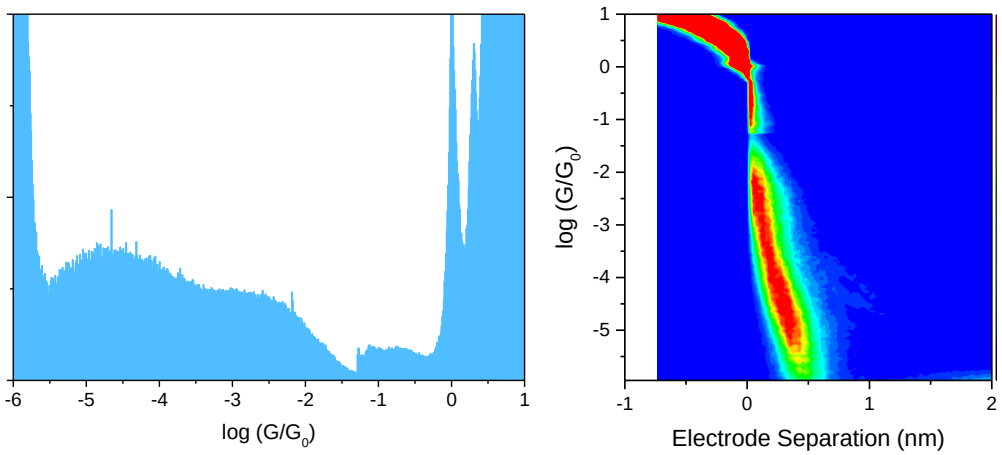

Figure A.9 SMC data (STM-BJ) for **$TSiPh_2T$** in air at 200 mV

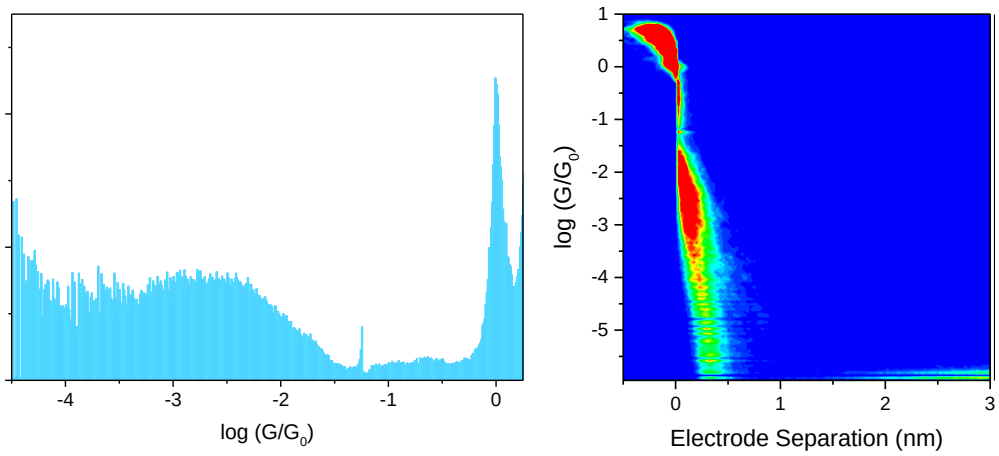

Figure A.10 SMC selected data (STM-BJ) for **$TSiPh_2T$** in air at 200 mV

A.9 $TCPh_2T$

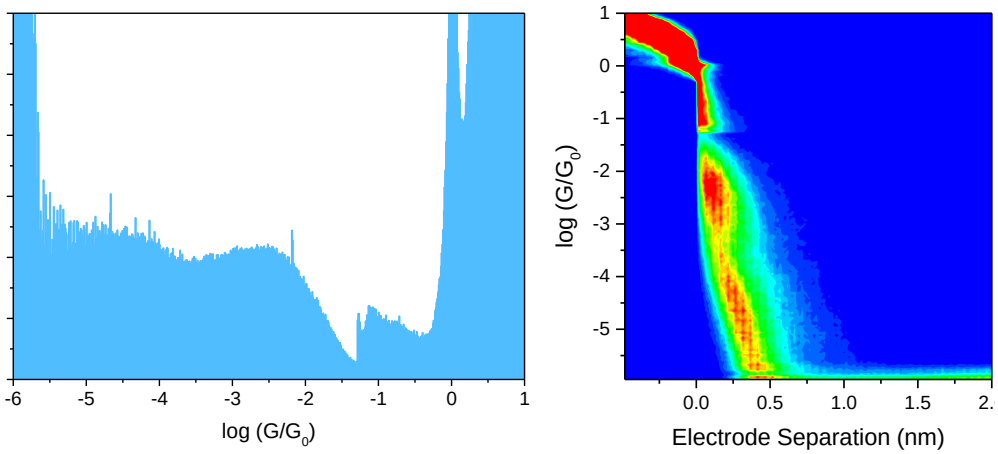

Figure A.11 SMC data (STM-BJ) for **$TCPh_2T$** in air at 200 mV

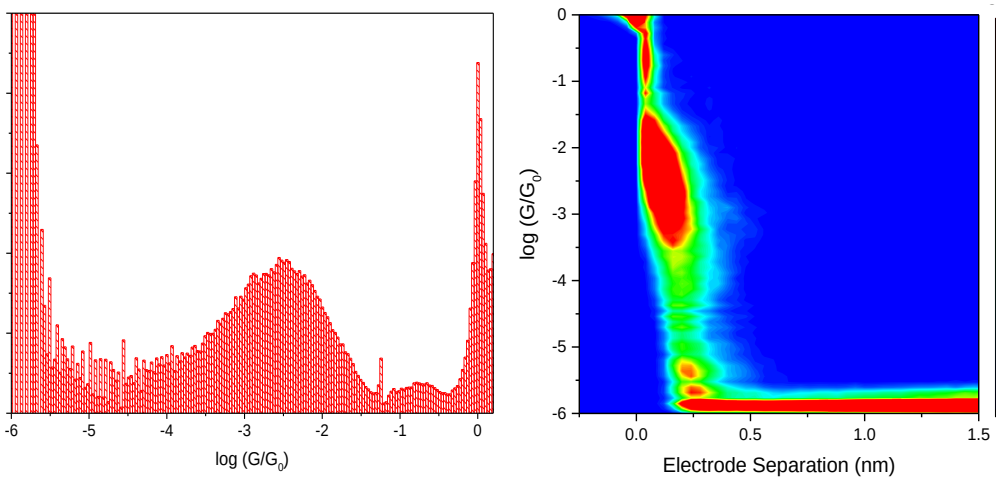

Figure A.12 *SMC selected data (STM-BJ) for* ***$TCPh_2T$*** *in air at 200 mV*

A.10 TKT

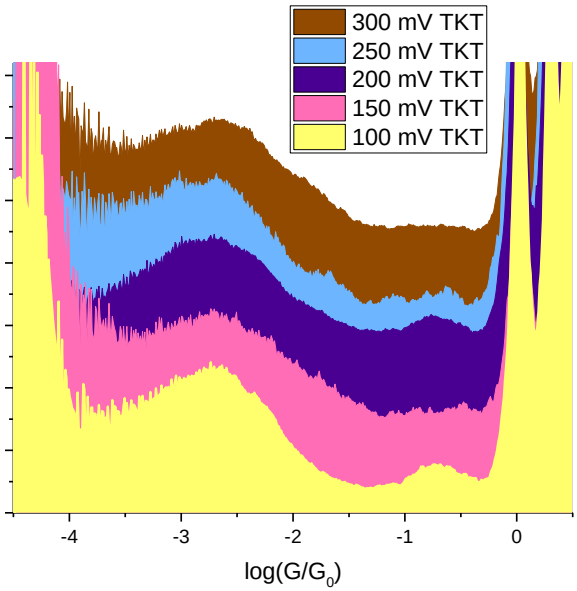

Figure A.13 SMC data (STM-BJ) for **TKT** in mesytilene at 100, 150, 200, 250 and 300 mV

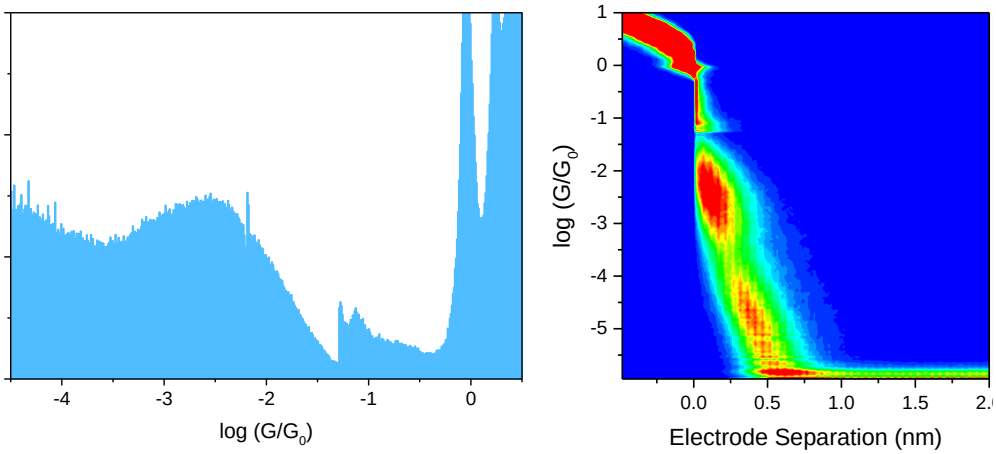

Figure A.14 SMC data (STM-BJ) for **TKT** in mesytilene at 200mV

A.11 $TCMe_2T$

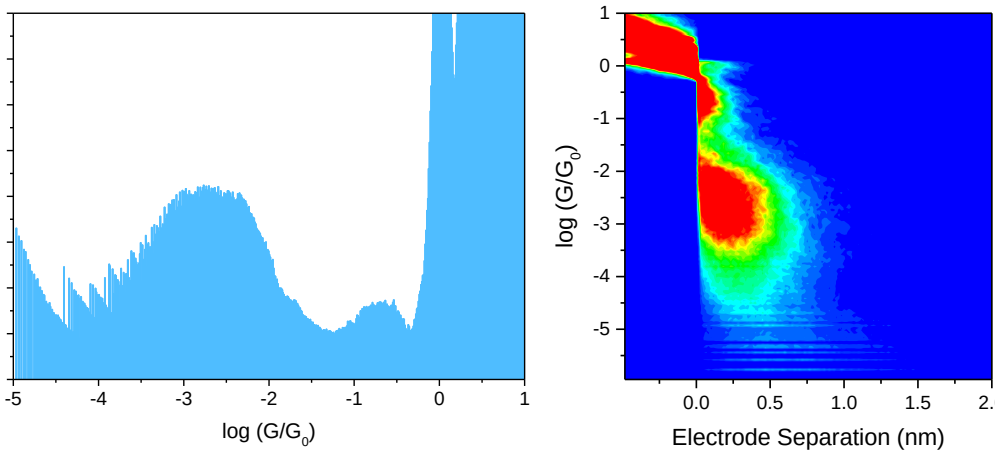

Figure A.15 SMC data (STM-BJ) for **$TCMe_2T$** in mesytilene at 200mV

A.12 TDKT

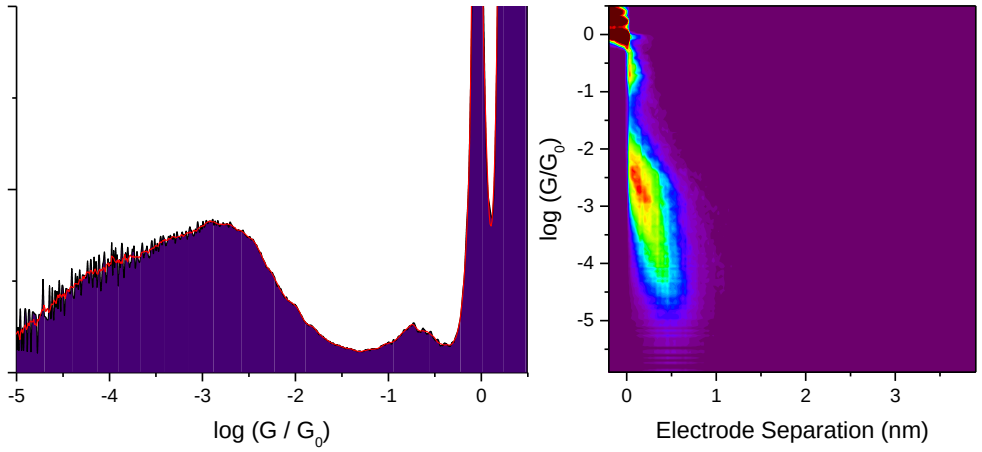

Figure A.16 SMC data (STM-BJ) for **TDKT** in mesytilene at 200mV

A.13 I/V experiments on bithiophenes

Here there are reported all the I/V histograms executed on the molecular wires bithiophene- based presented in this thesis.

A.13.1 TKT

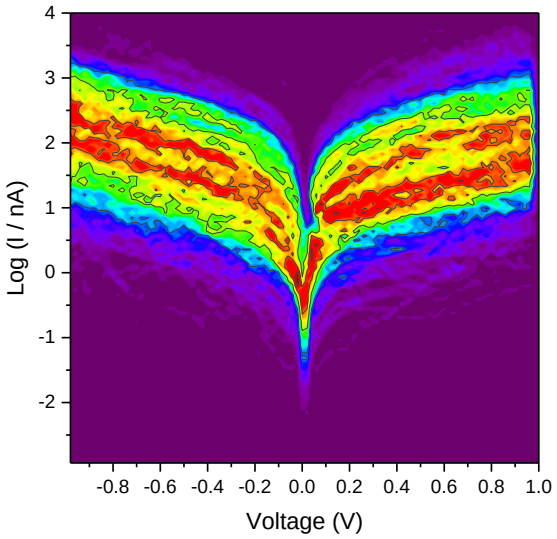

Figure A.17 I/V study for **TKT** between -1 and 1 V, in mesytilene

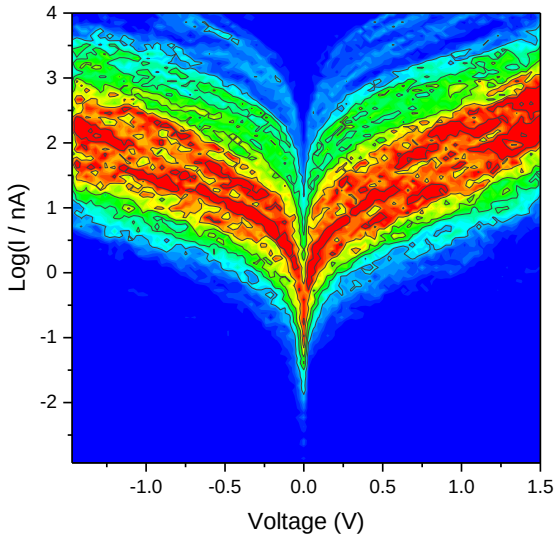

Figure A.18 I/V study for **TKT** between -1.5 and 1.5 V, in mesytilene

A.13.2 $TCMe_2T$

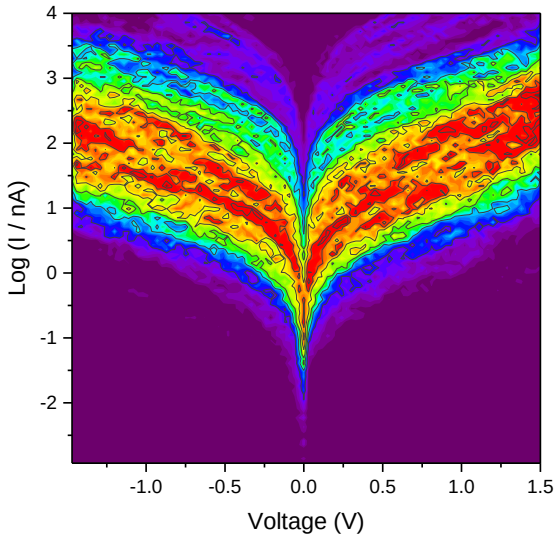

Figure A.19 I/V study for **$TCMe_2T$** between -1.5 and 1.5 V

A.13.3 3,3'bithiophene

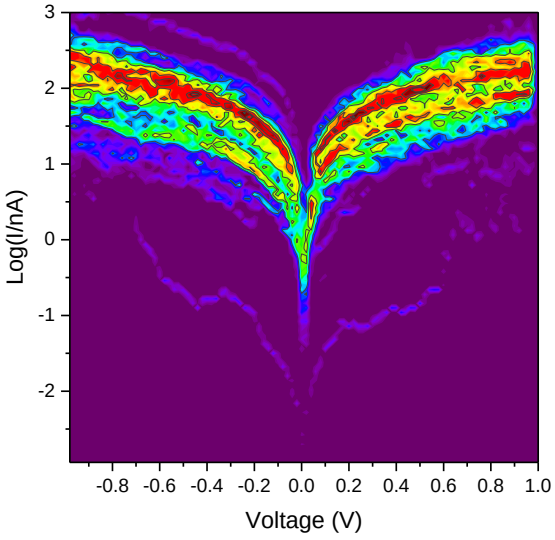

Figure A.20 I/V study for **3,3'bithiophene** between -1.5 and 1.5 V

A.13.4 Biphenyl-SME

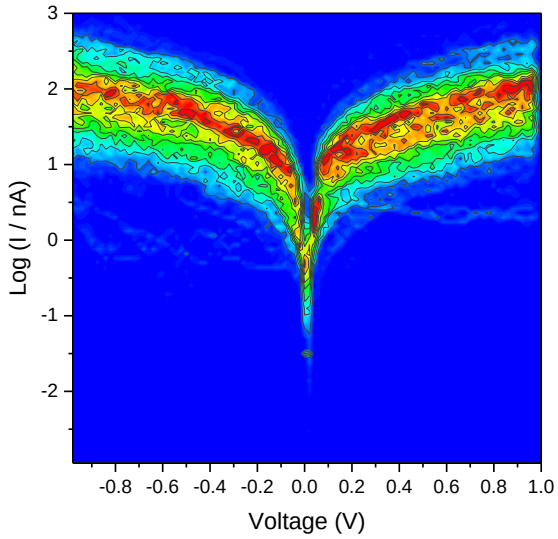

Figure A.21 I/V study for **biphenyl-SMe** between -1 and 1 V

A.14 Modulations experiments

Here there are reported all the I/V histograms executed on the bithiophene- based molecular wires presented in this thesis.

A.14.1 TKT

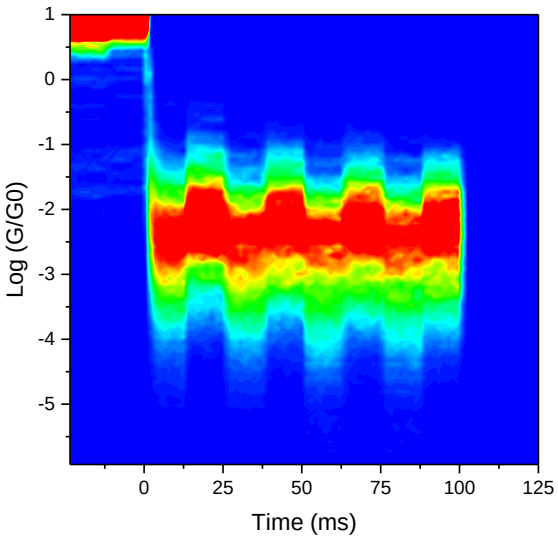

Figure A.22 0.2 nm modulation measurement for **TKT** at 100 mV

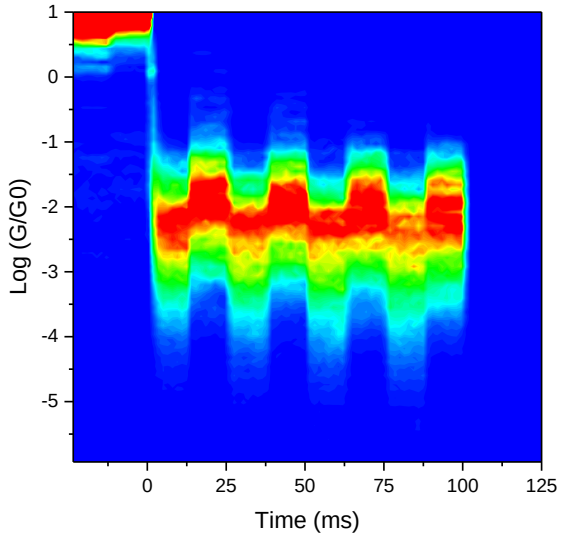

Figure A.23 0.3 nm modulation measurement for **TKT** at 100 mV

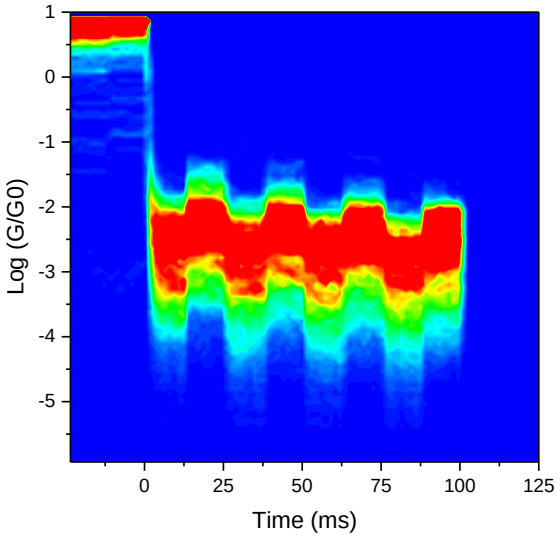

Figure A.24 0.2 nm modulation measurement for **TKT** at 200 mV

A.14.2 $TCMe_2T$

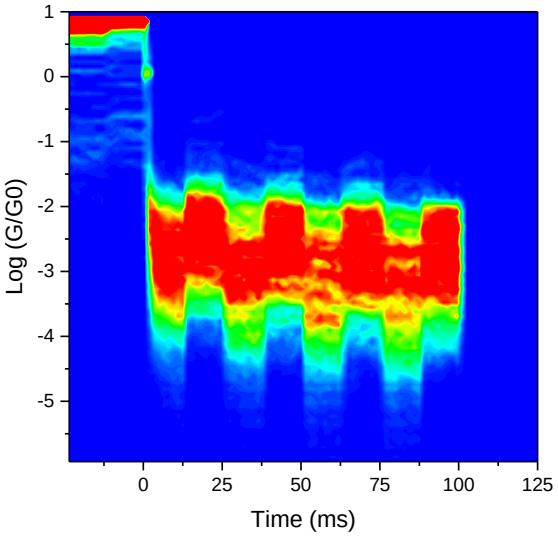

Figure A.25 0.2 nm modulation measurement for **$TCMe_2T$** at 200 mV

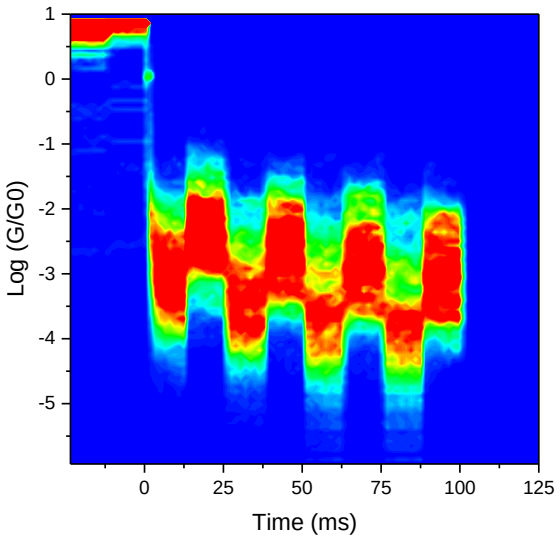

Figure A.26 0.3 nm modulation measurement for **$TCMe_2T$** at 200 mV

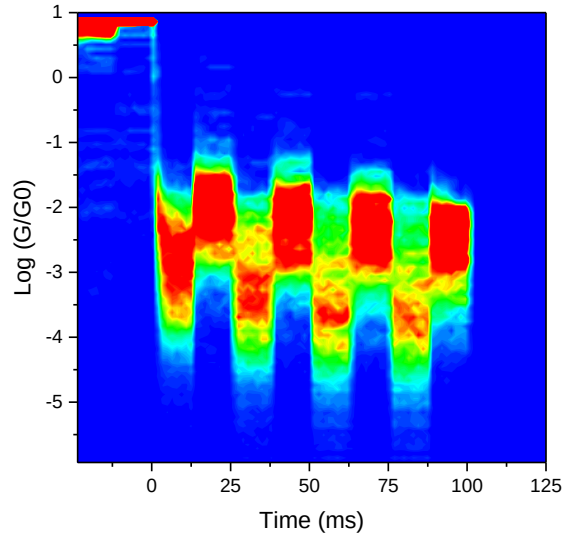

Figure A.27 0.4 nm modulation measurement for **$TCMe_2T$** at 200 mV

A.14.3 TDKT

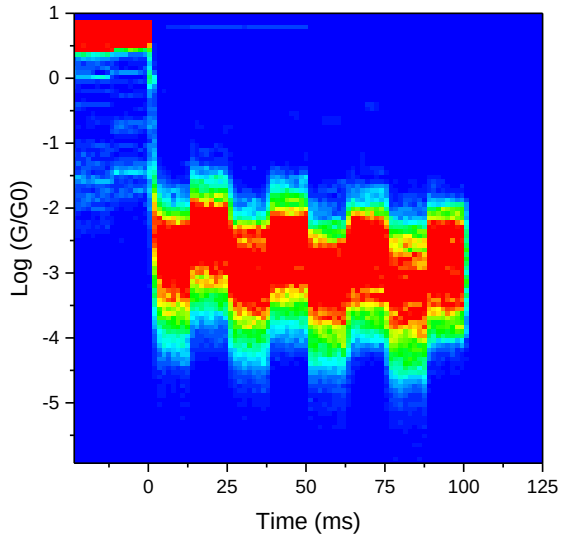

Figure A.28 0.2 nm modulation measurement for **TDKT** at 200 mV

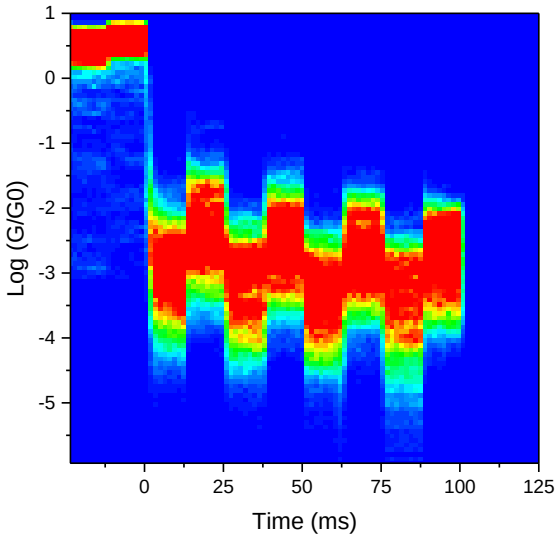

Figure A.29 0.3 nm modulation measurement for **TDKT** at 200 mV

A.14.4 Biphenyl-SMe

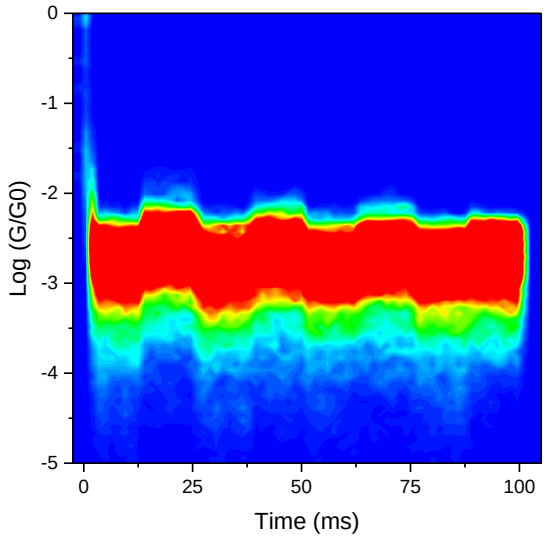

Figure A.30 0.2 nm modulation measurement for **Biphenyl-SMe** at 200 mV

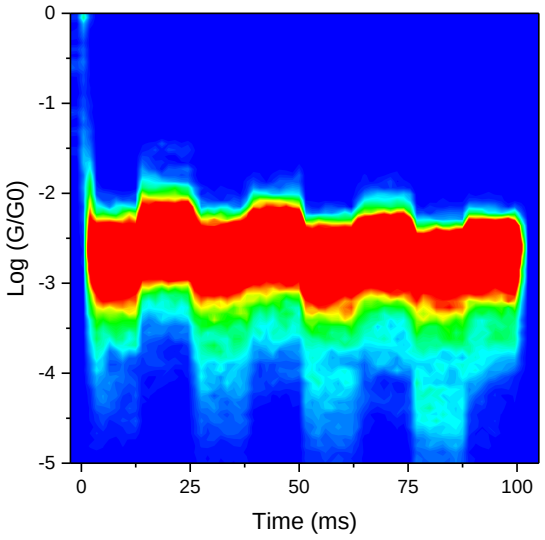

Figure A.31 0.3 nm modulation measurement for **Biphenyl-SMe** at 200 mV

A.15 TBPT

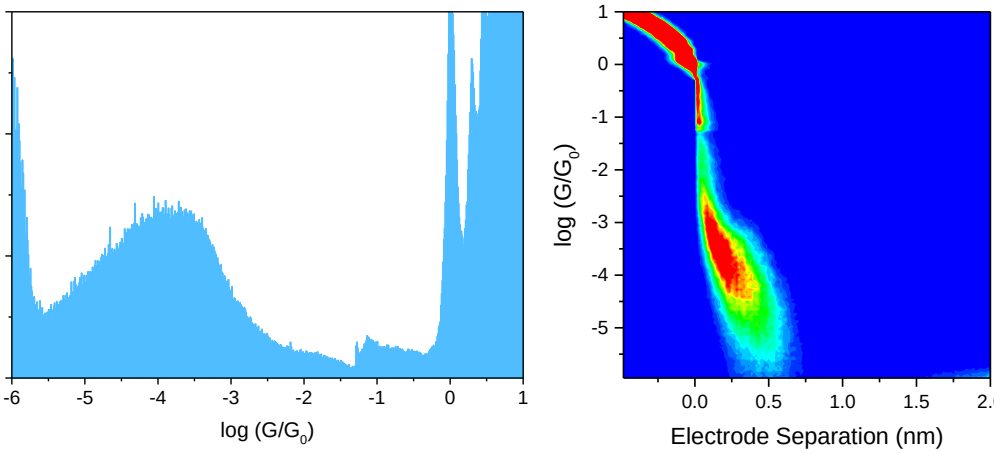

Figure A.32 SMC data (STM-BJ) for **TBPT** in mesytilene at 200Mv

A.16 TFOT

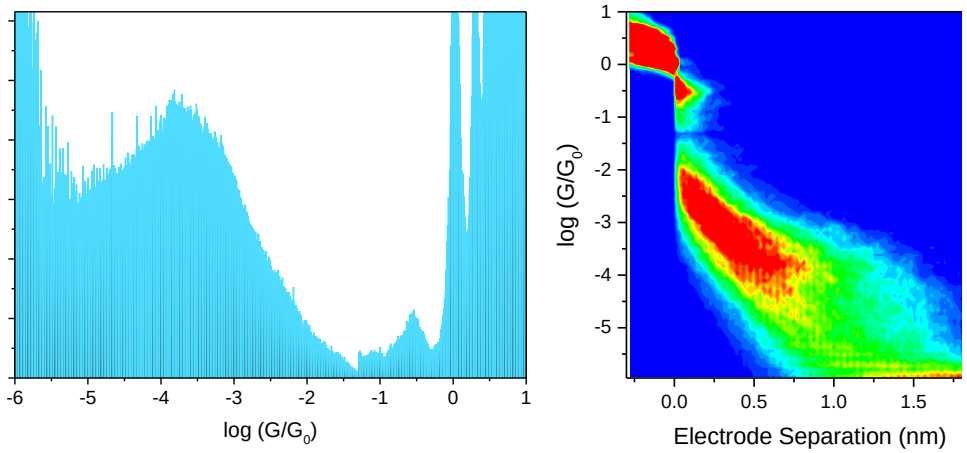

Figure A.33 SMC data (STM-BJ) for **TFOT** in mesytilene at 200mV

A.17 TFT

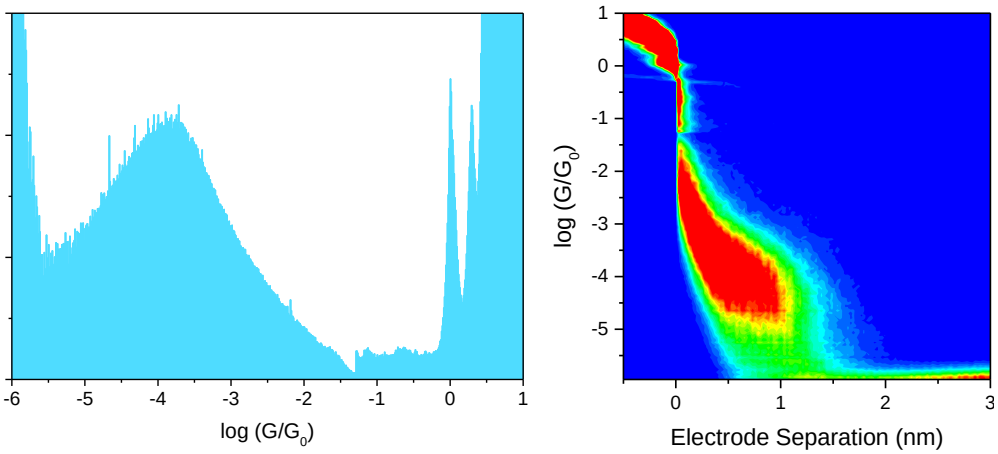

Figure A.34 SMC data (STM-BJ) for **TFT** in mesytilene at 200 mV

A.18 I/V experiment on TFT and TFOT

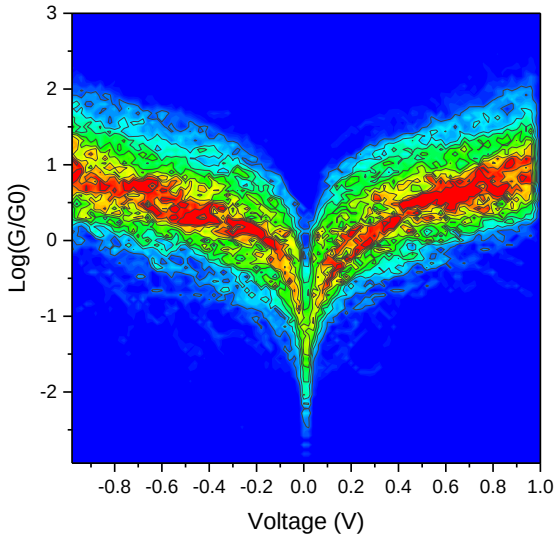

Figure A.35 I/V study for **TFOT** in mesytilene between -1 and 1 V

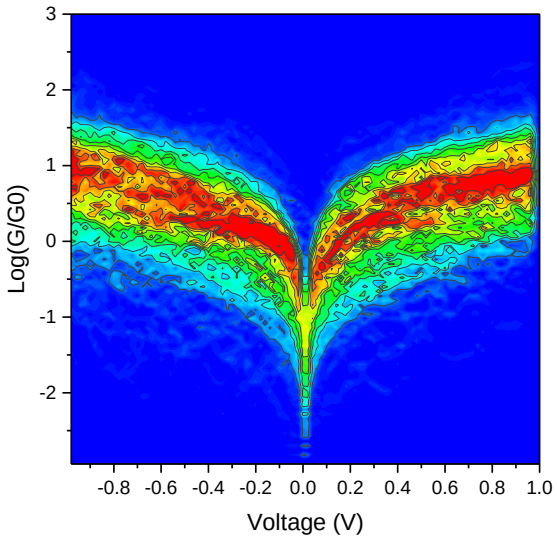

Figure A.36 I/V study for **TFT** in mesytilene between -1 and 1 V

A.19 BTBipy-MnBr(CO)$_3$

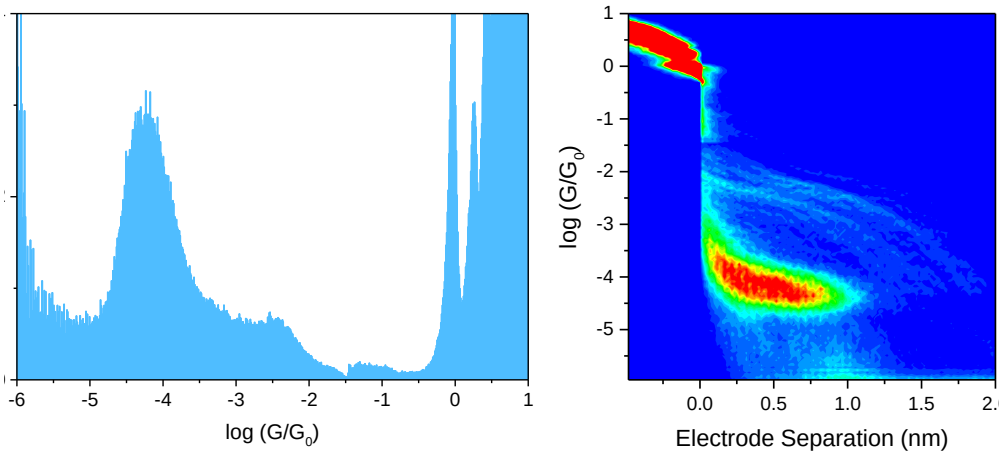

Figure A.37 SMC data (STM-BJ) for **BTBipy-MnBr(CO)$_3$** in mesytilene at 300 mV

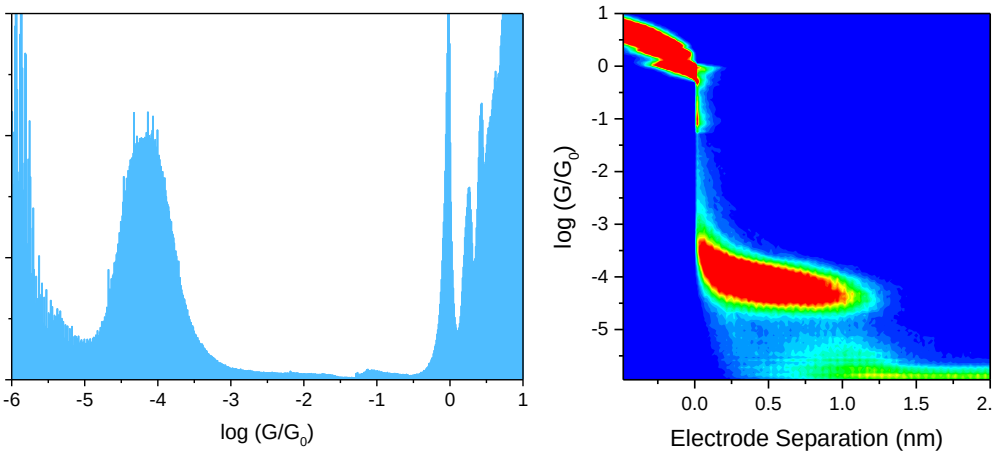

Figure A.38 SMC data (STM-BJ) for **BTBipy-MnBr(CO)$_3$** in mesytilene at 200 mV

A.20 BTBipy-Mo(CO)$_4$

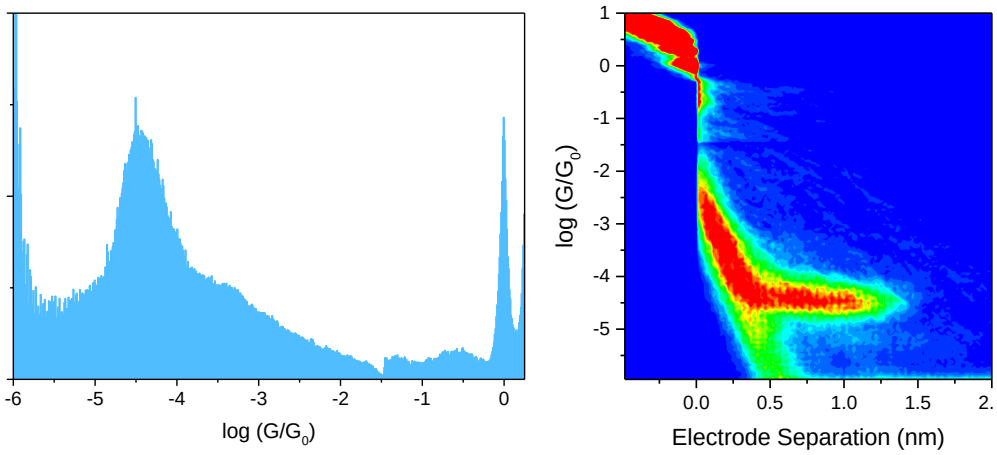

Figure A.39 SMC data (STM-BJ) for **BTBipy-Mo(CO)$_4$** in mesytilene at 300 mV

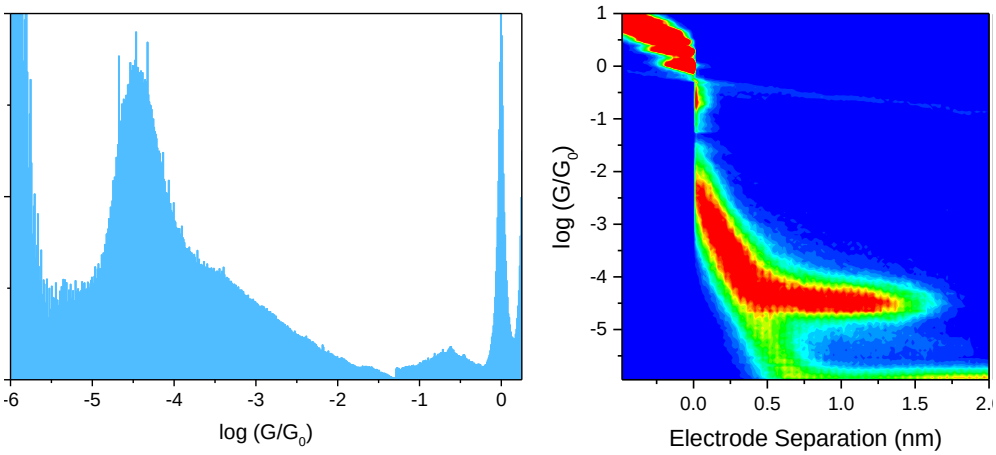

Figure A.40 SMC data (STM-BJ) for **BTBipy-Mo(CO)$_4$** in mesytilene at 200 mV

A.21 BTBipy-ReBr(CO)$_3$

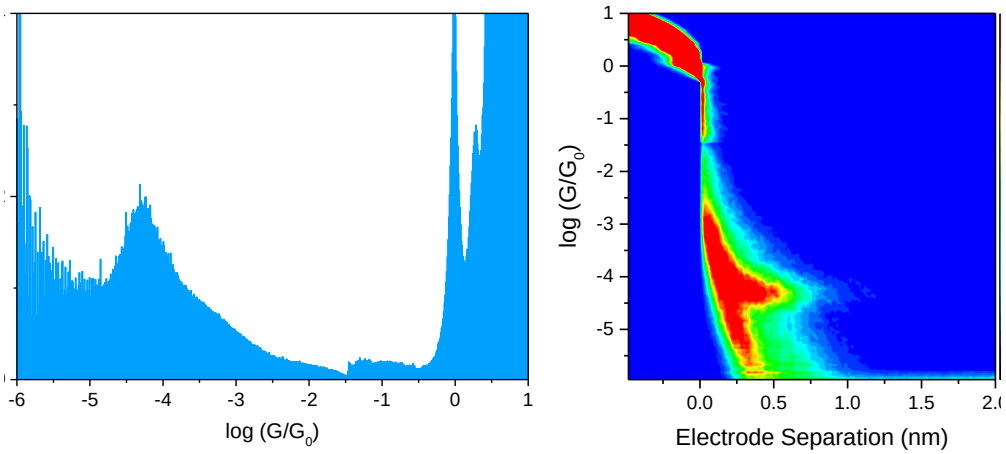

Figure A.41 SMC data (STM-BJ) for **BTBipy-ReBr(CO)$_3$** in mesytilene at 300 mV

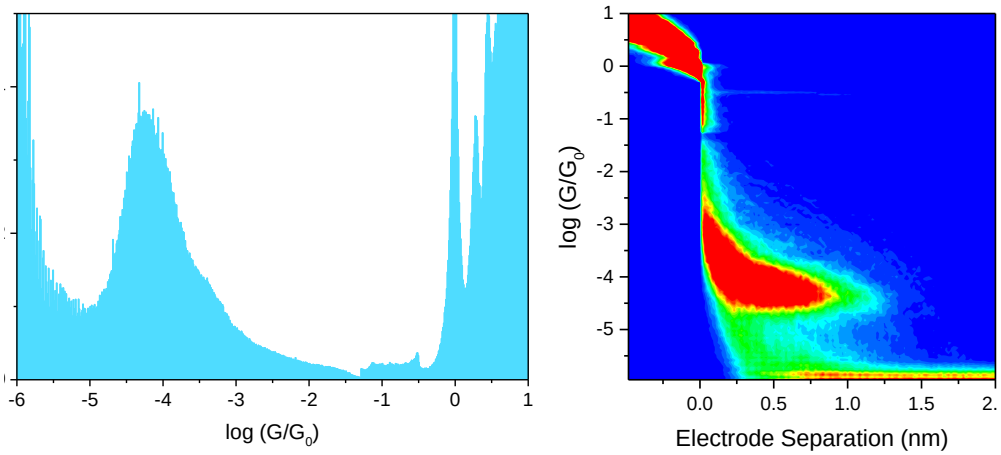

Figure A.42 SMC data (STM-BJ) for **BTBipy-ReBr(CO)$_3$** in mesytilene at 200 mV

A.22 BTBipy

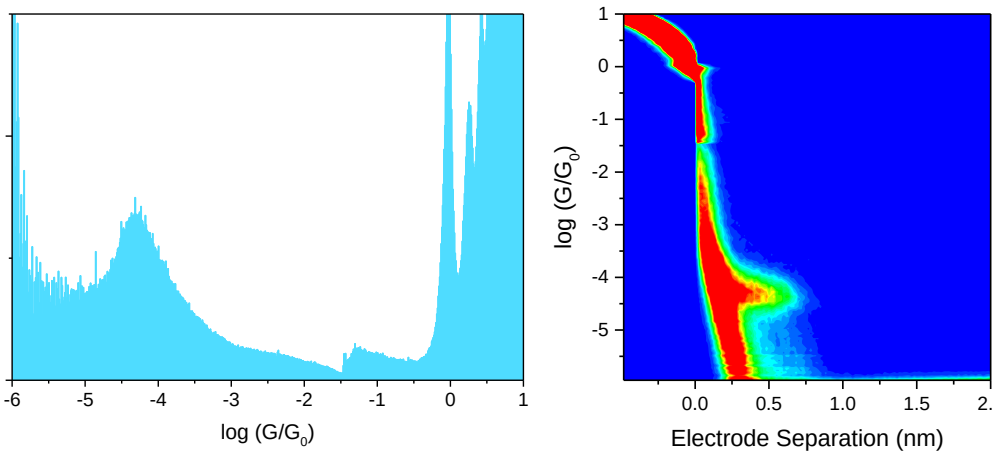

Figure A.43 SMC data (STM-BJ) for **BTBipy** in mesytilene at 300 mV

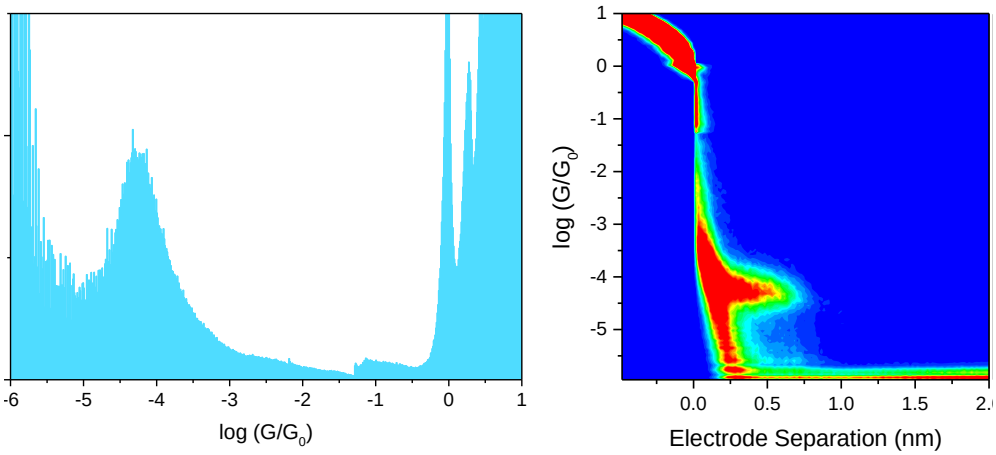

Figure A.44 SMC data (STM-BJ) for **BTBipy** in mesytilene at 200 mV

A.22.1 Comparison of bipyridine based-complexes

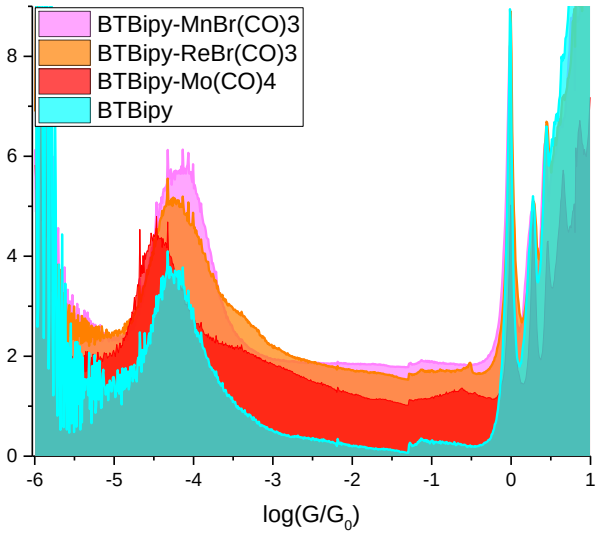

Figure A.45 SMC comparison (STM-BJ) of the BTBipy-based series of molecular wires in mesytilene at 200 mV, the comparison at 300 is reported in Chapter 4

A.23 1[Ph]1-SMe

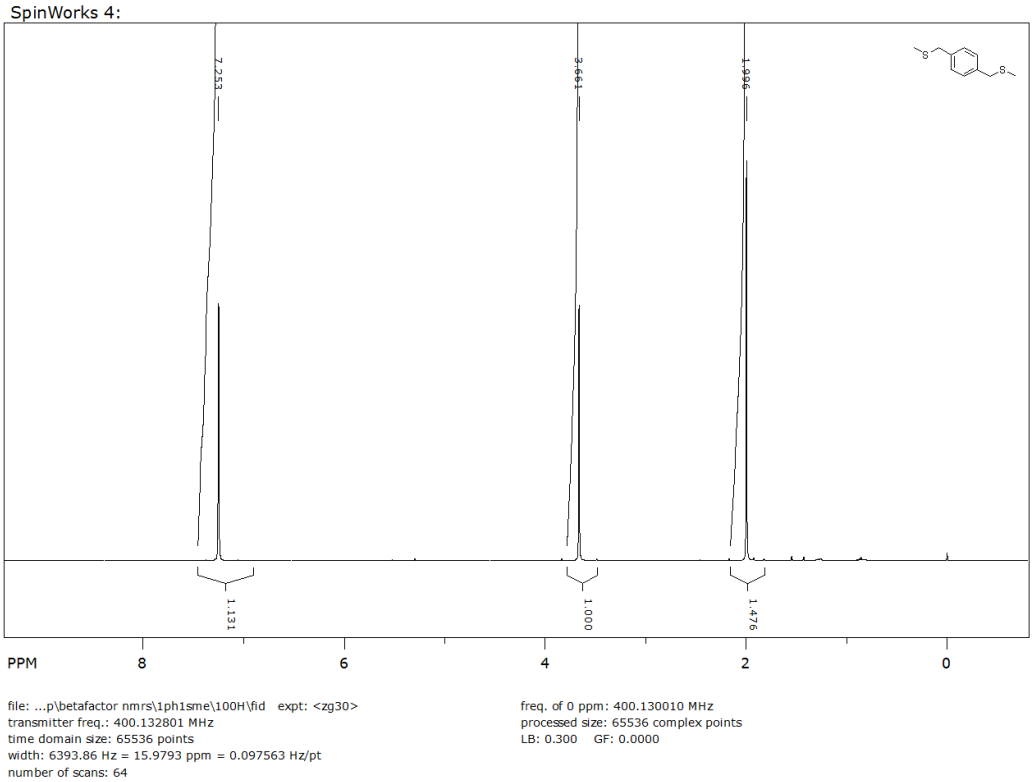

Figure A.46 ^{1}H NMR of **1[Ph]1-SMe**. 400 MHz, $CDCl_3$. Solvent peak obscured by resonance at 7.25 ppm.

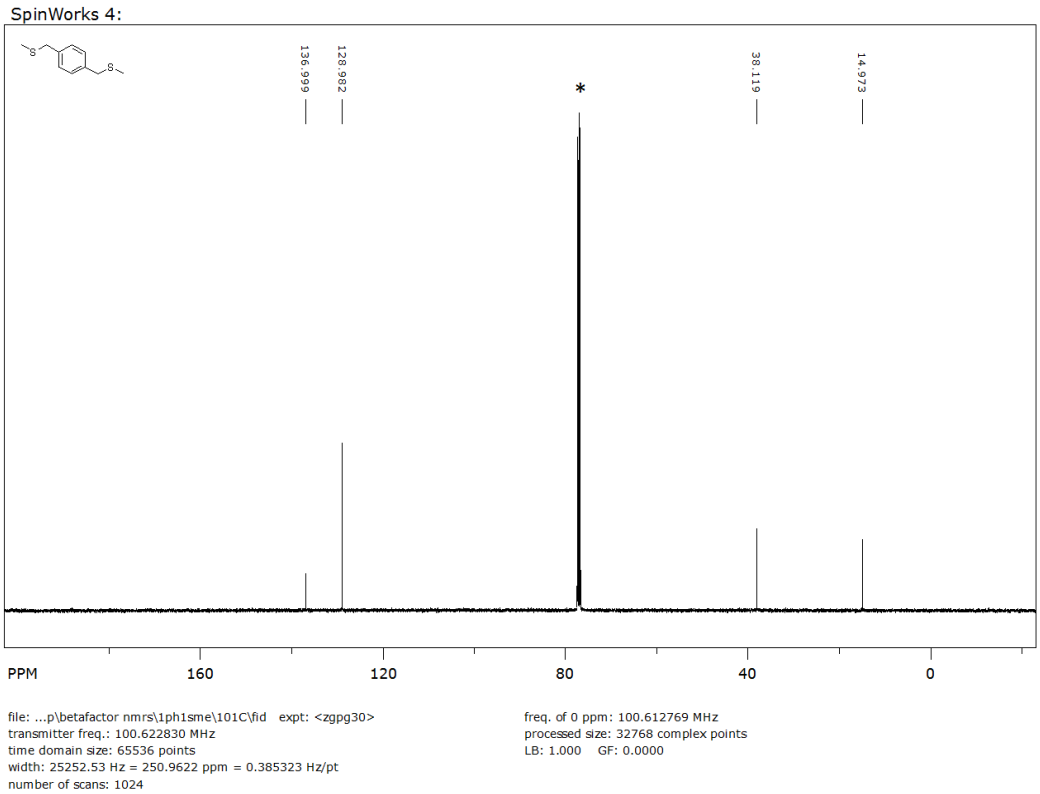

Figure A.47 ^{13}C NMR of **1[Ph]1-SMe**. 100 MHz, $CDCl_3$. Solvent peak starred.

A.24 3[Ph]3-SMe

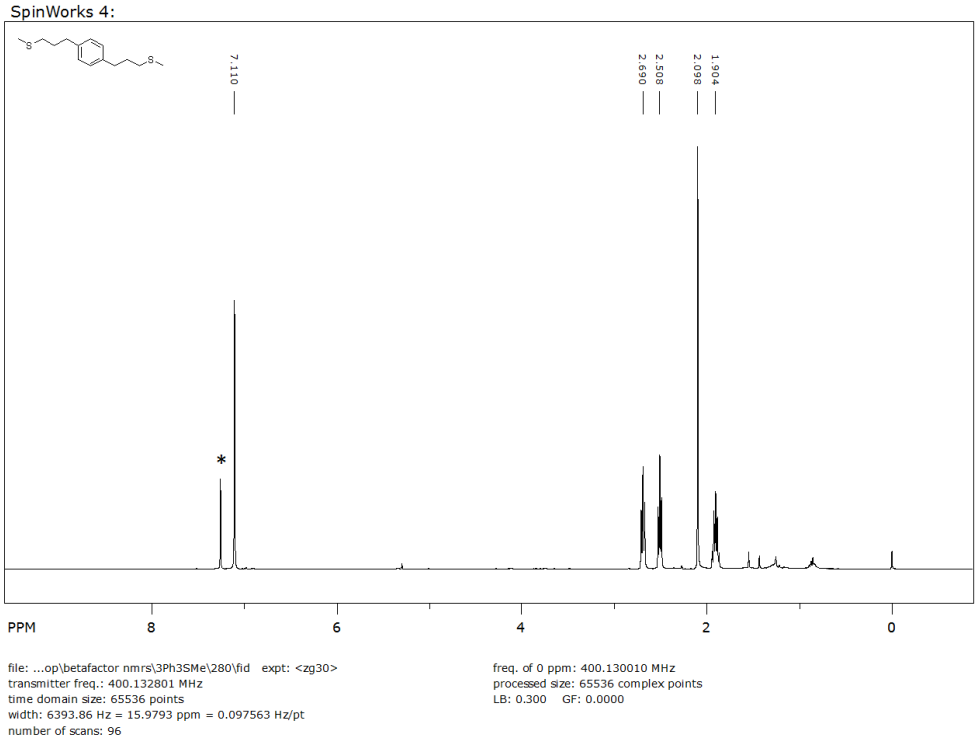

Figure A.48 ^{1}H NMR of **3[Ph]3-SMe**. 400 MHz, $CDCl_3$. Residual solvent peak starred.

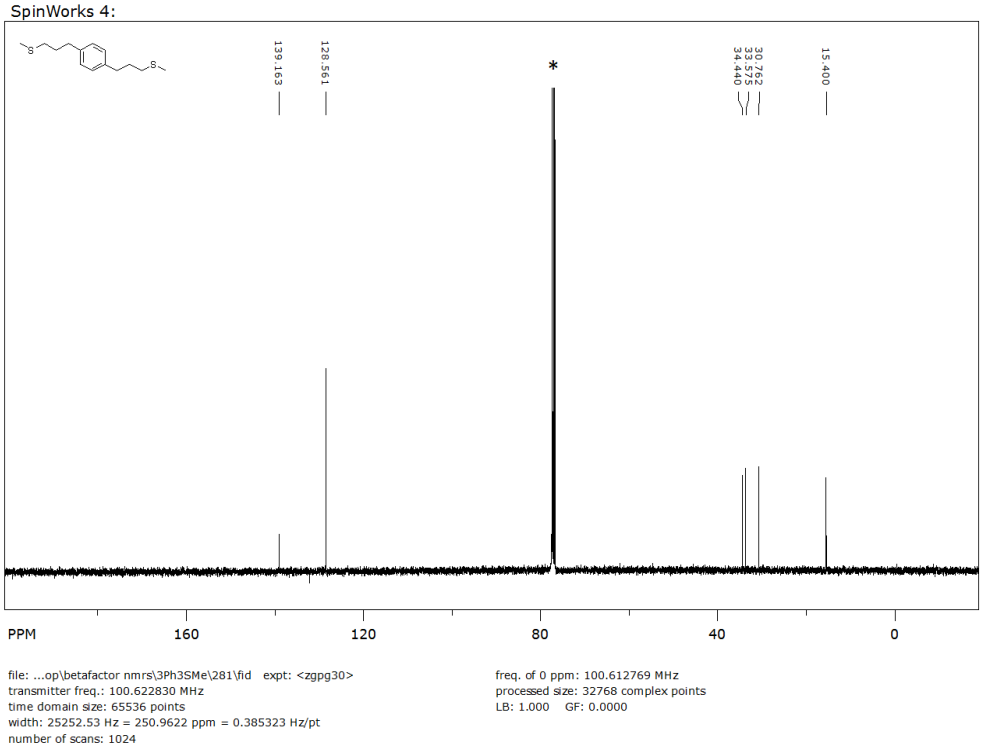

Figure A.49 ^{13}C NMR of **3[Ph]3-SMe**. 100 MHz, $CDCl_3$. Solvent peak starred.

A.25 4[Ph]4-SMe

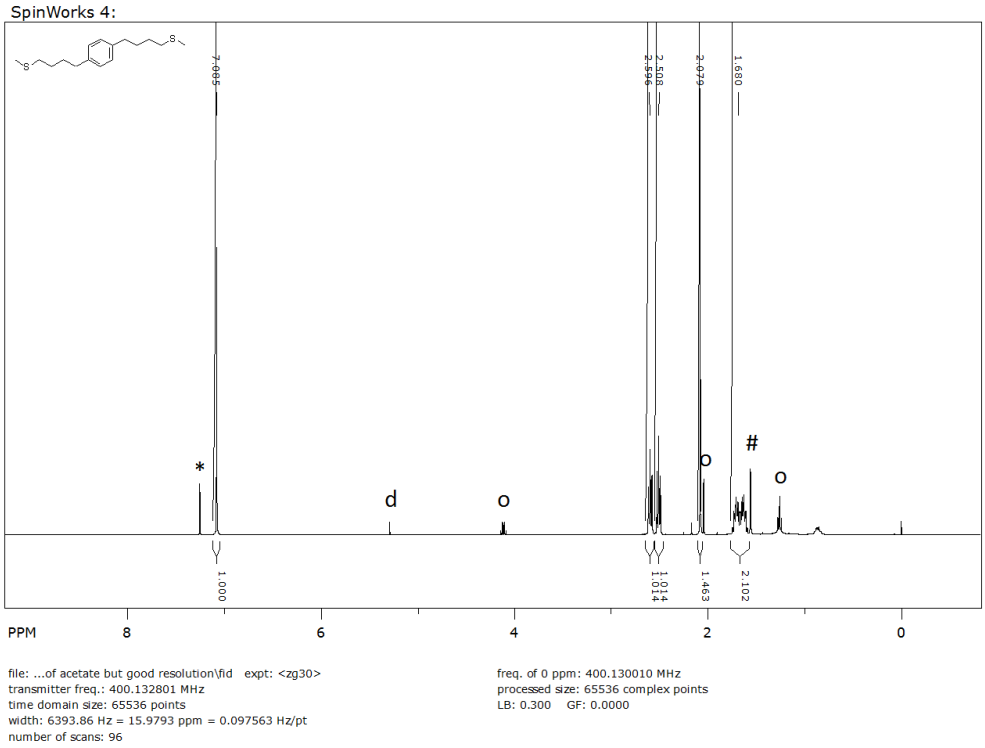

Figure A.50 ^{1}H NMR of **4[Ph]4-SMe**. 400 MHz, $CDCl_3$. Residual solvent peak starred, water peak hashed. O is residual ethyl acetate and d is residual dichloromethane that couldn't be removed on pumping in vacuo.

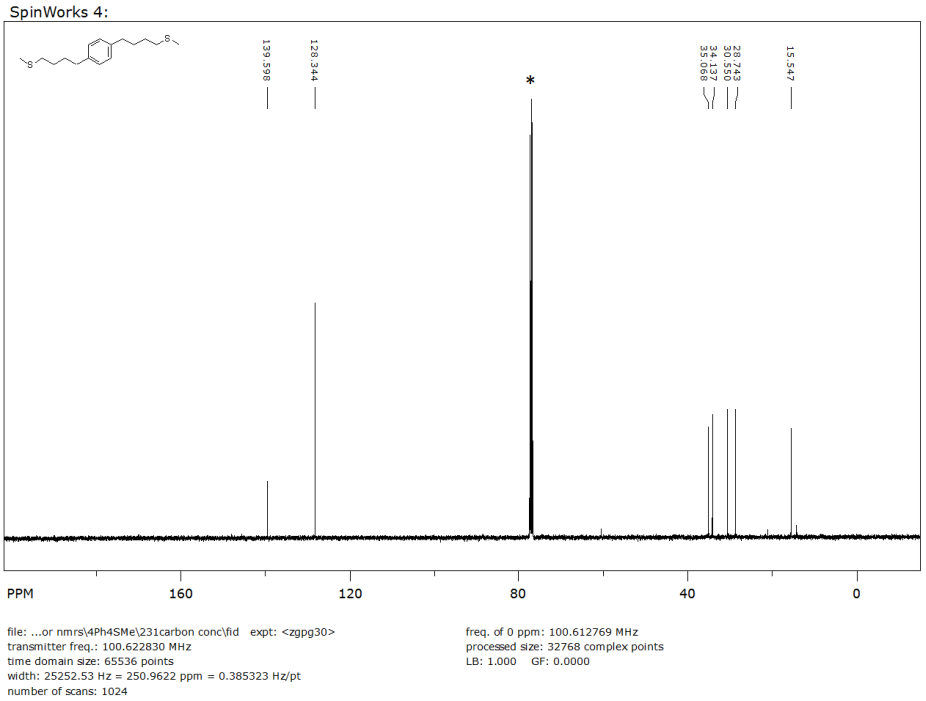

Figure A.51 ^{13}C NMR of **4[Ph]4-SMe**. 100 MHz, $CDCl_3$. Solvent peak starred.

A.26 5[Ph]5-SMe

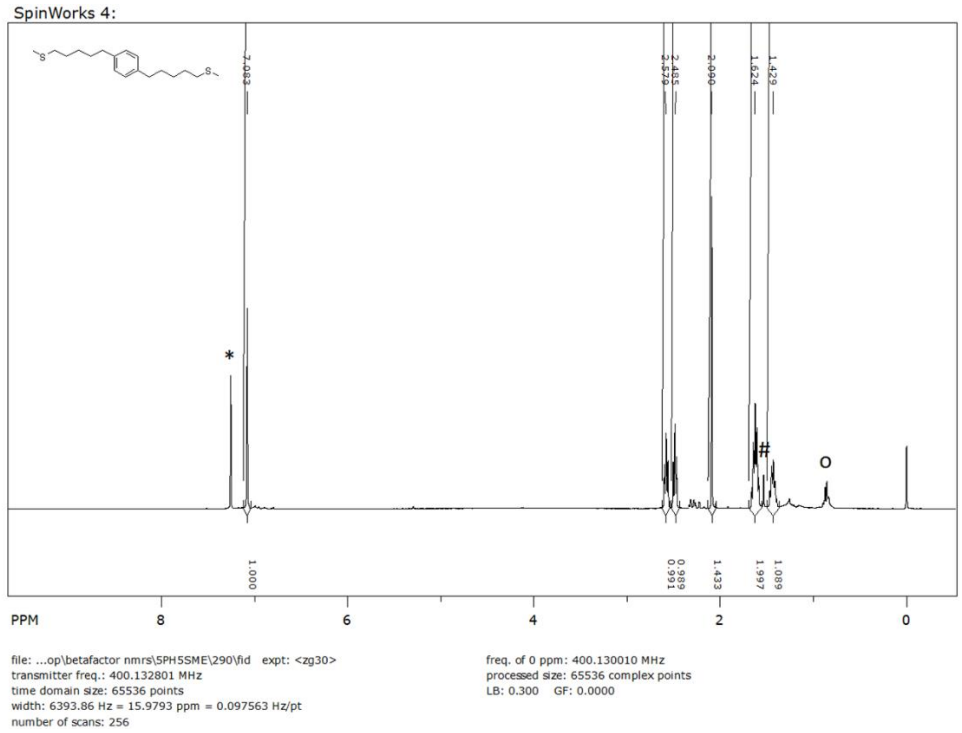

Figure A.52 ^{1}H NMR of **5[Ph]5-SMe**. 400 MHz, $CDCl_3$. Residual solvent peak starred, water peak hashed. O is residual hexane that couldn't be removed on pumping in vacuo.

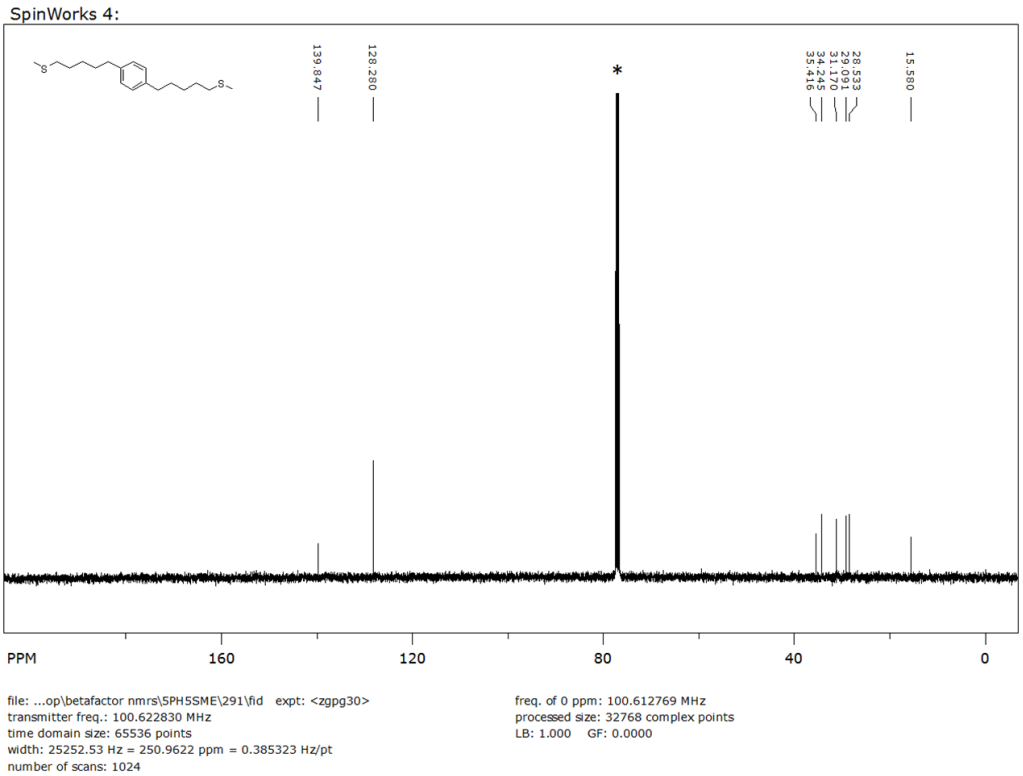

Figure A.53 ^{13}C NMR of **5[Ph]5-SMe**. 100 MHz, $CDCl_3$. Solvent peak starred.

A.27 6[Ph]6-SMe

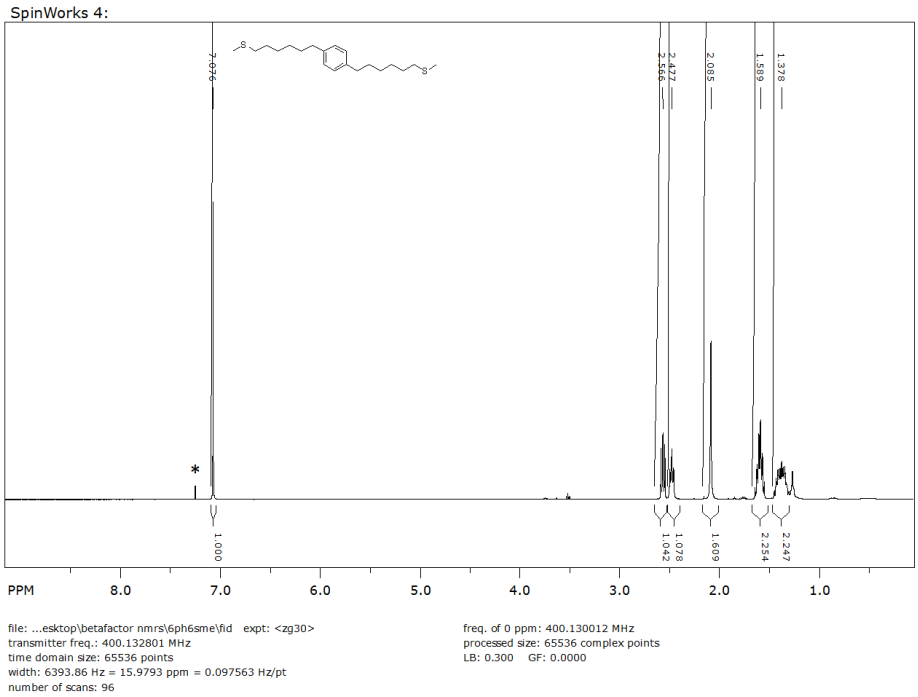

Figure A.54 ^{1}H NMR of **6[Ph]6-SMe**. 400 MHz, $CDCl_3$. Residual solvent peak starred, water peak obscured by the resonance at 1.59 ppm, increasing its integration.

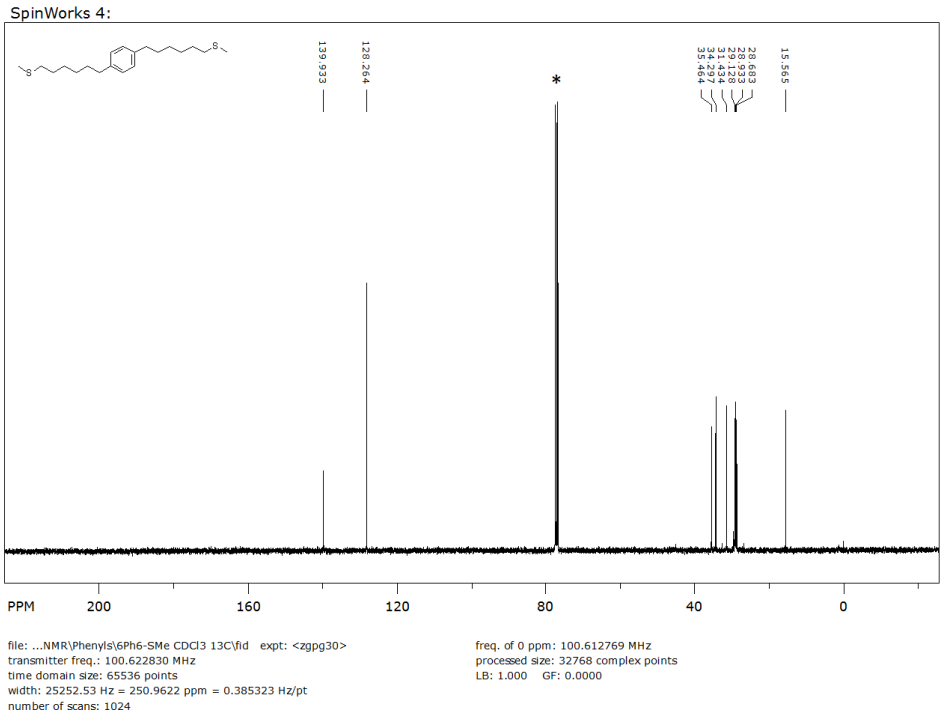

Figure A.55 ^{13}C NMR of **6[Ph]6-SMe**. 100 MHz, $CDCl_3$. Solvent peak starred.

A.28 $TCPh_2T$

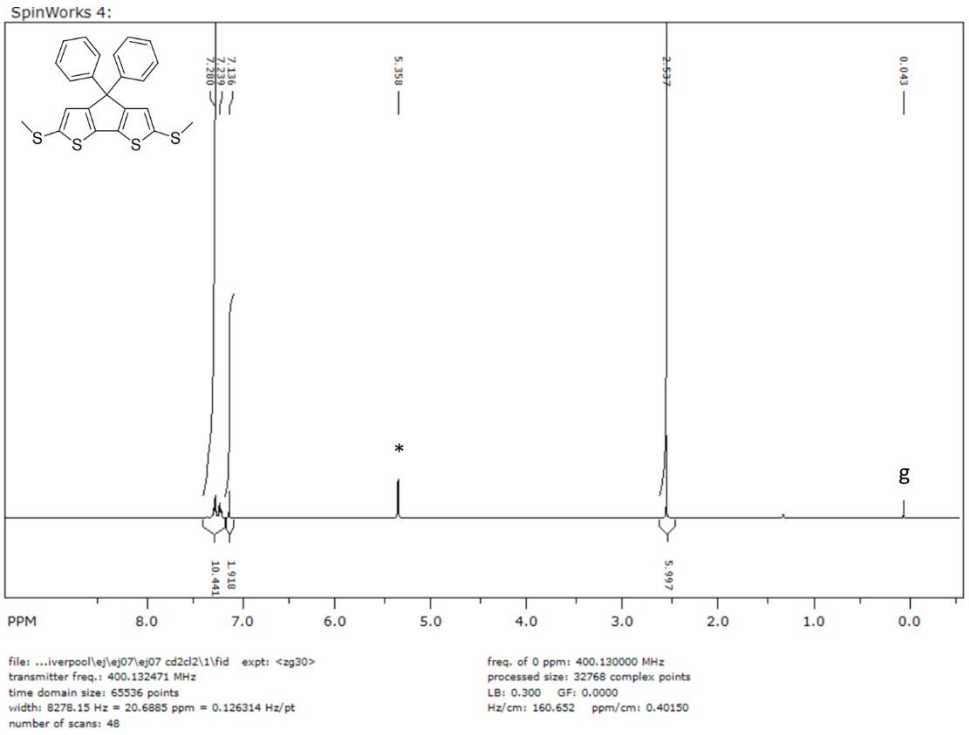

Figure A.56 ^{1}H NMR of **$TCPh_2T$**. 400 MHz, CD_2Cl_2. Residual solvent peak starred, TMS peak marked as g.

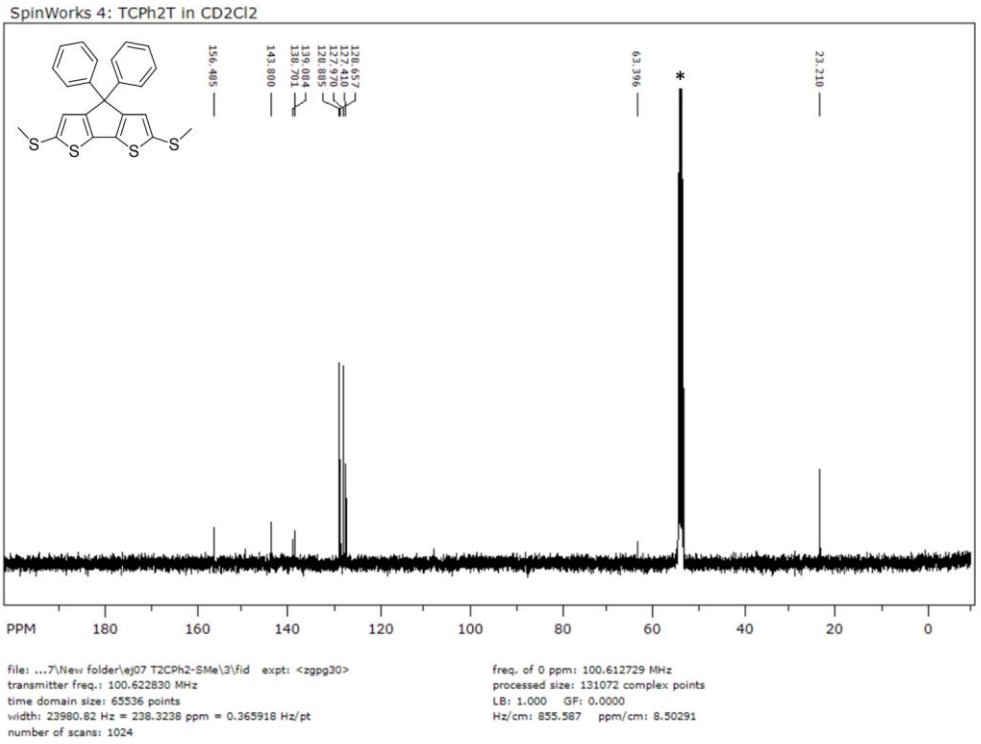

Figure A.57 ^{13}C NMR of **$TCPh_2T$**. 100 MHz, CD_2Cl_2. Solvent peak starred.

A.29 $TSiPh_2T$

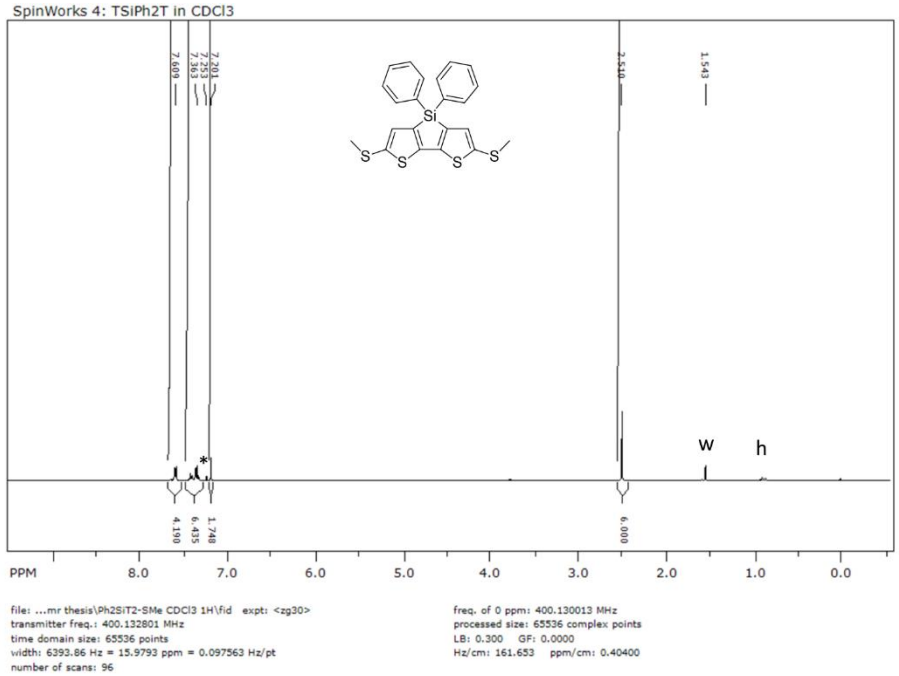

Figure A.58 ^{1}H NMR of **$TSiPh_2T$**. 400 MHz, CD_2Cl_2. Residual solvent peak starred, hexane peak marked as h.

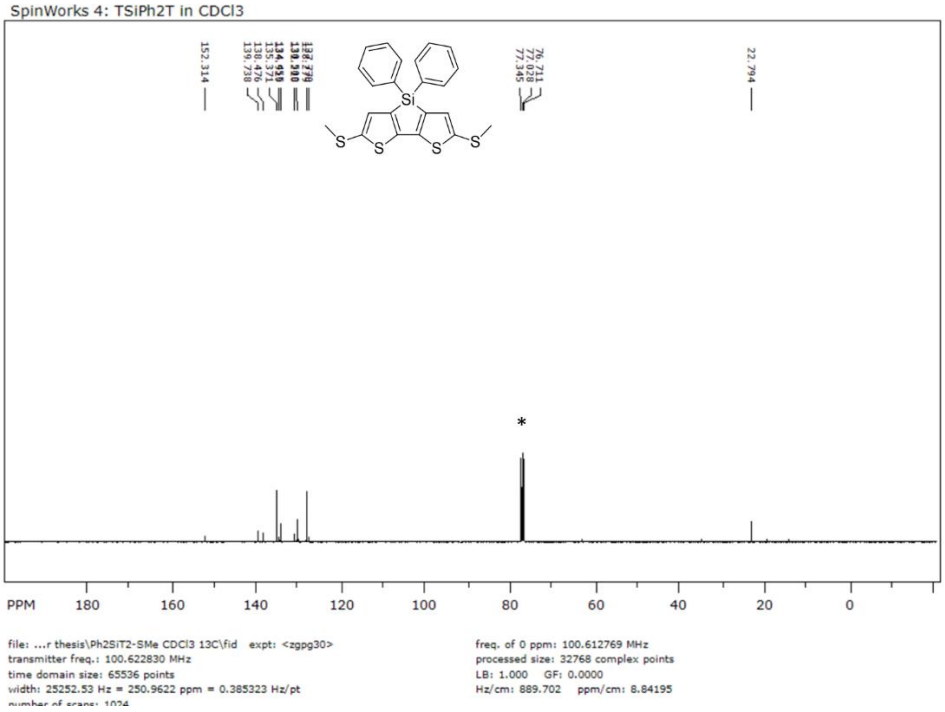

Figure A.59 ^{13}C NMR of **$TSiPh_2T$**. 100 MHz, CD_2Cl_2. Solvent peak starred.

A.30 $TGePh_2T$

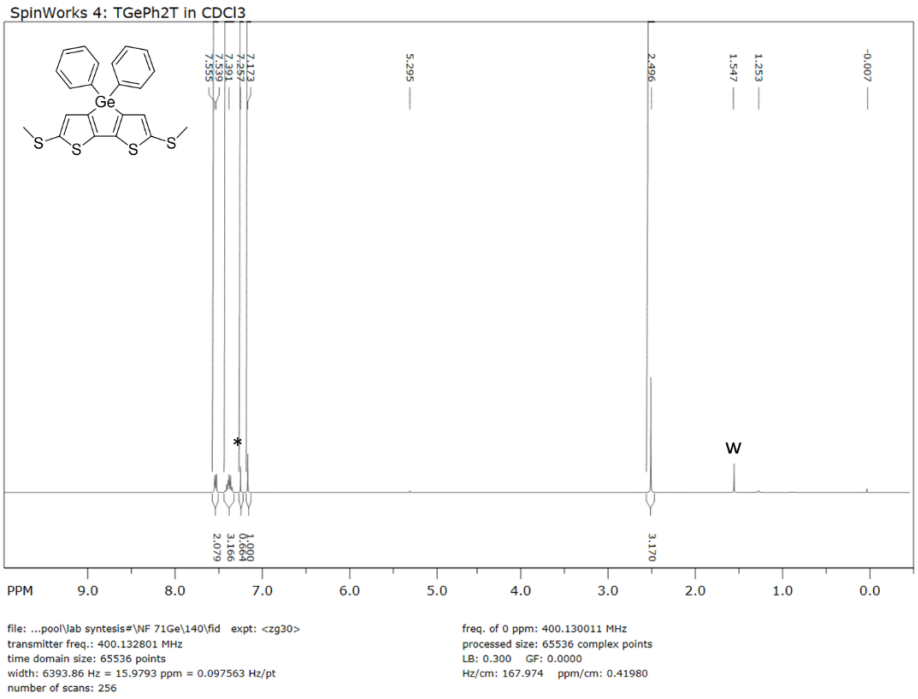

Figure A.60 ^{1}H NMR of **$TGePh_2T$**. 400 MHz, $CDCl_3$. Residual solvent peak starred, water peak marked as w.

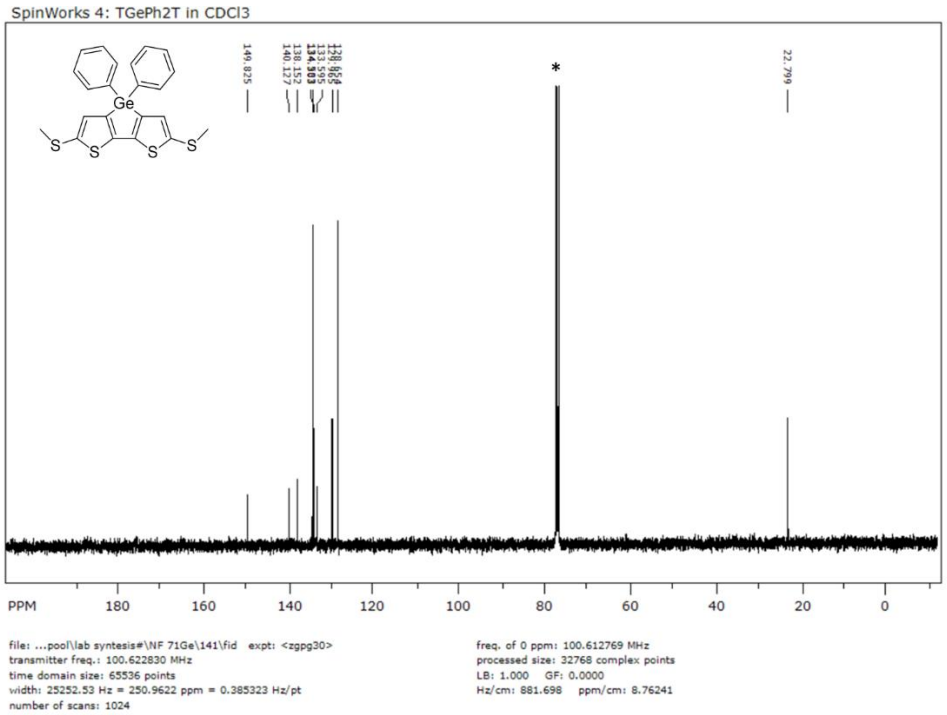

Figure A.61 ^{13}C NMR of **$TGePh_2T$**. 100 MHz, CD_2Cl_2. Solvent peak starred.

A.31 TKT

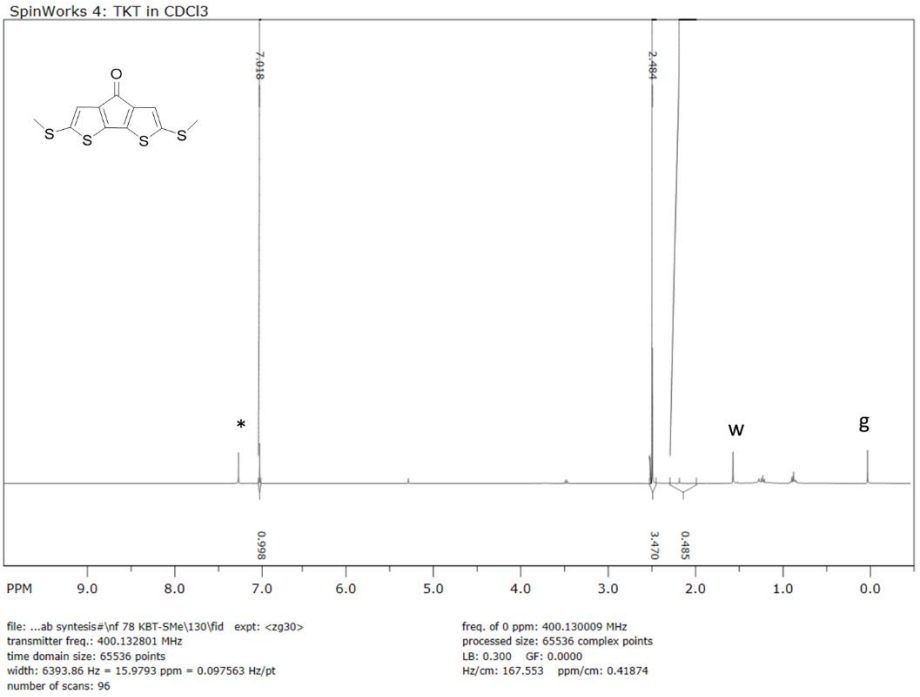

Figure A.62 ^{1}H NMR of **TKT**. 400 MHz, $CDCl_3$. Residual solvent peak starred, water peak marked as w, TMS marked as g.

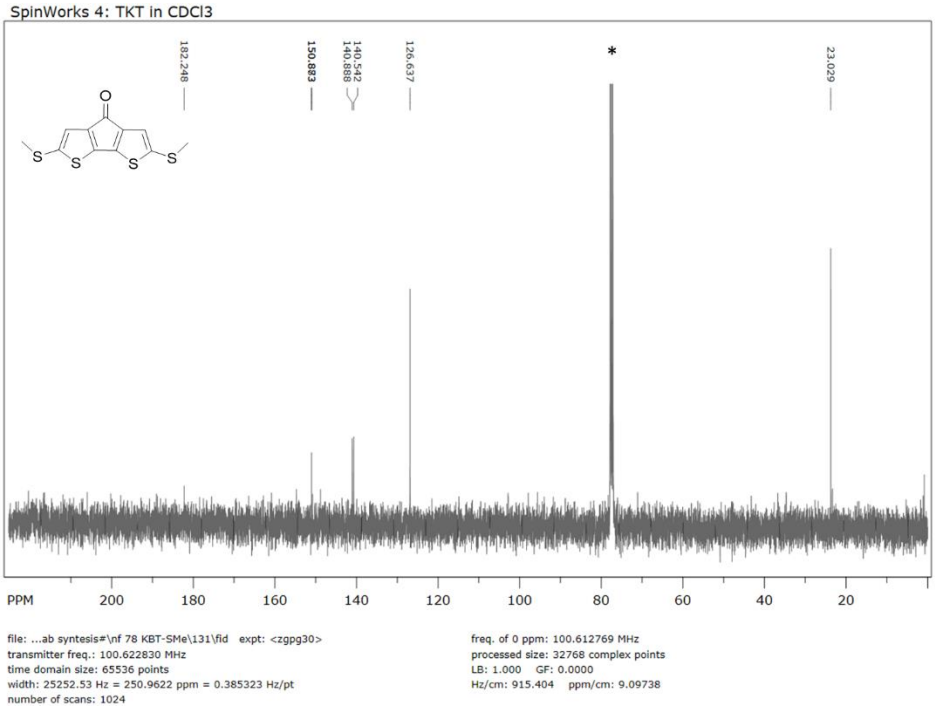

Figure A.63 ^{13}C NMR of **TKT**. 100 MHz, CD_2Cl_2. Solvent peak starred.

A.32 TDKT

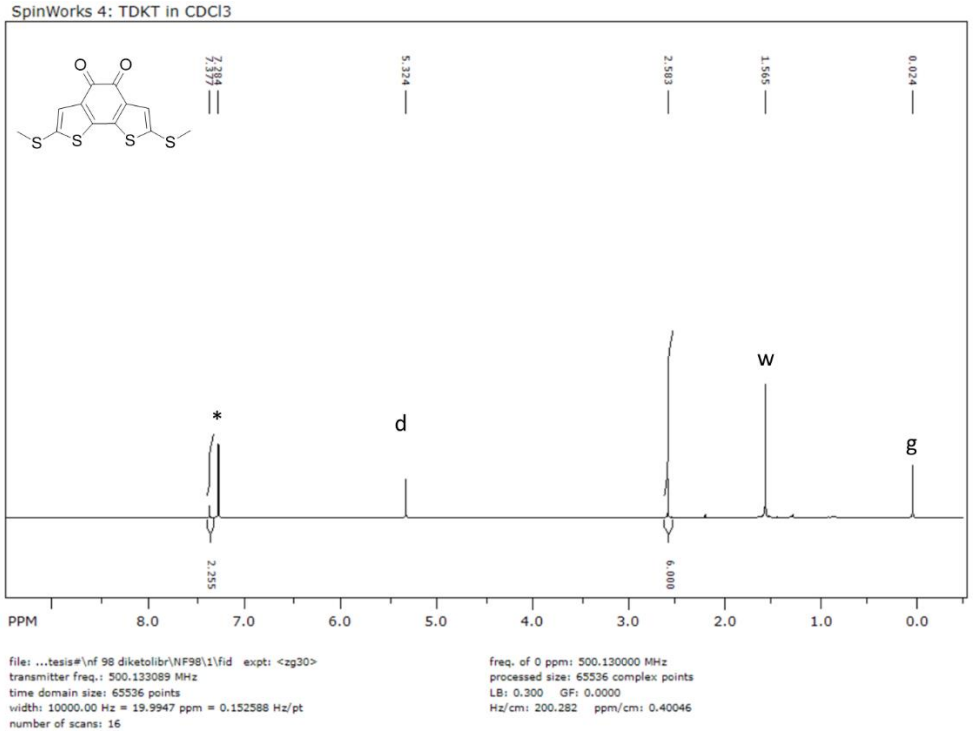

Figure A.64 ^{1}H NMR of **TDKT**. 400 MHz, $CDCl_3$. Residual solvent peak starred, water peak marked as w, TMS marked as g and CH_2Cl_2 marked as d.

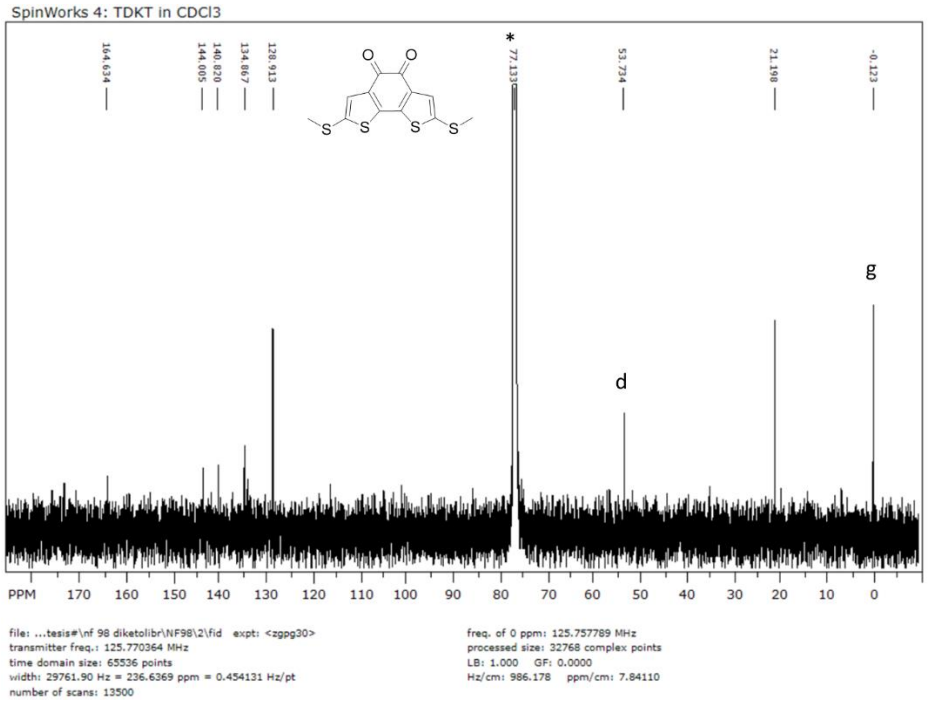

Figure A.65 ^{13}C NMR of **TDKT**. 100 MHz, CD_2Cl_2. Solvent peak starred, TMS marked as g and CH_2Cl_2 marked as d.

A.33 $TCMe_2T$

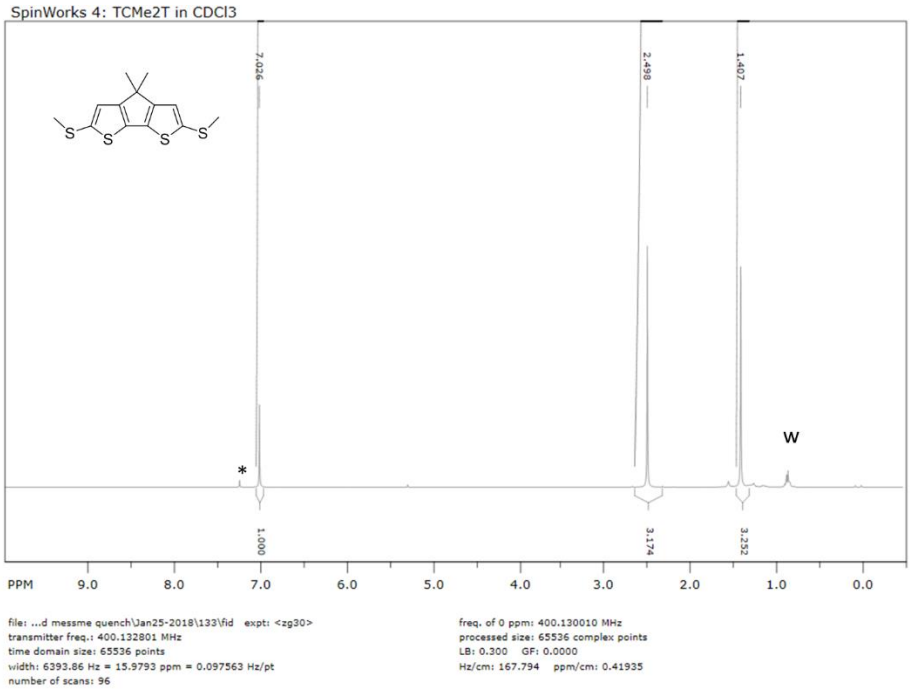

Figure A.66 ^{1}H NMR of **$TCMe_2T$**. 400 MHz, $CDCl_3$. Residual solvent peak starred, water peak marked as w.

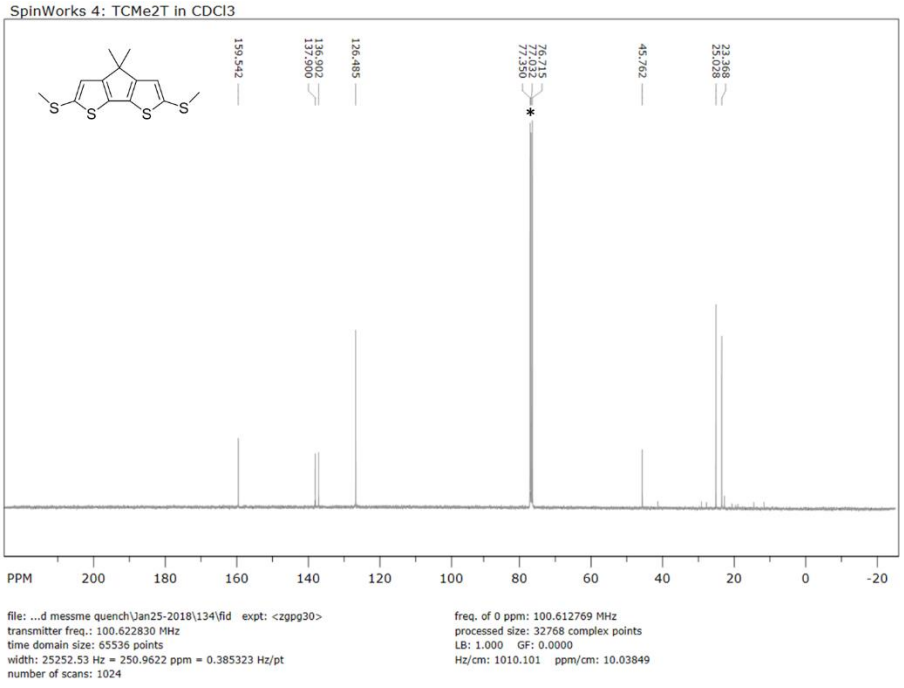

Figure A.67 ^{13}C NMR of **$TCMe_2T$**. 100 MHz, CD_2Cl_2. Solvent peak starred.

A.34 TFT

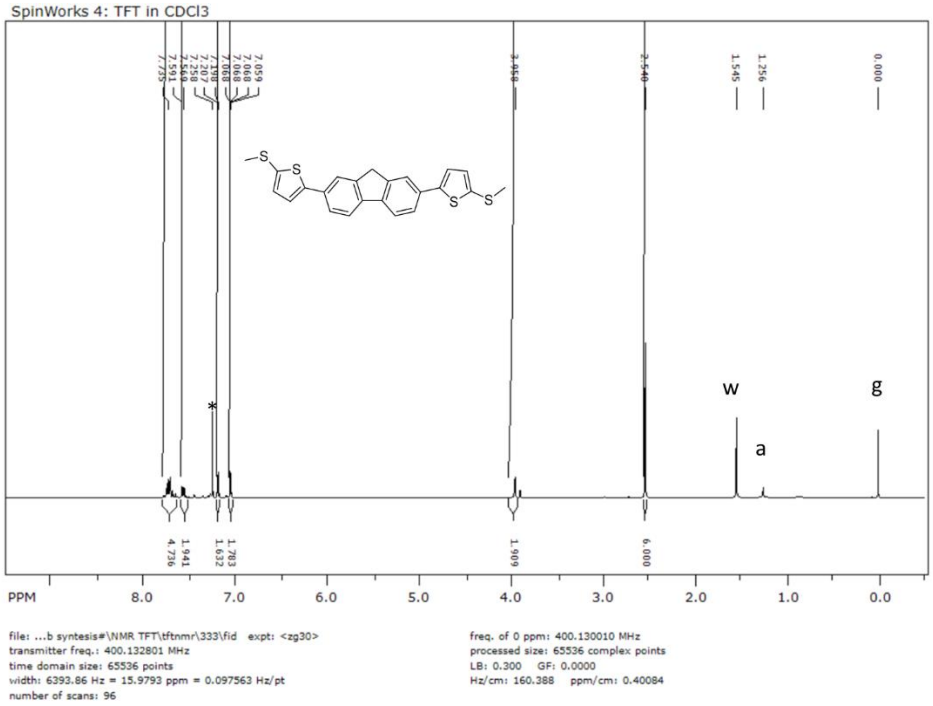

Figure A.68 ^{1}H NMR of **TFT**. 400 MHz, $CDCl_3$. Residual solvent peak starred, water peak marked as w, ethyl acetate marked as a and TMS as g.

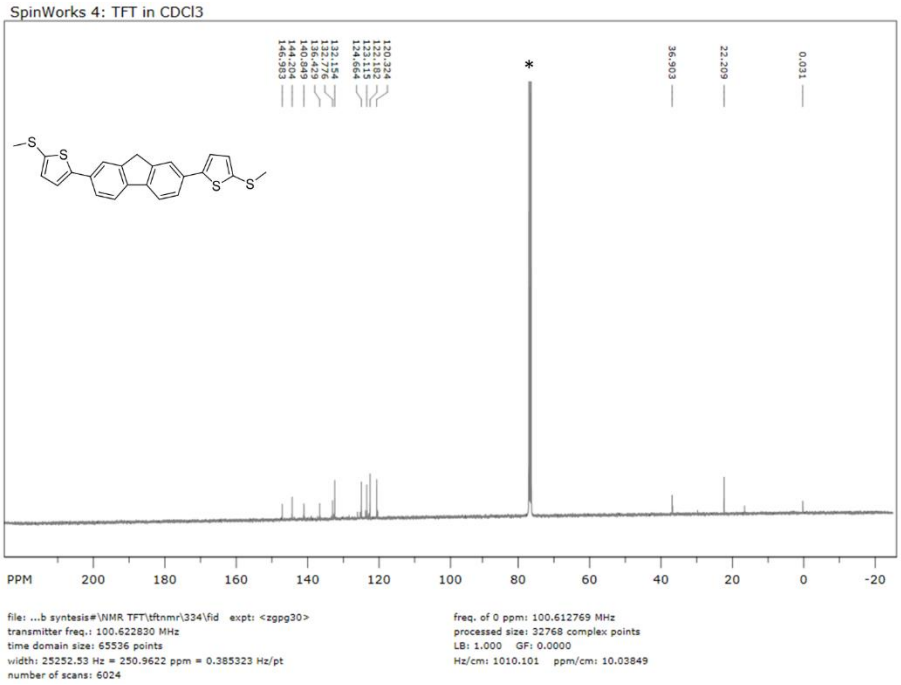

Figure A.69 ^{13}C NMR of **TFT**. 100 MHz, CD_2Cl_2. Solvent peak starred.

A.35 TFOT

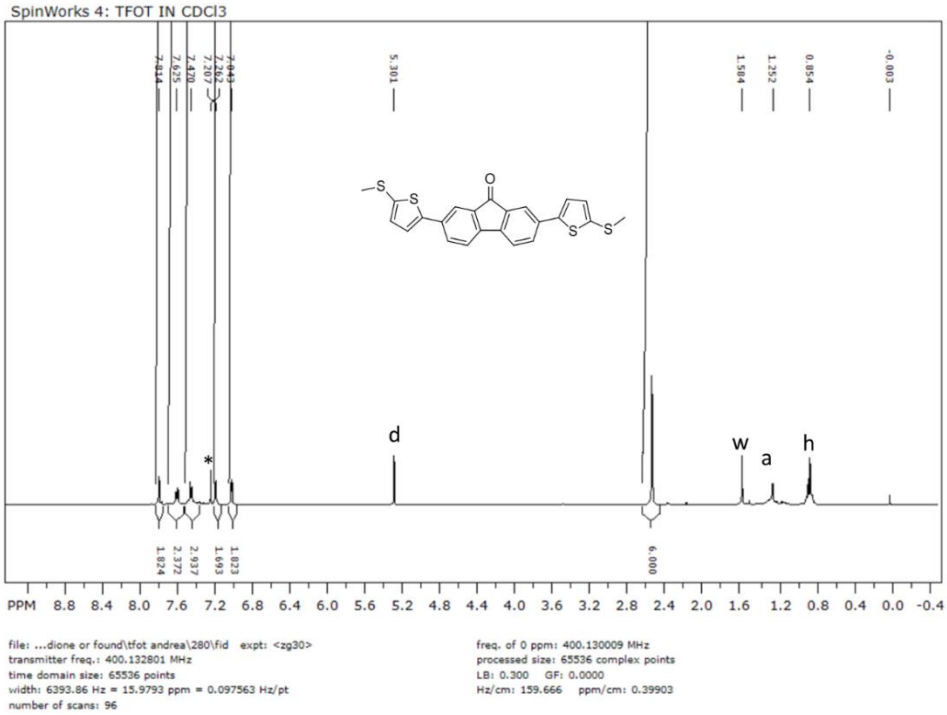

Figure A.70 ^{1}H NMR of **TFOT**. 400 MHz, $CDCl_3$. Residual solvent peak starred, DCM marked as d, water peak marked as w, ethyl acetate marked as a and hexane as h.

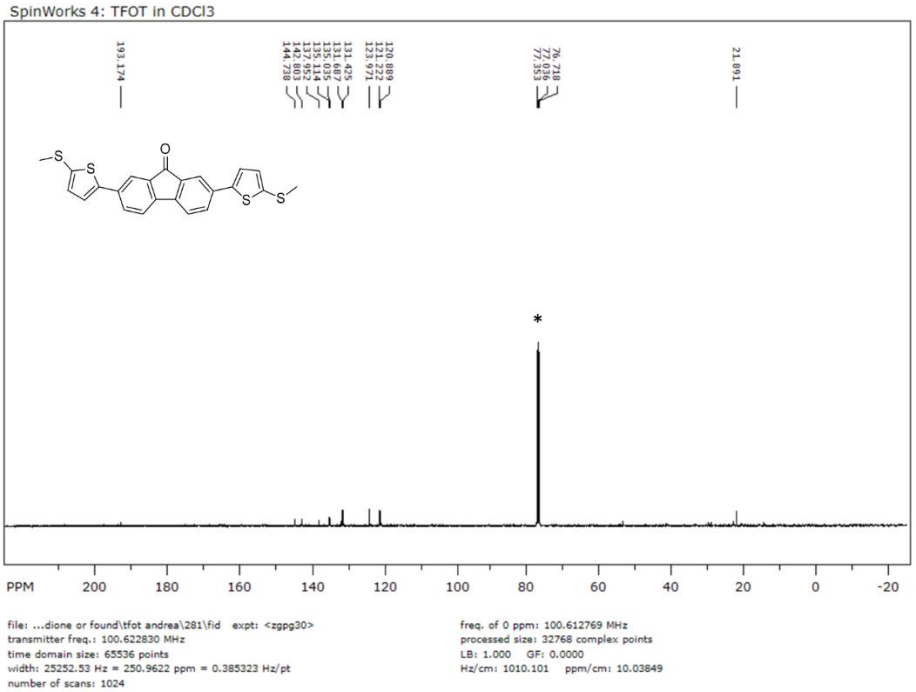

Figure A.71 ^{13}C NMR of **TFT**. 100 MHz, CD_2Cl_2. Solvent peak starred.

A.36 TPDT

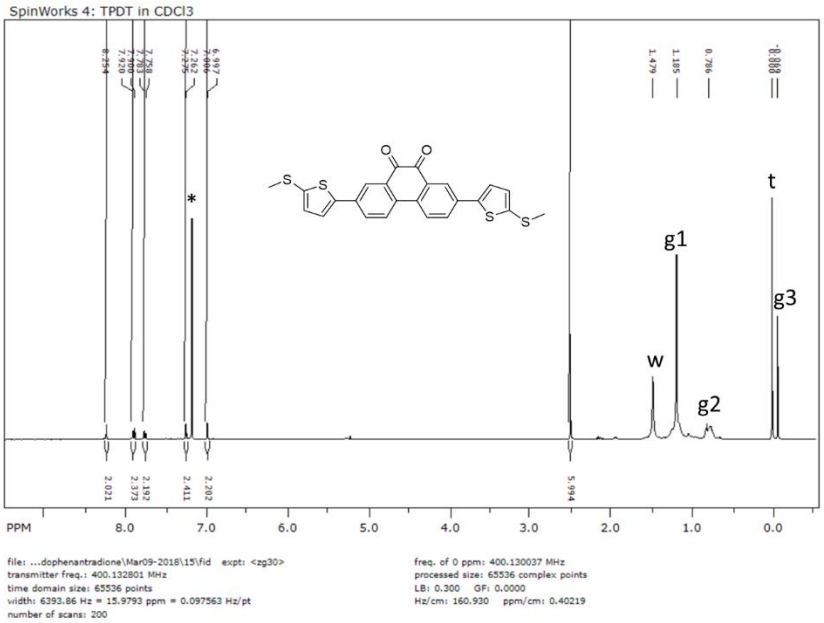

Figure A.72 ^{1}H NMR of **TPDT**. 400 MHz, $CDCl_3$. Residual solvent peak starred, grease peaks marked as g1-3, water peak marked as w, and TMS as t.

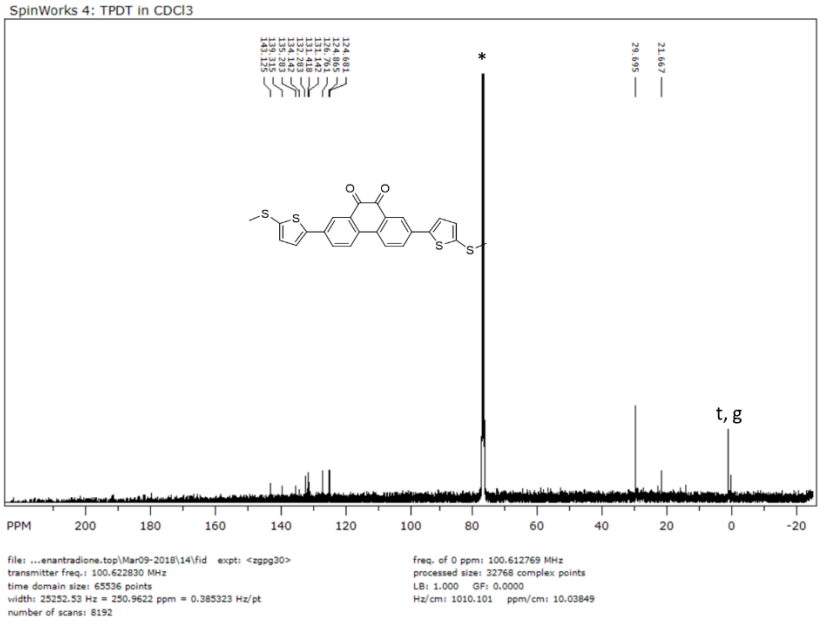

Figure A.73 ^{13}C NMR of **TFT**. 100 MHz, CD_2Cl_2. Solvent peak starred, TMS and grease peaks marked as t, g.

References

1 G. E. Moore, Craming more components onto integrated circuits, *Electronics*, 1965, **38**, 114–117.

2 R. H. Dennard, F. H. Gaensslen and H. Yl, Design of lon-Implanted MOSFET ' s with Very Small PhYSical Dimensions, 1999, **87**, 668–678.

3 M. Bohr, A 30 Year Retrospective on Dennard's MOSFET Scaling Paper, *IEEE Solid-State Circuits Newsl.*, 2007, **12**, 11–13.

4 S. E. Thompson and S. Parthasarathy, Moore's law: the future of Si microelectronics, *Mater. Today*, 2006, **9**, 20–25.

5 B. Mann, H. Kuhn, B. Mann and H. Kuhn, Tunneling through Fatty Acid Salt Monolayers Tunneling through Fatty Acid Salt Monolayers, *J. Appl. Phys*, 1971, **42**, 4398.

6 A. Aviram and M. A. Ratner, Molecular rectifiers, *Chem. Phys. Lett.*, 1974, **29**, 277–283.

7 M. A. Reed, C. Zhou, C. J. Muller, T. P. Burgin and J. M. Tour, Conductance of a molecular junction, *Science*, 1997, **278**, 252–254.

8 C. J. Chen, Introduction to Scanning Tunneling Microscopy Second Edition, *Oxford Univ. Press*, 2008, (2008).

9 Q. Lu, K. Liu, H. Zhang, Z. Du, X. Wang and F. Wang, From tunneling to hopping: A comprehensive investigation of charge transport mechanism in molecular junctions based on oligo(p-phenylene ethynylene)s, *ACS Nano*, 2009, **3**, 3861–3868.

10 X. D. Cui, A. Primak, X. Zarate, J. Tomfohr, O. F. Sankey, A. L. Moore, T. A. Moore, D. Gust, G. Harris and S. M. Lindsay, Reproducible measurement of single-molecule conductivity, *Science*, 2001, **294**, 571–574.

11 A. Vezzoli, R. J. Brooke, N. Ferri, S. J. Higgins, W. Schwarzacher and R. J. Nichols, Single-Molecule Transport at a Rectifying GaAs Contact, *Nano Lett.*,

2017, **17**, 1109–1115.

12 A. Vezzoli, R. Brooke, N. Ferri, C. Brooke, S. Higgins, W. Schwarzacher and R. J. Nichols, Charge Transport at a Molecular GaAs Nanoscale Junction, *Faraday Discuss.*, 2018, **210**, 397-408.

13 B. Xu and N. J. Tao, Measurement of single-molecule resistance by repeated formation of molecular junctions, *Science.*, 2003, **301**, 1221–1223.

14 Y. Zhao, S. Lindsay, S. Jeon, H. J. Kim, L. Su, B. Lim and S. Koo, Combined effect of polar substituents on the electronic flows in the carotenoid molecular wires, *Chem. - A Eur. J.*, 2013, **19**, 10832–10835.

15 C. R. Arroyo, S. Tarkuc, R. Frisenda, J. S. Seldenthuis, C. H. M. Woerde, R. Eelkema, F. C. Grozema and H. S. J. Van Der Zant, Signatures of quantum interference effects on charge transport through a single benzene ring, *Angew. Chemie - Int. Ed.*, 2013, **52**, 3152–3155.

16 C. Li, I. Pobelov, T. Wandlowski, A. Bagrets, A. Arnold and F. Evers, Charge transport in single Au | alkanedithiol | Au junctions: Coordination geometries and conformational degrees of freedom, *J. Am. Chem. Soc.*, 2008, **130**, 318–326.

17 X. S. Zhou, J. H. Liang, Z. Bin Chen and B. W. Mao, An electrochemical jump-to-contact STM-break junction approach to construct single molecular junctions with different metallic electrodes, *Electrochem. commun.*, 2011, **13**, 407–410.

18 C. A. Martin, D. Ding, J. K. Sørensen, T. Bjørnholm, J. M. van Ruitenbeek and H. S. J. van der Zant, Fullerene - based anchoring groups for molecular electronics, *J. Am. Chem. Soc.*, 2008, **130**, 13198–13199.

19 R. Parameswaran, J. R. Widawsky, H. Vázquez, Y. S. Park, B. M. Boardman, C. Nuckolls, M. L. Steigerwald, M. S. Hybertsen and L. Venkataraman, Reliable formation of single molecule junctions with air-stable diphenylphosphine linkers, *J. Phys. Chem. Lett.*, 2010, **1**, 2114–2119.

20 S. Marqués-González, D. S. Yufit, J. A. K. Howard, S. Martín, H. M. Osorio, V. M. García-Suárez, R. J. Nichols, S. J. Higgins, P. Cea and P. J. Low, Simplifying the conductance profiles of molecular junctions: the use of the trimethylsilylethynyl moiety as a molecule–gold contact, *Dalt. Trans.*, 2013, **42**, 338–341.

21 F. Chen, X. Li, J. Hihath, Z. Huang and N. Tao, Effect of anchoring groups on single-molecule conductance: Comparative study of thiol-, amine-, and carboxylic-acid-terminated molecules, *J. Am. Chem. Soc.*, 2006, **128**, 15874–15881.

22 L. Luo, S. H. Choi and C. D. Frisbie, Probing hopping conduction in conjugated molecular wires connected to metal electrodes, *Chem. Mater.*, 2011, **23**, 631–645.

23 L. Luo and C. D. Frisbie, Length-dependent conductance of conjugated molecular wires synthesized by stepwise 'click' chemistry, *J. Am. Chem. Soc.*, 2010, **132**, 8854–8855.

24 Z. Xie, I. Bâldea, A. T. Demissie, C. E. Smith, Y. Wu, G. Haugstad and C. D. Frisbie, Exceptionally Small Statistical Variations in the Transport Properties of Metal-Molecule-Metal Junctions Composed of 80 Oligophenylene Dithiol Molecules, *J. Am. Chem. Soc.*, 2017, **139**, 5696–5699.

25 A. Borges and G. C. Solomon, Effects of Aromaticity and Connectivity on the Conductance of Five-Membered Rings, *J. Phys. Chem. C*, 2017, **121**, 8272–8279.

26 H. Li, M. H. Garner, T. A. Su, A. Jensen, M. S. Inkpen, M. L. Steigerwald, L. Venkataraman, G. C. Solomon and C. Nuckolls, Extreme Conductance Suppression in Molecular Siloxanes, *J. Am. Chem. Soc.*, 2017, **139**, 10212–10215.

27 G. C. Solomon, C. Herrmann, T. Hansen, V. Mujica and M. A. Ratner, Exploring local currents in molecular junctions, *Nat. Chem.*, 2010, **2**, 223–228.

28 J. H. Smit, Quantum interference effects in molecular electronics, 2011, **15**.

29 M. Ratner, A brief history of molecular electronics, *Nat. Nanotechnol.*, 2013, **8**, 378–381.

30 C. J. Lambert, Basic concepts of quantum interference and electron transport in single-molecule electronics, *Chem. Soc. Rev.*, 2015, **44**, 875–888.

31 G. Sedghi, V. M. García-Suárez, L. J. Esdaile, H. L. Anderson, C. J. Lambert, S. Martín, D. Bethell, S. J. Higgins, M. Elliott, N. Bennett, J. E. MacDonald and R. J. Nichols, Long-range electron tunnelling in oligo-porphyrin molecular wires, *Nat. Nanotechnol.*, 2011, **6**, 517–523.

32 D. J. Wold, R. Haag, M. A. Rampi and C. D. Frisbie, Distance dependence of electron tunneling through self-assembled monolayers measured by conducting probe atomic force microscopy: Unsaturated versus saturated molecular junctions, *J. Phys. Chem. B*, 2002, **106**, 2813–2816.

33 S. H. Choi, C. Risko, M. Carmen Ruiz Delgado, B. Kim, J. L. Brédas and C. Daniel Frisbie, Transition from Tunneling to Hopping Transport in Long, Conjugated Oligo-imine Wires Connected to Metals, *J. Am. Chem. Soc.*, 2010, **132**, 4358–4368.

34 G. Sedghi, K. Sawada, L. J. Esdaile, M. Hoffmann, H. L. Anderson, D. Bethell, W. Haiss, S. J. Higgins and R. J. Nichols, Single molecule conductance of porphyrin wires with ultralow attenuation, *J. Am. Chem. Soc.*, 2008, **130**, 8582–8583.

35 Z. Li, T. H. Park, J. Rawson, M. J. Therien and E. Borguet, Quasi-ohmic single molecule charge transport through highly conjugated meso-to-meso ethyne-bridged porphyrin wires, *Nano Lett.*, 2012, **12**, 2722–2727.

36 Q. Ferreira, A. M. Bragança, L. Alcácer and J. Morgado, Conductance of well-defined porphyrin self-assembled molecular wires up to 14 nm in length, *J. Phys. Chem. C*, 2014, **118**, 7229–7234.

37 C. Wang, A. S. Batsanov, M. R. Bryce, S. Martín, R. J. Nichols, S. J. Higgins, V. M. García-Suárez and C. J. Lambert, Oligoyne single molecule wires, *J. Am. Chem. Soc.*, 2009, **131**, 15647–15654.

38 B. Q. Xu, X. L. Li, X. Y. Xiao, H. Sakaguchi and N. J. Tao, Electromechanical and conductance switching properties of single oligothiophene molecules, *Nano Lett.*, 2005, **5**, 1491–1495.

39 E. Leary, H. H??benreich, S. J. Higgins, H. Van Zalinge, W. Haiss, R. J. Nichols, C. M. Finch, I. Grace, C. J. Lambert, R. McGrath and J. Smerdon, Single-molecule solvation-shell sensing, *Phys. Rev. Lett.*, 2009, **102**, 1–4.

40 E. Pires, J. E. Macdonald and M. Elliott, Chain length and temperature dependence of alkanedithiol molecular conductance under ultra high vacuum, *Nanoscale*, 2013, **5**, 9397.

41 W. Haiss, S. Martin, L. E. Scullion, L. Bouffier, S. J. Higgins and R. J. Nichols, Anomalous length and voltage dependence of single molecule conductance, *Phys. Chem. Chem. Phys.*, 2009, **11**, 10831.

42 C. Brooke, A. Vezzoli, S. J. Higgins, L. A. Zotti, J. J. Palacios and R. J. Nichols, Resonant transport and electrostatic effects in single-molecule electrical junctions, *Phys. Rev. B - Condens. Matter Mater. Phys.*, 2015, **91**, 1–9.

43 F. Pauly, E. Scheer, Y. Kim, T. J. Hellmuth, B. Marius and K. I. M. E. T. Al, Characteristics of Amine-Ended and Junctions Revealed by Inelastic Electron Tunneling Spectroscopy, 2011, **5**, 4104–4111.

44 F. Hüser and G. C. Solomon, From Chemistry to Functionality: Trends for the Length Dependence of the Thermopower in Molecular Junctions, *J. Phys. Chem. C*, 2015, 150612131913005.

45 Z. Xie, I. Bâldea, C. E. Smith, Y. Wu and C. D. Frisbie, Experimental and Theoretical Analysis of Nanotransport in Oligophenylene Dithiol Junctions as a Function of Molecular Length and Contact Work Function, *ACS Nano*, 2015, **9**, 8022–8036.

46 E. Leary, S. J. Higgins, H. van Zalinge, W. Haiss and R. J. Nichols, Chemical control of double barrier tunnelling in α,ω-dithiaalkane molecular wires, *Chem. Commun.*, 2007, 3939–3941.

47 E. Leary, S. J. Higgins, H. Van Zalinge, W. Haiss, R. J. Nichols, S. Nygaard, J. O. Jeppesen and J. Ulstrup, Structure-property relationships in redox-gated single molecule junctions - A comparison of pyrrolo-tetrathiafulvalene and viologen redox groups, *J. Am. Chem. Soc.*, 2008, **130**, 12204–12205.

48 Z. Li, I. Pobelov, B. Han, T. Wandlowski, A. Błaszczyk and M. Mayor, Conductance of redox-active single molecular junctions: An electrochemical approach, *Nanotechnology*, 2006, **18**, 2745–2779 .

49 S. Sangtarash, A. Vezzoli, H. Sadeghi, N. Ferri, H. M. O 'brien, I. Grace, L. Bouffier, S. J. Higgins, R. J. Nichols and C. J. Lambert, Gateway state-mediated, long-range tunnelling in molecular wires, *Nanoscale*, 2018, **10**, 3060-3067.

50 J. M. Soler, E. Artacho, J. D. Gale, A. García, J. Junquera, P. Ordejón and D. Sánchez-Portal, The SIESTA method for ab initio order- N materials, *J. Phys. Condens. Matter*, 2002, **14**, 2745–2779.

51 J. Ferrer, C. J. Lambert, V. M. García-Suárez, D. Z. Manrique, D. Visontai, L. Oroszlany, R. Rodríguez-Ferradás, I. Grace, S. W. D. Bailey, K. Gillemot, H. Sadeghi and L. A. Algharagholy, GOLLUM: A next-generation simulation tool for electron, thermal and spin transport, *New J. Phys.*, 2014, **16**, 093029

52 W. B. Chang, C. K. Mai, M. Kotiuga, J. B. Neaton, G. C. Bazan and R. A. Segalman, Controlling the thermoelectric properties of thiophene-derived single-molecule junctions, *Chem. Mater.*, 2014, **26**, 7229–7235.

53 B. Capozzi, J. Z. Low, J. Xia, Z. F. Liu, J. B. Neaton, L. M. Campos and L. Venkataraman, Mapping the Transmission Functions of Single-Molecule Junctions, *Nano Lett.*, 2016, **16**, 3949–3954.

54 J. Z. Low, B. Capozzi, J. Cui, S. Wei, L. Venkataraman and L. M. Campos, Tuning the polarity of charge carriers using electron deficient thiophenes, *Chem. Sci.*, 2017, **8**, 3254–3259.

55 B. Capozzi, E. J. Dell, T. C. Berkelbach, D. R. Reichman, L. Venkataraman and L. M. Campos, Length-dependent conductance of oligothiophenes, *J. Am.*

Chem. Soc., 2014, **136**, 10486–10492.

56 A. K. Ismael, K. Wang, A. Vezzoli, M. K. Al-Khaykanee, H. E. Gallagher, I. M. Grace, C. J. Lambert, B. Xu, R. J. Nichols and S. J. Higgins, Side-Group-Mediated Mechanical Conductance Switching in Molecular Junctions, *Angew. Chemie - Int. Ed.*, 2017, **56**, 15378–15382.

57 K. MURAKAMI, J. OHSHITA, S. INAGI and I. TOMITA, Synthesis, and Optical and Electrochemical Properties of Germanium-Bridged Viologen, *Electrochemistry*, 2015, **83**, 605–608.

58 J. Ohshita, M. Nodono, H. Kai, T. Watanabe, A. Kunai, K. Komaguchi, M. Shiotani, A. Adachi, K. Okita, Y. Harima, K. Yamashita and M. Ishikawa, Synthesis and optical, electrochemical, and electron-transporting properties of silicon-bridged bithiophenes, *Organometallics*, 1999, **18**, 1453–1459.

59 D. Tanaka, J. Ohshita, Y. Ooyama, N. Kobayashi, H. Higashimura, T. Nakanishi and Y. Hasegawa, Synthesis, optical properties, and crystal structures of dithienostannoles, *Organometallics*, 2013, **32**, 4136–4141.

60 H. Hanamura and N. Nemoto, Synthesis and properties of cyclopentadithiophene-based poly(silarylenesiloxane) derivatives, *Polym.*, 2011, **52**, 5282–5289.

61 M. Lemmer, M. S. Inkpen, K. Kornysheva, N. J. Long and T. Albrecht, Unsupervised vector-based classification of single-molecule charge transport data, *Nat. Commun.*, 2016, **7**, 1–10.

62 O. A. Al-Owaedi, S. Bock, D. C. Milan, M.-C. Oerthel, M. S. Inkpen, D. S. Yufit, A. N. Sobolev, N. J. Long, T. Albrecht, S. J. Higgins, M. R. Bryce, R. J. Nichols, C. J. Lambert and P. J. Low, Insulated molecular wires: inhibiting orthogonal contacts in metal complex based molecular junctions, *Nanoscale*, 2017, **9**, 9902–9912.

63 E. J. Dell, B. Capozzi, K. H. Dubay, T. C. Berkelbach, J. R. Moreno, D. R. Reichman, L. Venkataraman and L. M. Campos, Impact of molecular symmetry on single-molecule conductance, *J. Am. Chem. Soc.*, 2013, **135**,

11724–11727.

64 T. L. Schull, J. G. Kushmerick, C. H. Patterson, C. George, M. H. Moore, S. K. Pollack and R. Shashidhar, Ligand Effects on Charge Transport in Platinum(II) Acetylides, *J. Am. Chem. Soc.*, 2003, **125**, 3202–3203.

65 K. Liu, X. Wang and F. Wang, Probing Charge Transport of Ruthenium-Complex-Based Molecular Wires at the Single-Molecule Level, *ACS Nano*, 2008, **2**, 2315–2323.

66 J. Ponce, C. R. Arroyo, S. Tatay, R. Frisenda, P. Gavin, D. Aravena, E. Ruiz, H. S. J. Van Der Zant and E. Coronado, E ff ect of Metal Complexation on the Conductance of Single- Molecular Wires Measured at Room Temperature, *J. Am. Chem. Soc.*, 2014, ***136*** (23), 8314–8322.

67 S. Scheerer, N. Rotthowe, O. S. Abdel-Rahman, X. He, S. Rigaut, H. Kvapilová, S. Záliš and R. F. Winter, Vinyl ruthenium-modified biphenyl and 2,2'-bipyridines, *Inorg. Chem.*, 2015, **54**, 3387–3402.

68 R. W. Date, E. F. Iglesias, K. E. Rowe, J. M. Elliott and D. W. Bruce, Metallomesogens by ligand design, *Dalt. Trans.*, 2003, **10**, 1914–1931.

69 Y. Fan, L. Zhang, F. Dai, L. Shi and Z. Chen, Preparation , Characterization , and Photophysical Properties of Pt - M (M) Ru , Re) Heteronuclear Complexes with 1 , 10-Phenanthrolineethynyl Ligands, 2008, **47**, 2811–2819.

70 J. Ponce, C. R. Arroyo, S. Tatay, R. Frisenda, P. Gavin, D. Aravena, E. Ruiz, H. S. J. Van Der Zant and E. Coronado, E ff ect of Metal Complexation on the Conductance of Single- Molecular Wires Measured at Room Temperature, *J. Am. Chem. Soc.*, 2014, **136**, 8314–8322.

71 D. B. G. Williams and M. Lawton, Drying of organic solvents: Quantitative evaluation of the efficiency of several desiccants, *J. Org. Chem.*, 2010, **75**, 8351–8354.

72 D. S. Kopchuk, A. F. Khasanov, I. S. Kovalev, G. V. Zyryanov, G. A. Kim, I. L. Nikonov, V. L. Rusinov and O. N. Chupakhin, The extension of conjugated

system in pyridyl-substituted monoazatriphenylenes for the tuning of photophysical properties, *Chem. Heterocycl. Compd.*, 2014, **50**, 871–879.

73 E. Leary, S. J. Higgins, H. van Zalinge, W. Haiss and R. J. Nichols, Chemical control of double barrier tunnelling in α,ω-dithiaalkane molecular wires, *Chem. Commun.*, 2007, 3939–3941.

74 A. Vezzoli, R. J. Brooke, N. Ferri, S. J. Higgins, W. Schwarzacher and R. J. Nichols, Single-Molecule Transport at a Rectifying GaAs Contact, *Nano Lett.*, 2017, **17** (2), 1109–1115.

75 P. M. Beaujuge, H. N. Tsao, M. R. Hansen, C. M. Amb, C. Risko, J. Subbiah, K. R. Choudhury, A. Mavrinskiy, W. Pisula, J. L. Brédas, F. So, K. Müllen and J. R. Reynolds, Synthetic principles directing charge transport in low-band-gap dithienosilole-benzothiadiazole copolymers, *J. Am. Chem. Soc.*, 2012, **134**, 8944–8957.

76 H. Hanamura and N. Nemoto, Synthesis and optical properties of poly(tetramethylsilarylenesiloxane) derivative bearing diphenylcyclopentadithiophene moiety, *Polym.*, 2014, **55**, 6672–6679.

77 Y. A. Getmanenko, C. Risko, P. Tongwa, E. G. Kim, H. Li, B. Sandhu, T. Timofeeva, J. L. Brédas and S. R. Marder, Mono- and dicarbonyl-bridged tricyclic heterocyclic acceptors: Synthesis and electronic properties, *J. Org. Chem.*, 2011, **76**, 2660–2671.

78 F. A. Arroyave, C. A. Richard and J. R. Reynolds, Efficient synthesis of benzo[1,2- b:6,5- b']dithiophene-4,5-dione (BDTD) and its chemical transformations into precursors for π-conjugated materials, *Org. Lett.*, 2012, **14**, 6138–6141.

79 H. Hanamura, R. Haneishi and N. Nemoto, Fluorescent cyclopentadithiophene derivatives having phenyl-substituted silyl moieties, *Tetrahedron Lett.*, 2011, **52**, 4039–4041.

80 S. J. Higgins and R. J. Nichols, Metal/molecule/metal junction studies of organometallic and coordination complexes; What can transition metals do

for molecular electronics?, *Polyhedron*, 2018, **140**, 25–34.

81 C. Xu, A. Guenet, N. Kyritsakas, J.-M. Planeix and M. W. Hosseini, Molecular tectonics: heterometallic (Ir,Cu) grid-type coordination networks based on cyclometallated Ir(iii) chiral metallatectons, *Chem. Commun.*, 2015, **51**, 14785–14788.

82 S. D. Oosterhout, V. Savikhin, J. Zhang, Y. Zhang, M. A. Burgers, S. R. Marder, G. C. Bazan and M. F. Toney, Mixing Behavior in Small Molecule:Fullerene Organic Photovoltaics, *Chem. Mater.*, 2017, **29**, 3062–3069.

Acknowledgements

After almost 4 years I have a lot of people to thank for their support and these few words are not going to be enough!

Firstly, I must thank the person who firstly believed in me from a modest CV and a very bad internet connection and decided to give the opportunity to start a PhD under his wing: Prof. Simon Higgins. He also really helped me a lot through my PhD including this thesis!

I would like to thank also Prof. Richard Nichols that believed in me as well from the beginning and also co-supervised me and really helped me during all these years.

Important mention must be given to Dr Andrea Vezzoli that showed me and helped me with most of the things I did during my PhD, from how to synthetize a compound really pure to how to use an STM. I couldn't have achieved half of my work without your help!

I must also thank all the other scientists from the group that really helped with all their knowledge and time: Prof Don Bethell (always right on basically everything), Dr David Costa Milan (the best STM Dr that I know), Dr Edmund Leary, Inco Planje, Saman Naghibi for the support and also as friends. I would like also to thank the others PhD students that supported and accompanied me throughout the years (mostly to the AJ): Dr Matthew Pye, Davide Gastaldello, Martino Jakoobi, Claudia Gatti in particular for their friendship, but also all the others from the 4th floor and from other labs!

Additionally, also thanks to the students I had the chance to help for their projet: Helen, Emma, Aidan and all the other hundreds during my GTA-time.

A big thanks also goes to all our collaborators that worked hard: Prof. Colin lambert and his group from Lancaster: Sara, Iain, Mohsin, Ali, Prof Walter Schwarzacher and Richard from Bristol.During my PhD I haven't maturated only as a scientist but also as a person and for that I would like to thank all the very nice people that I had the chance to meet during the years within and outside my PhD: Robert, Daria, Alex, Robyn, Rhiannon, Eika, Jinghong, Sara, Stefàno, Celine, Ryan, Tom, Rachel and Jacko.

I would also thank my family: my mom Mara, my brother Lele and my two Grandmas for believing in me during all this time.

Finally, I would like to thank my soulmate Cecilia that supported me during all these years and helped me to get through the day. I will always remember your love and your patience that accompanied me all the way down to the end of this thesis.

Nicolò Ferri, 25th October 2018